AD-A062 441 VIRGINIA MASON RESEARCH CENTER SEATTLE WASH F/G 6/19
HYPERBARIC DECOMPRESSION BY MEANS OF BUBBLE DETECTION.(U)
APR 78 K H SMITH, L STAYTON N00014-69-C-0402
UNCLASSIFIED NL

1 OF 2
AD
A062441

LEVEL II (4) SC

708426

Hyperbaric Decompression by Means of Bubble Detection

Final Report

#N000 14 69-C-0402

by

Kent H. Smith
and
Lee Stayton

April 20, 1978

Virginia Mason Research Center
1000 Seneca Street
Seattle, Washington 98101

(6) Hyperbaric Decompression by Means of Bubble Detection,

(9) Final Report,

#NOOO 14 69-C-0402

(11) 20 Apr 78 (15) N0014-69-C-0402

(10) by
Kent H. Smith
and
Lee Stayton

April 20, 1978

(12) 146 p.

Virginia Mason Research Center
1000 Seneca Street
Seattle, Washington 98101

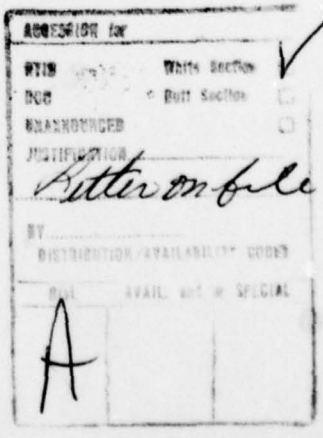

Section I

Animal Decompression Studies

Section I

Table of Contents

I. ABSTRACT

Present decompression procedures, based on the Haldane concept, allow the maximum possible degree of supersaturation without producing decompression sickness in an attempt to provide the greatest rate of gas elimination and the shortest possible safe decompression. The initially large supersaturation values experienced in a Haldane type decompression were shown to predispose bubble formation. Using the Doppler detector implanted on the pulmonary artery or posterior vena cava in sheep and goats, we have demonstrated the presence of gaseous emboli in all Haldane model decompressions. Emboli signals from implanted cuffs were clear with a high signal to noise ratio and were therefore adaptable for signal analysis and absolute quantitation with a gas emboli counter. Gas emboli-free ascent procedures were developed using the ultrasonic detector and the emboli counter.

These gaseous emboli when detected in large numbers heralded the onset of decompression sickness. Even in small numbers these emboli caused changes in platelet and fibrinogen survival times. We conclude that the most probable cause of bubble formation in a Haldane type decompression is the initial ascent rate and that gas emboli are pathogenic and should be eliminated to provide a truly safe decompression.

II. INTRODUCTION

Paul Bert in 1878 (1) conclusively demonstrated that nitrogen gas bubbles occurred in the blood of animals decompressed from increased atmospheric pressures. That these bubbles were in some way connected with the clinical signs of decompression sickness came about circumstantially as no direct relationship was shown. Because the causitive mechanism was not known, much effort went into providing a technique for preventing symptoms which divers call decompression sickness or "bends."

That bubbles form and grow within the body during decompression and whether they have an absolute relation to decompression sickness is of considerable importance. While authors disagree on whether bubbles always exist during decompression (4,7), there is little disagreement in the fact that intra- and extravascular bubbles can, and most probably do, exist during decompression sickness.

An objective appeared clear that an effort should be made to detect the presence of bubbles during decompression and hopefully to correlate this detection with the onset of clinical decompression sickness. Various optical (2) and acoustic systems (3,5,6) have been developed recently to detect the presence of bubbles in both intra- and extravascular locations.

We proposed to evaluate the applicability of the Doppler ultrasonic flowmeter system to the detection of bubbles in decompressed animals and to assess the relation of

Doppler detected bubbles and the incidence of decompression sickness. Finally, we proposed to construct decompression procedures from the detection of newly formed bubbles.

The following document details instrument and animal systems development. It describes procedural techniques for the evaluation of the Ultrasonic Doppler bubble detection system.

References

1. Bert, Paul. 1878. La Presion Barométrique. Masson, Paris.
2. Buckles, R.G. The Physics of Bubble Formation and Growth. Aerospace Med. 39:1062-1069, 1968.
3. Gillis, M.F., Peterson, P.L. and Karagianes, M.T.: In Vivo Detection of Circulating Gas Emboli Associated with Decompression Sickness Using the Doppler Flowmeter. Nature. 217:965-967, 9 March 1968.
4. Hempleman, H.V., Crocker, W.E., and Taylor, H.J.: Gt. Britain MRC RNPRC, U.P.S. Rept. R.N.P. 52/708, U.P.S. 131, June 1959.
5. Spencer, M.P., and Campbell, S.D.: Development of Bubbles in Venous and Arterial Blood During Hyperbaric Decompression. Bull. Mason Clinic. 22:1, March 1968.
6. Walder, D.N., Evans, A., and Hempleman, H.V.: Ultrasonic Monitoring of Decompression. The Lancet. 897-898, 27 April 1968.

References, cont.

7. Wyman, J., Jr., Scholander, P.F., Edwards, C.A., and Irving, L.: On the Stability of Gas Bubbles in Sea Water. J. Maine Res. 11: 47-62, 1952.

V. EXPERIMENTAL ANIMAL SELECTION AND PREPARATION

A. Specie Selection.

The selection of an animal model must be done with respect to simulating man's susceptibility to decompression sickness. However, several criteria are important in the proper selection of an animal model to be used in decompression sickness:

1) A minimum perfusion rate very close to that of man;
2) Control of regional blood flow (that is, response to neurological, hormonal and pharmacological entities) similar to that of man;
3) Predictable susceptibility to and a display of objectively assessable signs of decompression sickness;
4) Convenient size; and
5) Ease of handling.

In several mathematical models used for the calculation of tissue gas loading, elimination and uptake are limited by the perfusion rate of a specific compartment, either anatomical or theoretical and defined by a half-time (t 1/2). In the development of tissue saturation values, we have taken advantage of the perfusion limited system. The use of limiting tissue perfusion rates facilitated comparison of animal models. Although mathematical models of this sort neglect diffusion or other limitations of gas transfer, they were available, were backed by empirical data, and could easily be used for evaluation.

The autonomic nervous system (that section of the nervous system responsible for most physiologic compensatory responses) of the laboratory and the domestic animals contempleted were generally similar to that found in man. Certain regional controls which regulate blood flow differed in origin, however general vascular responses appeared to be uniform. If one were to study the neurological, hormonal or pharmacologic responses to decompression sickness and desired to extrapolate the information to man, these regional specie variations would have to be taken into greater consideration.

The ability of an animal to objectively display signs of decompression sickness was considered important for the comparison of objectively detected signs and the onset time of clinically manifested signs. We have observed that the larger domestic animals, i.e., pig, sheep, goat and dog, better display signs of discomfort than do the smaller laboratory animals such as the rat, mouse, guinea pig or rabbit. The latter animals are known to require a more severe insult to produce an equally observable sign than do the former group of animals.

Excepting physiologic differences, animal size is important only in relation to available equipment and facilities. As long as proper handling equipment and facilities are available, any animal model that satisfies other criteria and fits into the existing chamber could be used.

Ease in handling and adaptability to experimental procedure are very important criteria. The physiologic response to experimental stimuli of the animal is in part a result of the way the animals responded to handling. One must review all handling procedures prior to animal selection including daily care, surgical procedures, and routine daily experimentation. An excited animal presents an entirely different physiological model than does an animal that is relaxed and comfortable. For this reason, docile or conditioned animals make better experimental subjects.

The medium-sized domestic animals, i.e., dog, goat, sheep and pig, are probably more physiologically similar to man than many of the species usually found in the research laboratory, e.g., rodents. Some of the similarities between these animals and man are body weight, respiratory rate, heart rate, systemic blood pressure, etc. The seeming similarity between two species usually is a function of body size. Body size seems to be especially important with respect to decompression sickness.

The variety of species previously used in decompression studies has been somewhat limited. Of these, the goat has been most often used. Investigators have reported that the onset of symptoms observed in the goat are not unlike those observed in man. Certain physiologic and metabolic parameters of the goat differ

distinctly from man however. One anatomic difference which possibly could introduce physiologic variation is the compound structure of the ruminant digestive tract. The microbiological activity and gas production in these stomach areas of the ruminant may make these species undesirable for some types of decompression studies. Nevertheless, the animal is easy to handle, is usually of a good working size and does have general physiologic response to compressed gas atmospheres similar to that of man.

The dog is a well-established laboratory animal for many physiologic investigations and has been used successfully in diving decompression work. However, we were not satisfied that the dog was endowed with the same quantitative physiologic characteristics which were in the end responsible for man's susceptibility to decompression sickness. Body mass of dogs varies considerably between various breeds as do fat water ratios and minimum perfusion rates. For these reasons it is necessary to specify canine characteristics as well as evaluate them with respect to the study attempted. Because other more uniform animal models were available, the dog was not considered the best candidate for the decompression studies.

No small and easily handled nonhuman primates were available that had body mass or fat water ratios to suggest that they might be suitable. Large nonhuman

primates which do represent man very closely are both hard to handle and expensive.

When comparing various domestic nonprimate, simple stomached animals to man, the most physiologically similar is the pig. Recent increases in the application of this laboratory species supports this statement (3). New strains of miniature swine have been developed and are finding increasing use in the field of cardiovascular physiology research. Withstanding certain obvious phenotypic variation, the similarity between pig and man is not limited to the cardiovascular system but includes the integumentary system, respiratory system, and digestive system, as well as other functions of note. Because of the lack of much experimental data, more study is necessary for the use of the pig as a model for studying decompression sickness.

The sheep, because of its similar relative mass to man, has also been used successfully as a decompression model. It is easy to handle, adapts easily to laboratory situations and is readily available. For these reasons the sheep was chosen as the animal of choice for this study.

B. Surgical Procedure

Several different surgical approaches were attempted to apply ultrasonic bubble detectors to the major cardiac vessels. The first approach was by

resection of the third rib. This approach gave adequate accessibility to the pulmonary artery, but anterior and posterior caval vessels were not easily reached with this approach. The final and satisfactory approach appeared to be by sternotomy.

Feed and water were removed from the animals 36 hours prior to surgery. One hour prior to surgery, 1/75th of a grain of atrophine was administered subcutaneously. The animals were then brought to surgery, placed on the operating table in dorsal recumbency and prepared by clipping, scrubbing and disinfecting with alcohol and Zepharin. The patient was induced with 5% halothane in oxygen administered by cone using a NarkoVet anesthesia machine with Drager Vapor. The animal was then intubated with a 12 mm Rusch endotracheal catheter connected to the anesthetic machine and positively ventilated with a Mark 9 and a Mark 4 Bird respirator. Animals were maintained on 1.5% halothane in oxygen. The sensitivity level of the respirator was set such that normal respiratory movements would control the respiratory rate but in the event of their absence, the unit would automatically cycle 7 times per minute. During the sugical procedure with the thorax open, the lungs were manually inflated by bag 5 times every 15 minutes to reduce atelectasis.

The surgical site was finally prepared and a sternotomy incision was made using a sternotomy knife. Retractors were used to spread open the thoracic cage presenting

the heart, lungs and major cardiac vessels. Cuff-type Doppler probes were placed on: 1) the pulmonary artery in juxtaposition to its exit from the right ventricle; 2) the anterior vena cava just cephalad to the common cava and 3) the posterior vena cava, some 3 cm caudad to the common cava (Figure 1). Lead wires from the cuff-type Doppler ultrasonic probes were brought through the 2nd and 3rd intercostal spaces at the level of the olecranon. At the completion of this procedure, the sternotomy incision was closed. A sharp penetrating stylette with an eye in the most distal end was forced through the ventral thoracic wall just lateral to the sternum. Stainless steel sutures were then threaded through the eye and pulled up and from within the thoracic cavity, externally. This procedure was done on both sides of the thoracic cage with a continuous suture. The stainless steel sutures were placed in every other intercostal space.
The thorax was then closed and the sutures tied. A stainless steel vent tube was left in place at the most caudal end of the sternotomy incision. The remainder of the subcutaneous incision was closed with No. 2 catgut. Prior to closure and removal of the bent tube, the lungs were forcefully expanded and held in full inspiratory position. Suction was used on the vent tube which was removed simultaneously with closure of the vent tube site.

Following closure of the skin of the thoracic incision, the right lateral inguinal area was prepared for implantation

of the femoral cuff. An incision was made over, and parallel to, the femoral vessels approximately 10 cm in length. Blunt dissection of the sartorious muscle anteriorly and the pectineus muscle posteriorly revealed the femoral vein lying posterior and deep to the femoral artery. The 1/2 cm cuff was placed on the femoral vein and the incision was closed.

Before the animal was taken from the operating table, the probes were checked for electronic integrity and flow signal. The animal was then placed in a sling and positive pressure respiration was continued with 100% oxygen or air until the animal had recovered sufficiently to be returned to the animal quarters. Animals were routinely administered 1 million units of procaine Penicillin G and 1 gram of Dyhydrostreptomycin prophylactically by intramuscular route. Ten milligrams of Talwin* were also administered intramuscularly. This was repeated at 12 hour intervals for the first 36 postsurgical hours. A recuperative period of 3 weeks was allowed each experimental animal prior to exposure in the chamber.

C. Discussion

Prior to refinement of the surgical exercise, the technique proved to be both difficult and sometimes unsuccessful. The lateral approach by thoracotomy and rib dissection did not allow proper accessibility to

(* Talwin, a brand of pentazocine (as lactate) Winthrop Laboratories, N.Y., N.Y.)

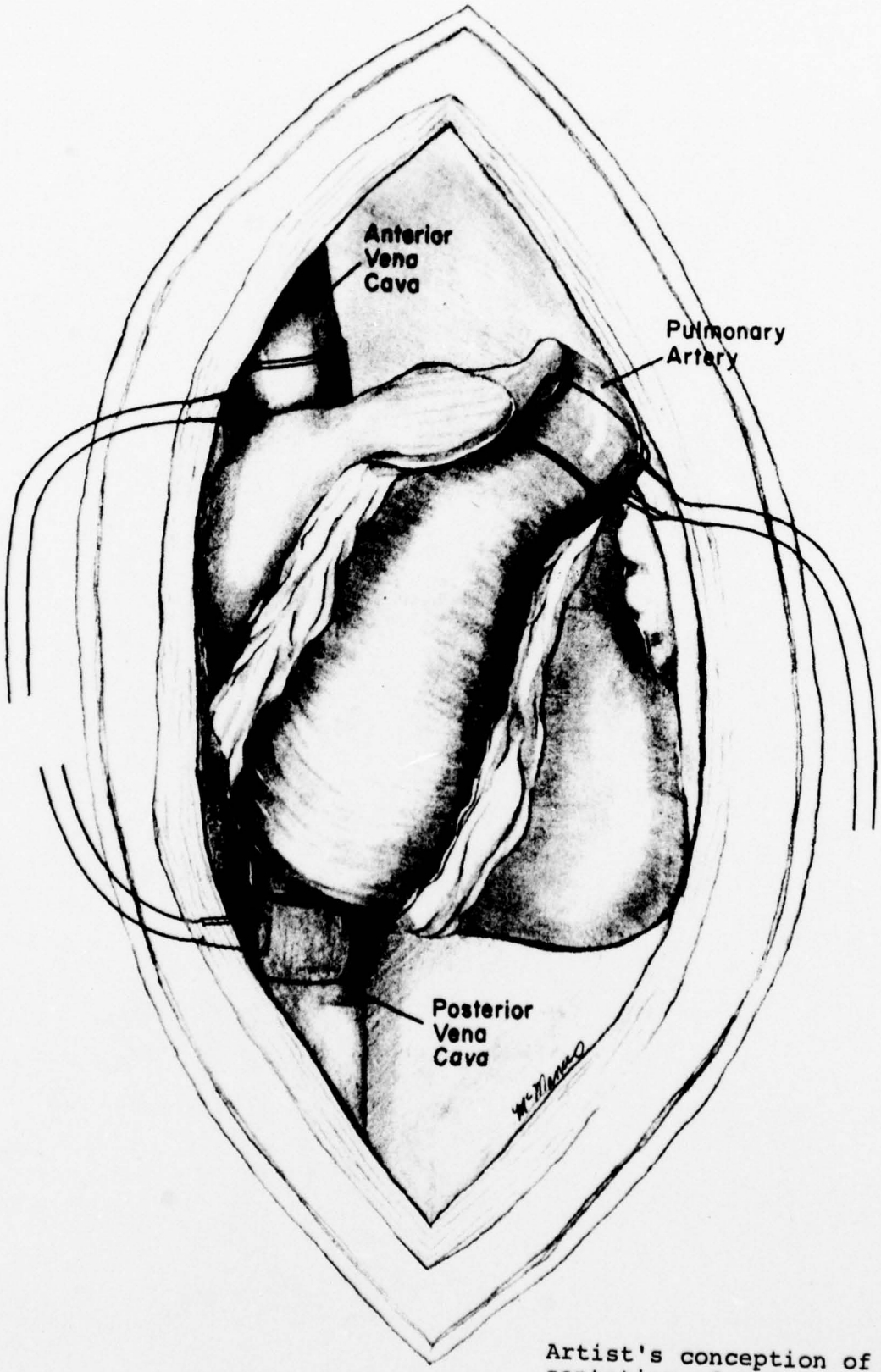

Fig. 1.

Artist's conception of presentation of major cardiac vessels with sternotomy incision. Ultrasonic transducer cuffs are in place.

the desired vessels. Three animals were lost; severe pleural adhesions were present which caused numerous points of pneumothorax when the lungs were bluntly dissected from the wall of the thorax. The third animal expired from inhalation pneumonia subsequent to emesis after removal of the endotracheal catheter.

In general the sternotomy incision proved to be successful as it allowed good accessibility to all of the major cardiac vessels and could be done quickly and safely. The great disadvantage to the sternotomy incision was the amount of postoperative pain. Close confinement of the animal during its early postoperative period in combination with the administration of a non-narcotic analgesic agent (Talwin) relieved the animals from experiencing much pain. The postoperative animals would routinely be back on feed within four or five hours after the surgical exercise.

IV. ANIMAL DECOMPRESSION STUDIES

A. Introduction.

Decompression from exposure to increased ambient pressures has historically been a human titration. Routine decompression procedures have been based on empirical evidence of success for an "average diver." Success was defined as no subjective sign of decompression sickness. This somewhat gross technique has been highly refined with interesting theoretical and sometimes mathematically complex equations. These refinements plus the accumulation of continuing expirical data vastly improved the heretofore hazardous procedure.

We desired to establish an end point in the development of decompression profiles which could announce the onset of decompression sickness prior to any clinical manifestation. The question to be answered appeared to be what tool could detect newly formed bubbles in either the tissue or the vascular system. The principles of ultrasound seemed to lend themselves to such an application. Doppler ultrasonic flow measurement was frequently encumbered by undesirable sounds if bubbles were present in the fluid whose flow was to be measured. When applied to the detection of bubbles, this system signaled the presence of bubbles in both *in vitro* and *in vivo* systems.

Decompression sickness has long been identified with the unphysiologic evolution of gas from body stores in the form of bubbles (4,5). That bubbles were present in a diver was not suspected until he presented signs of decompression sickness. Techniques for the ultrasonic detection of gas bubbles in tissue and blood have now been developed that allow their acoustic visualization. In the original Doppler studies, Spencer and Campbell (6) implanted Doppler blood flow transducers on the posterior vena cava and descending aorta of domestic sheep. They demonstrated that Doppler bubble signals in the posterior vena cava preceded signs of decompression sickness and that bubble sounds later became evident in the descending aorta. Their hypothesis for the presence of arterial bubbles was that although the lung served as a filter to dissipate many venous bubbles, an overloading of the pulmonary bed with gaseous emboli might allow passage of bubbles into the systemic arterial circulation. Denovo bubbles in the arterial system were also suspected on severe profiles. Other studies using this technique supported the satisfactory use of the Doppler in the detection of decompression bubbles (7).

Continuous wave and pulsed ultrasound systems have been employed to detect both vascular and tissue bubbles (8,9,10,11,12). In these applications, either

the reflected signal (echo), with respect to time of signal return (11,12) or attenuation of a through transmission of sound (8,10), was examined to indicate a new tissue interface such as a bubble might produce. The addition of a retention cathode ray tube and scanning instruments allowed one to visualize an entire tissue density matrix.

B. Objectives

1. To develop decompression procedures based on ultrasonic bubble detection,
2. To determine onset time of bubble formation with respect to depth/time profiles,
3. To investigate anatomical bubble development sequence during decompression from hyperbaric exposures, and
4. To determine best body location for bubble detection sensor.

C. Methods

1. Experimental Plan

a. Bubble Detection

Doppler ultrasonic flowmeters were to be used to detect bubbles formed in the anterior vena cava, posterior vena cava, pulmonary artery and femoral vein, using implantable sensors in domestic sheep. 10 MHz carrier frequencies were the frequencies of choice

considering the resonant frequency and bubble size that we wished to detect.

Spectographic frequency and amplitude analyses were planned to quantitate velocity, number, size and position.

b. Animal Exposures

Adult domestic sheep were to be instrumented with Doppler blood flow transducers. Varying exposures to pressures up to 89 psig in air were to be explored for immediate return limits. Decompression profiles with sufficient severity to produce signs of decompression sickness were desired and were to be correlated with Doppler indications of bubble formation. Following the use of these bends producing profiles, no decompression return limits from various depths were to be evaluated using the first indication of bubble formation as the limiting criterion in an ascent profile. Ascent rates were 60 fpm.

Bubble formation was to be evaluated for origin, quantity and its relation to clinically manifested signs of decompression sickness.

2. Equipment and Materials

A hyperbaric chamber was put into service at the Virginia Mason Research Center, during the

first Contract Year covered by this report and was the chamber facility used for the exposure of all experimental animals. The chamber was designed for a working pressure of 700 psig with an entirely manual control system. Oxygen content of the chamber was measured with a Beckman E2 Oxygen Analyzer. Temperature and humidity were controlled by periodic venting of the chamber with compressed air. Acceptable carbon dioxide levels were also maintained during animal exposures by the periodic venting procedure.

3. Procedure

Domestic sheep (Ovis aires) weighing approximately 57 kilograms were surgically prepared by sternotomy and 10 mHz Doppler ultrasonic transducers in cuff-form were placed on the anterior vena cava (AVC), posterior vena cava (PVC), pulmonary artery (PA), and femoral vein (FV). In one animal, an ultrasonic transducer in cuff-form was placed on the aorta approximately 2 cm distal to its attachment to the left ventricle. A two- [illegible] ost surgical recovery period was allowe[illegible]r all animals after which control recordings were taken to establish baseline bubble-free flow signals (Figure 2 and 3).

The animals were then individually exposed to compression followed by decompression during which

they were monitored for bubble formation. The Doppler ultrasonic flow-bubble information was recorded on magnetic tape. The initial dive profiles were severe in order to definitely produce signs of decompression sickness in the exposed animals. An example of one of these profiles is demonstrated in Figure 4. The signs of decompression sickness manifested were anxiety, restlessness, increased heart rate, and joint pain, indicated by characteristic leg movement. These signs of decompression sickness were clearly apparent. Animals that exhibited these signs were recompressed to a level which appeared to alleviate pain and then were decompressed slowly at some spontaneously determined rate. From the initial studies, dive profiles were developed which would produce Doppler detected bubble signs without decompression sickness. Values of allowable surfacing tissue supersaturation (M) were calculated from these latter depth-time profiles and compression cycles were determined which would uniquely insult 1 compartment of a 9 compartment model with half-times ranging from 5 to 240 minutes (Table 1). Data were collected for: (1) The detection of the first appearance of venous bubbles; (2) The development and distribution of bubbles; and (3) Data reduction to demonstrate

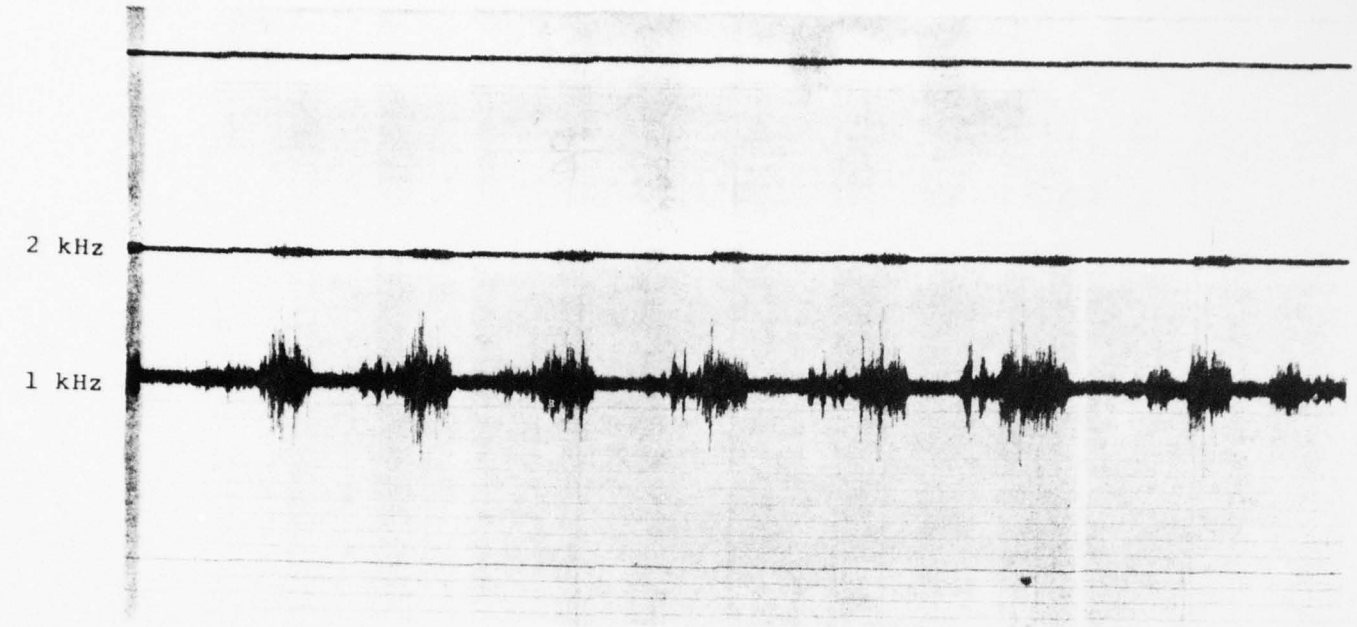

CONTROL PULMONARY ARTERY SIGNAL

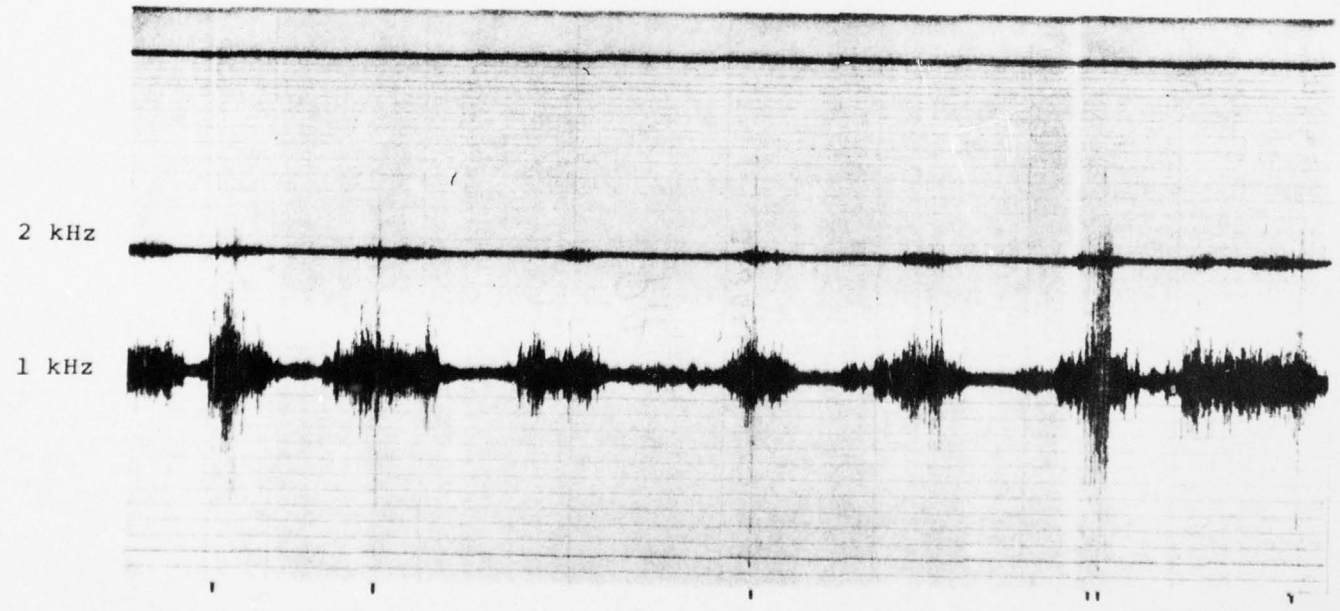

PULMONARY ARTERY SIGNAL POST DECOMPRESSION WITH BUBBLES

Fig. 2. Oscillographic recordings of pulmonary arterial blood flow.

Top: Control recording.
Bottom: Post decompression.
Marks at bottom of recording indicate location of bubble signal.

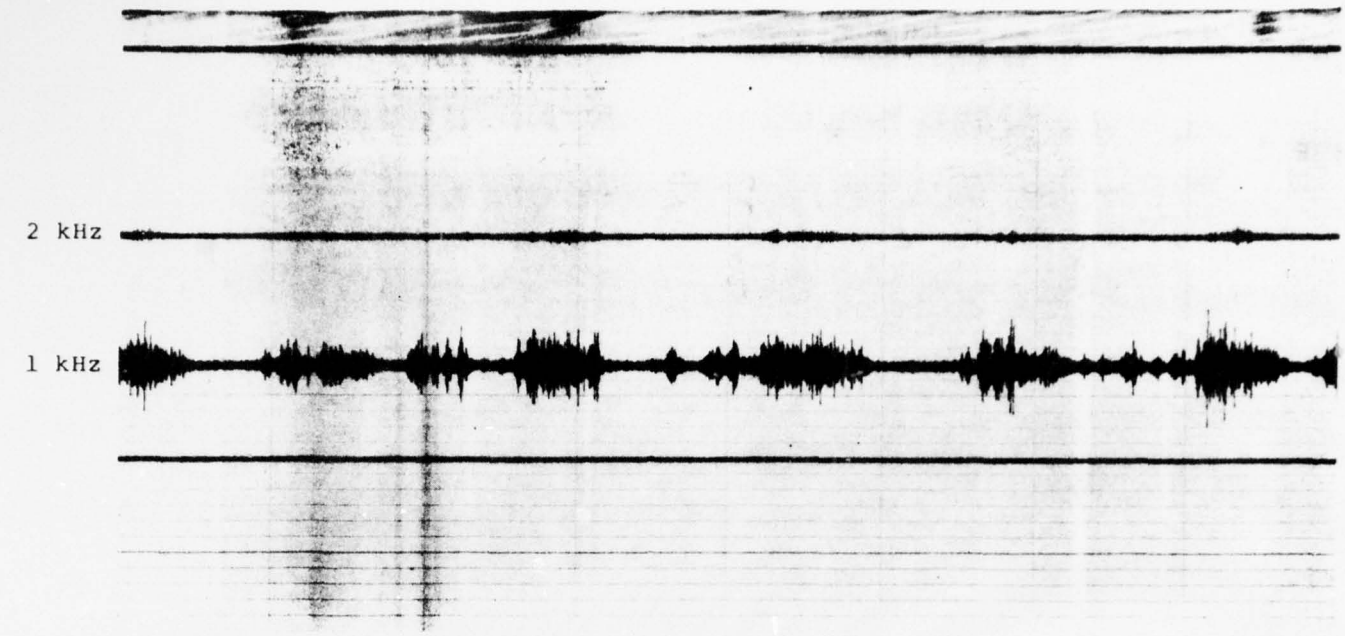

CONTROL ANTERIOR VENA CAVA SIGNAL

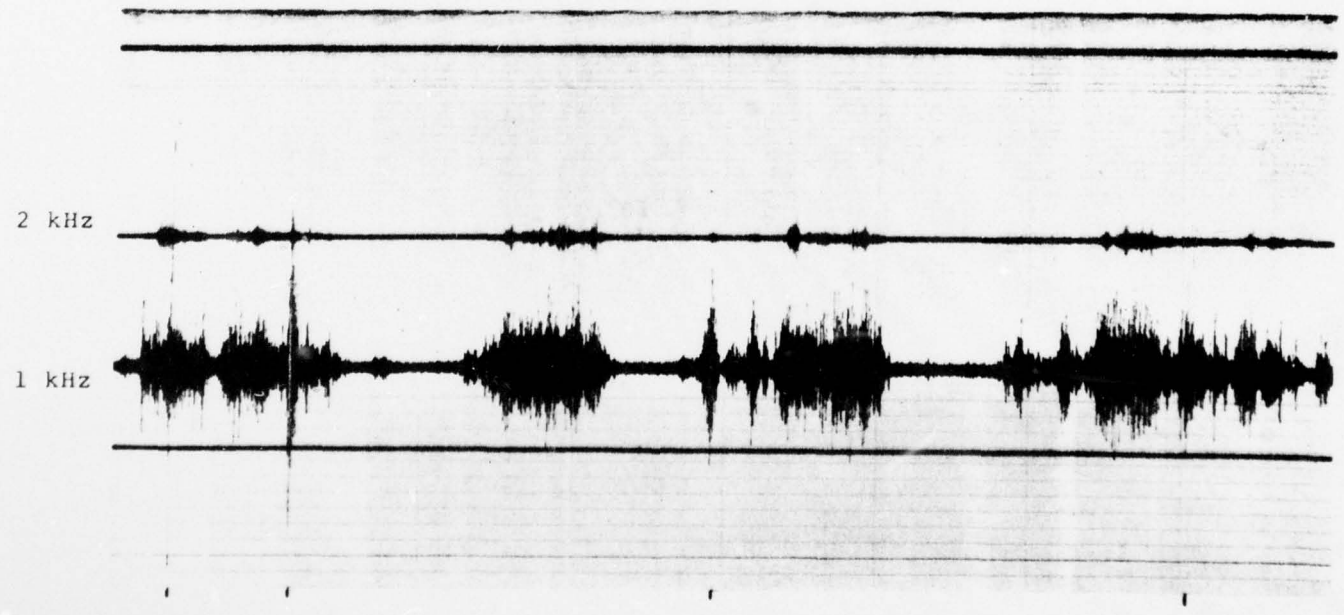

ANTERIOR VENA CAVA SIGNAL POST DECOMPRESSION WITH BUBBLES

Fig. 3 . Oscillographic recordings of anterior vena cava blood flow
Top: Control recording.
Bottom: Post decompression.
Marks at bottom of recording indicate location of bubble signal.

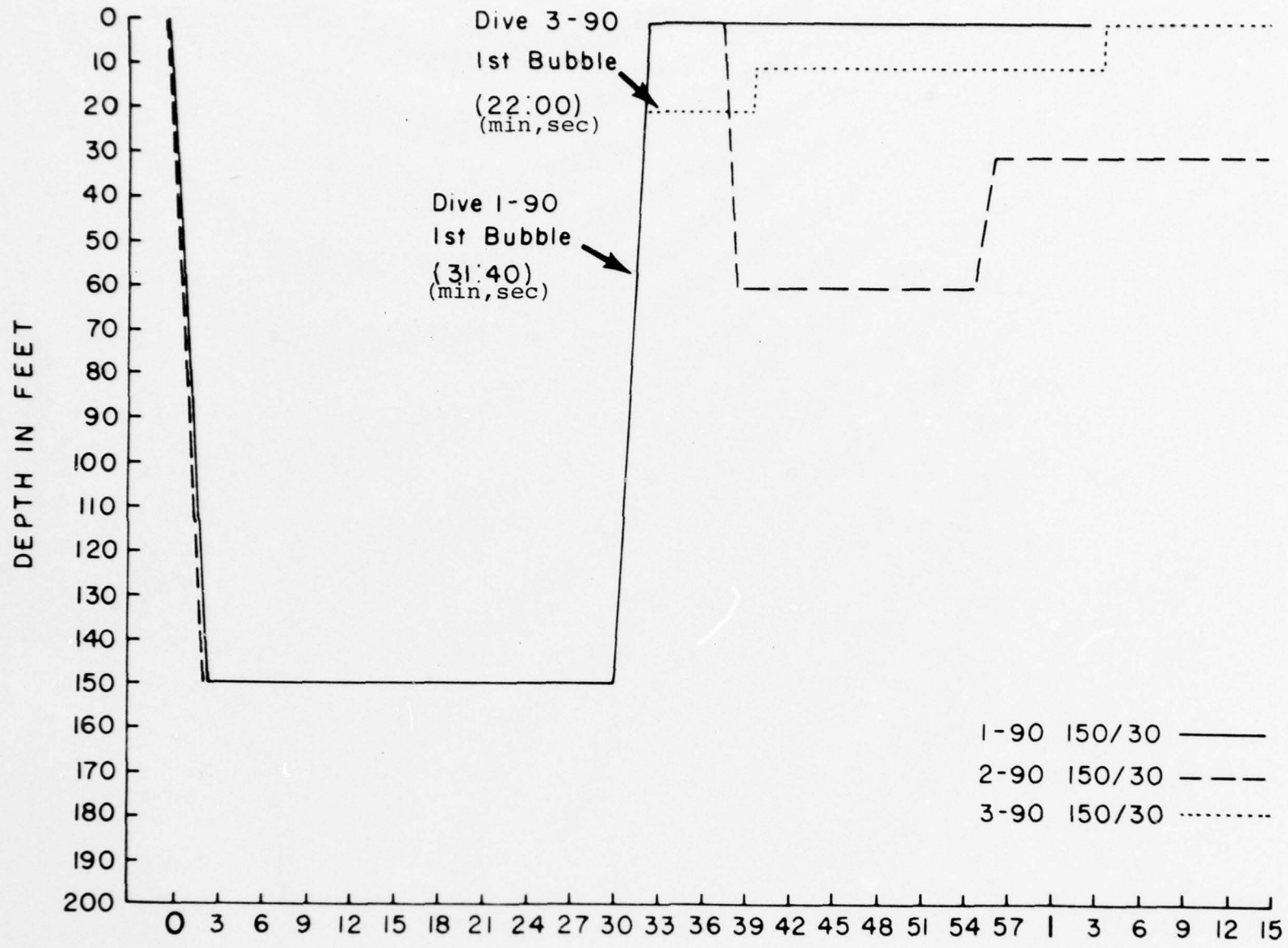

Fig. 4 . Dive profile showing U.S. Navy decompression schedule (3-90) and recompression after no-decompression ascent (2-90).

TABLE 1.

T I S S U E I N E R T G A S L O A D I N G S

Depth (fsw)	Time (min)	$t_{1/2}$ 5	10	20	40	80	120	160	200	240
188	10	139	102	71	50	39	35	33	32	31
120	30	121	110	88	65	48	41	38	36	34
92	58	100	99	90	73	56	47	43	40	38
76	90	87	87	85	74	59	51	46	43	40
58	150	73	73	73	69	60	53	50	45	43
45	270	62	62	62	62	59	55	51	48	46
36	540	55	55	55	55	55	54	53	50.7	49

(___indicates value exceeds M value)

the best location for routine bubble detection.

D. Results

Characteristic Doppler bubble sounds continued to be present for long periods of time after decompression insult. Routinely these sounds could be detected at 24 hours and in one animal these sounds were still present at 72 hours post-decompression. Doppler sounds which did remain long after decompression insult seemed logically to be some entity other than gaseous emboli. In that the sounds did not alter significantly upon recompression, it appeared even more likely that a non-gaseous embolus was the causative factor. Other sources of emboli have been hypothesized (13) which could account for their long-term appearance.

A total of 41 dives was completed on 9 animals. In all animals which experienced decompression sickness, Doppler indications of bubble formation were present prior to the onset of clinical manifestations. In the profiles listed in Table 1, only small numbers of bubbles were detected with the Doppler system. The underlined number indicates that this tissue value exceeded the theoretically calculated allowable supersaturation for that compartment (Table 2). Only one animal on the 45 ft/270 min profile exhibited any sign of decompression sickness. All other runs of animals tested on these profiles were asymptomatic, however all demonstrated obvious bubbles.

TABLE 2.

ALLOWABLE SURFACE TISSUE SUPERSATURATION VALUES IN FEET OF SEA WATER

(SURFACING M VALUES)

$t_{1/2}$	5	10	20	40	80	120	160	200	240
M.	120	100	86	73	59	54	51.5	51.5	51.5

These were identified in post-decompression recordings as seen in Figures 1 and 2.

First Bubble Location:

Anterior vena cava bubble sounds were detected first in 18 cases out of 21 monitoring comparisons. In one case when the AVC sounds were not detected first, bubble detection was hampered severly by static noise on the AVC channel. The aorta, the only other channel monitored during Dive 16-90, manifested bubbles 4 minutes and 7 seconds after surfacing from a 130 ft. dive for 20 minutes.

TABLE 3.

LOCATION OF FIRST BUBBLE DETECTION

Vessel Comparison		Number of Comparisons	Number of First Bubbles (__)
AVC	PVC	5	AVC (5) PVC (0)
AVC	PA	3	AVC (1) PA (2)
AVC	FV	2	AVC (1) FV (1)
AVC	Aorta	11	AVC (11) Aorta (0)
PVC	PA	1	PVC (1) PA (0)
PVC	FV	2	PVC (0) FV (2)
PVC	Aorta	1	Both detected at same time.
Aorta	FV	1	Aorta (0) FV (1)

Demonstrated in Table 3 is the comparison of first bubble detection with respect to the location of the monitored vessel. Much of the data reported here was obtained prior to the development of the four channel system when only 2 vessels could be recorded during a single dive. Consequently comparisons were made only on two vessels at a time.

Time of Bubble Detection:

The first appearance of bubbles in a vessel was usually followed by detection in other vessels. Appendix A presents the time of first bubbles in all vessels monitored. From this data it is clearly seen that the AVC detector had a high probability of demonstrating the presence of bubbles before they occured in other vessels monitored. The PA detector represented a confluence of bubbles, as one would expect, from the two venous returns, AVC and PVC, at a time interval shortly after first detection.

Anterior vena cava bubbles appeared a mean time of 2.61 ± 2.31 sd* minutes after surfacing with a linear ascent from bottom depth. PVC bubbles appeared an average of 9.5 ± 5.3 sd minutes and PA bubbles 6.9 ± 5.1 sd minutes after surfacing. Time of onset seemed to have little relation to depth or length of profile while there appeared clear relation between the vessel and first bubble appearance.

(* sd - Standard Deviation)

Best location for routine bubble detection should be that site where bubbles can be routinely picked up by the Doppler transducer at the earliest possible time. The PA, while not first in the presentation of detectable bubbles in this study, does represent the venous admixture of gas-laden blood returning from all parts of the body. Since it can be monitored from a transcutaneous location in both animals and man, in addition to manifesting bubbles routinely, the PA appears to be the vessel of choice.

B. Goats

1. Specific Aims

a. Through direct monitoring of goats implanted with the Doppler ultrasonic detector, record the actual physical presence of gas emboli as a result of tissue and blood gas disequilibrium.

b. Using the U.S.N. exceptional exposure profile for 220 fsw for 20 minutes, exposing the experimental subjects on 5 days of each week for 2 consecutive weeks with one dive per day, to determine if gas emboli occur randomly or with an ordered nature.

c. Using the same dive series mentioned in 2 above, if decompression sickness is present, compare the number of detectable gas emboli to the presence of decompression sickness signs and symptoms.

d. Employing the same dive series mentioned in 2 above, determine if the number of detected gas emboli are influenced by the daily repetitive diving.

e. Using 220 fsw, 20 minute; and 60 fsw, 4 hour, profiles with varying ascent rates, determine the relationship of rate of ascent and detection of gaseous emboli.

f. Using a 220 fsw for 20 minutes profile, determine the rate of ascent that produces zero detectable gas emboli.

g. Determine if the number of detectable gas emboli present in the vascular system can be controlled by varying the ascent rate.

h. Determine the feasibility of using the doppler detection of vascular gas emboli to control decompression procedures.

i. Examine radiographically for the presence or absence of dysbaric osteonecrosis following this dive series.

j. Monitor human subjects during deep helium/oxygen exposures for the presence of gaseous emboli and relate that presence to the occurrence of decompression sickness.

2. Rationale

Present decompression procedures allow the maximum possible degree of tissue supersaturation without producing decompression sickness in order to provide the greatest rate of gas elimination and the shortest possible safe decompression. Previously a low incidence of bends was viewed as an indication that the optimal decompression was taking place. Our experience with the doppler has demonstrated that detectable emboli were usually present before the onset of

symptoms and were often detected when no symptoms appeared. Since bubble formation is a function of the degree of supersaturation, the decompression procedure treads a fine line between the appearance of symptoms in divers and the possibility of wasted time if no symptoms appear.

The recurrent failure of present decompression procedures reflects the difficulty of bringing together both theoretical concepts and a knowledge of physiologic dynamics. A good method of observing what is acutally happening in the body without significant delay, in relation to a particular depth/time profile has not yet been adequately defined.

Past experience of dives being monitored by Doppler show a definite relationship in the number of venous gas emboli and the eventual development of decompression sickness. These studies were designed to give data which could be used in defining more exactly the nature of this relationship.

Data expressed in a graphic format, gathered from dives whose decompression profiles will be determined by a constant number of bubbles being present throughout the ascent, will be compared to presently used U.S.N. profiles. This information will be valuable in understanding the discontinuities of decompression tables now used and perhaps demonstrate faults

in present theoretical concepts. This empirical data will also be useful in understanding the area of ill-defined physiologic concepts. Defining the quantity of bubbles that could be considered a safe threshold would provide a significant forewarning to the possible development of decompression sickness. This would allow corrections to be made to a potentially hazardous profile.

That a particular dive profile will work for one individual and not for another has been demonstrated in many dives in which more that one diver participated. Situations where a profile will work for a particular individual diver one time and not at another time has also been noted. A defined safe gas emboli number would make the Doppler effective in evaluating a decompression profile according to the particular individual's susceptibility. In this manner Doppler detection of venous gas emboli may provide one with a prophylactic device for safer decompression. The proposed experiments will use the doppler in an attempt to show this potential as an important investigative instrument which can be applied with little difficulty to further define parameters involved in decompression.

Use of the Doppler can be considered both a more conservative and a more objective way of

testing decompression profiles. From both a practical and medical point of view it renders less important previous controversies regarding use of either a constant tension gradient (ΔP) between tissue and ambient hydrostatic pressure or a constant pressure ratio (P_i/P_f) (Behnke, 1969) for limiting ascent rates. It provides an experimentally objective means of establishing safe decompression schedules by relating symptoms, signs and sequelae of decompression sickness to the appearance and number of gas emboli.

3. Methods

a. Animal preparation and exposure

Three 40 kilogram goats were implanted by thoracotomy with a doppler sensor which was placed on the posterior vena cava. A two week post operative period was allowed to ensure the health of the experimental animal. Radiographs were taken of the long bones prior to any hyperbaric exposure.

Two of the experimental animals were restrained in the chamber during the dive procedures. The type of restraint used gave the animals room to move and lie down, but kept them sufficiently restrained to allow attachment of the necessary doppler monitoring instrumentation.

Closed curcuit television and port holes allowed observation of the animals from several angles throughout the dive. If it became necessary, it was possible to enter the pressurized chamber to assist the animals, repair equipment, etc.

The signal from the implanted Doppler was fed through the chamber to the signal analysis system, which was used to detect, count, and record the bubble signals as they were carried past the Doppler probe by the blood stream. Emboli detection instrumentation was developed by the Applied Physics Laboratory of the University of Washington under this grant and consisted of three basic components, a transducer, transmitter, and receiver. The transducer was a piezoelectric crystal (PZT-4) set in acrylic and mounted in a cuff. This cuff was implanted around the posterior vena cava proximal to its entry through the diaphragm. Approximately 3 cm distance was maintained between the cuff and the heart in order to preclude heart movement sounds. Sylastic-covered transmission wires led from the cuff through the chest cavity at which point a nylon pack was sutured to the

to the animal's skin and was used to contain the transmission wires. This pack served as the storage container when the leads were not in use. Careful daily cleansing was necessary to prevent infections at the point where the wires exited from the body.

Implantation of the transducer gave signals of high quality with large signal to noise ratios, providing reliable analysis and counting of ultrasonic Doppler events (UDE).

A Wang 700 C calculator, in conjunction with a 701 output writer and a 712 plotter system was programed to sample the bubble count at specified intervals, and to plot the bubble count vs. the dive time. After a dive's completion, a representative profile of the dive was plotted over the bubble count. This data collection system yielded a real time count of the bubbles as the dive progressed and a retrieval store of data on magnetic tape for subsequent analysis.

Bubble profile graph: Figure 5

The abcissa, or x-axis, of the graph represents the dive time in minutes from the beginning of the dive to some point in time after

reaching the surface. The ordinate, or y-axis, represents the bubble count on a logarithmic scale of 1 to 1,000. The solid line of the figure represents the dive profile. It begins at the upper left hand corner with zero depth and zero time. It then descends to the x-axis representing pressurization to 220 fsw where it remains for 20 minutes dive time. It then ascends depicting the decompression profile. Rates of ascent (ROA) and depths of stop are all indicated on the graph. The stars and circles on the graph in the results sections represent the emboli count for a specific animal represented by either the star or the circle. Other information on the graph includes the initial rate of ascent from 220 feet to the first stop and the total time of dive (TTD).

The dive series began with a 9-dive baseline study using the USN 220 feet/20 minute Exceptional Exposure standard air profile. This particular profile was chosen because it was known to produce bubbles and bends in certain human subjects. Following that baseline study, no further profile was examined as a baseline because the USN 220 ft/20 min. profile did produce great numbers of Doppler events, or emboli, in the subject goats.

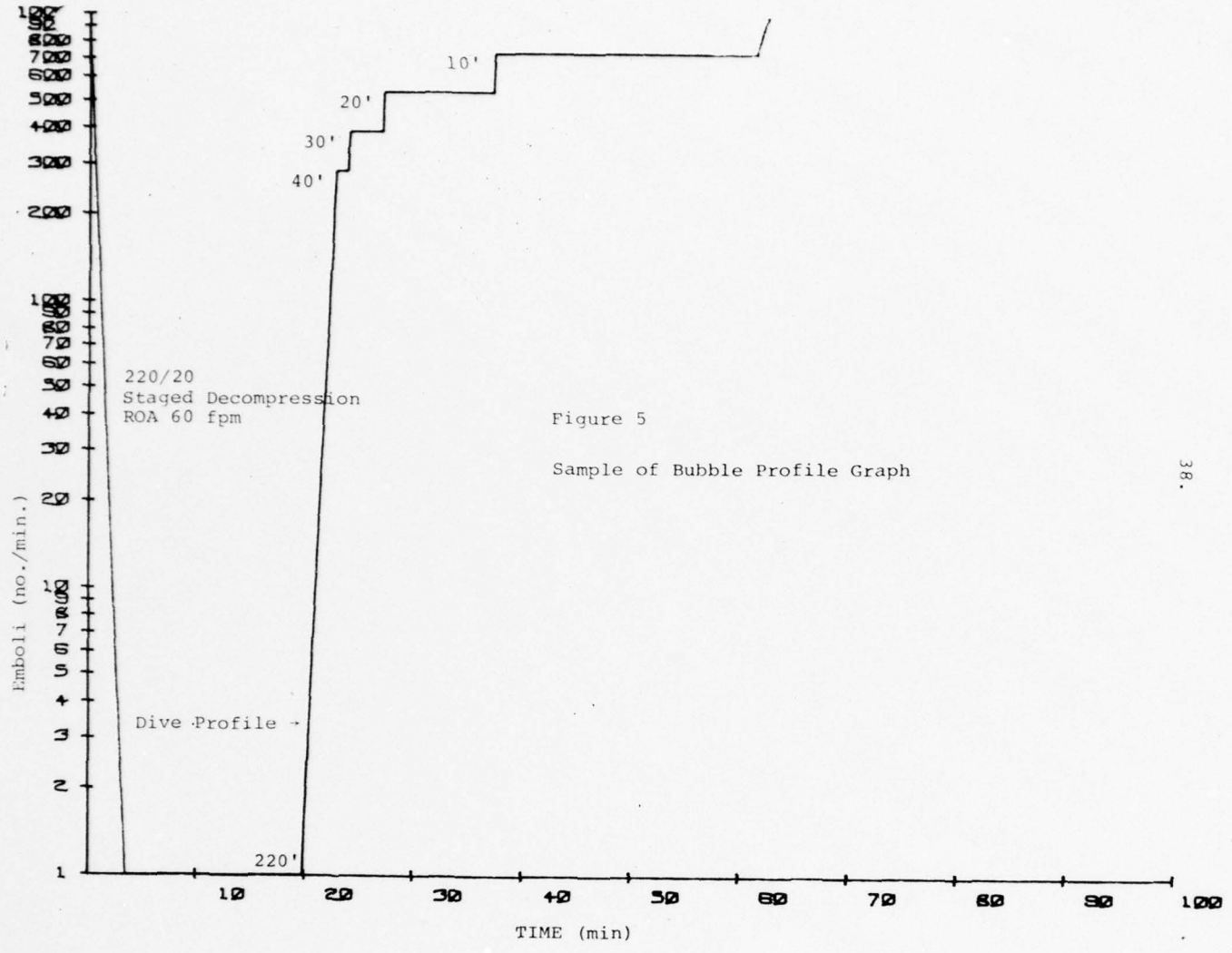

Figure 5

Sample of Bubble Profile Graph

4. Results

The initial baseline exposures using the USN standard air Exceptional Exposure profile revealed large numbers of gaseous emboli in all the experimental subjects, which are depicted in graphs 001, 002, 005, and 008.

Profile 90-008 was the first positive bends inducing dive of the experimental series. It appeared that both pain and central nervous system signs were exhibited by the animals. During this exposure and subsequent exposures, in which bends were induced, certain signs were most frequently exhibited:

tachycardia
agitation (anxiety, fright)
loss of balance
loss of bladder/bowel control
dyspnea
cyanosis

Less severe symptoms were stomping of affected limb, favoring of limb in weight support or limping while walking.

Sound characteristics of the Doppler signal changed significantly immediately prior to animals exhibiting severe bends symptoms. The distinctive individual bubble signals would be replaced by a continuing frothing type signal. This was followed by a complete eclipse of the Doppler signal. (It is possible that sufficient air was being returned

to the vena cava that little or no blood flow was occurring, perhaps being blocked by a large gas pocket). Very shortly following this type of signal, the animal collapsed and experienced severe dyspnea. Immediate recompression to 60 feet was initiated, during which time the blood flow signal returned and the bubble count dropped off rapidly following the re-institution of the bubble signal. This result was experienced in profiles 008,009, 0011, and 0012. The animals quickly recovered after only a short period at the 60 foot treatment depth.

The stay at 60 feet was determined by the length of time it took for the disappearance of detectable gas emboli, which ranged from 20 to 60 minutes. Decompression was then commenced at 2 feet per minute to the surface or depth that bubbles again were detected. A reoccurance of bubbles halted the ascent until such time as it was determined safe to proceed with the decompression.

It is interesting to note the significant sharp decline in the bubble count following the recompression in profile 008.

Effect of change of rate of ascent;

The United States Navy rate of ascent for air tables is 60 ft/min. To see what effect the change of rate of ascent would have, the initial rate was

changed to 30 fpm. Profile 009 demonstrates the ascent from the bottom at 30 fpm, which intersects with the second minute of the 30 foot stop of the baseline profile, and was continued using the depth of stop and stop times used in the baseline. The total time of dive was 62 min, 40 sec, which is identical with the USN Exceptional Exposure table. As can be seen from the bubble data, emboli were observed, however, their occurance was later in the profile and substantially fewer in number in one animal.

In profiles 009 to 0013, the 30 ft per minute initial ascent rate did reduce the time of onset, or first occurance of emboli detection, so it was decided to use 30 ft/min as an initial ascent rate, and with that ascent rate, to establish a first stop depth, following which, emboli would not be detected.

Dives 014 - 021 all used the 30 ft/min rate of ascent to differing initial stop depths in order to find the minimum depth that could be decompressed to without initiating bubble formation. It was discovered that 40 ft. of seawater could be ascended to at 30 ft/min from 220 ft without initiating bubble formation. Following this revelation, further dives were done employing the 30 ft/min ascent to the 40 foot level with subsequent decompression as

is shown in Figures 022 - 035. We discovered that while the decompression to 40 ft at 30 ft/min did not produce detectable emboli, we were nevertheless unable to ascend beyond that point at what would seem to be a reasonable decompression rate without inducing bubble formation. While the attempts at a zero-UDE decompression from 40 feet to the surface were unsuccessful these profiles nevertheless illustrate the effects of type of decompression relative to where emboli occur.

Since the 40 foot stop seems to be too shallow from which to jump off into additional decompression, even though it appeared to be emboli free as the initial stop point, the subsequent dives employed a deeper first stop depth. This reduced the amount of decompression stress, i.e., the effect of decompression per se, on bubble formation, and in addition, allowed dissolved gases more time to be given off before reaching the critical emboli formation point. Profiles 037 and 038 depict an initial stop depth of 60 feet with a subsequent 1.343 ft/min rate of ascent which appeared to be virtually emboli free. Elongation of the ascent time from 60 feet to the surface by reducing the rate of ascent time to

1.09 ft/min still appeared to allow the presence of detectable emboli (profiles 039 and 040).

The Royal Navy Decompression Schedule for the 220 foot-20 min exposure were also run. The total dive time was 127 min., which proved to be sufficient time for degassing and few emboli were produced. The last dives of the series were two dives using a linear decompression with a total dive time of 127 min. and a first stop at 60 fsw. Few emboli were detected.

VII. Discussion

Failure of currently employed decompression schedules to prevent decompression sickness has been proposed by Kidd and Elliott to be a result of 1) an error in decompression theory, 2) an error in decompression practice, and 3) an anomalous response of the individual.

Whatever the explanation for an inadequate decompression, minute bubbles of inert gas are thought to form, coalesce and grow, exert pressure on nerve elements, interact with the hemostatic mechanism, damage vascular endothelia, and/or occlude some part of the circulation. The presenting symptoms may be sudden and dramatic, involving vital centers, or delayed, localized and merely uncomfortable. Secondary effects of tissue damage and edema may be superimposed on this picture. Few decompression profiles now in use can be considered absolutely safe in spite of many years of

attempts to solve the complexing decompression problem. In other studies in this laboratory, we have determined what we think is part of the pathogenesis of certain types of decompression sickness, but until the exact cause and pathologic course of decompression sickness are well defined, the problem will continue to be as elusive as it has been for the past many years.

The recent evidence indicating that gas emboli are present in divers using "acceptable" decompression schedules alerts us that such separated gas may have a variety of hematologic, vascular, and tissue effects, any of which may not be sufficient to produce symptoms. It is therefore in the diver's best interest to prevent as much bubble formation as possible.

Doppler ultrasound is the most widely used non-invasive method to detect gaseous emboli, and appears to be a satisfactory means of heralding the onset of decompression sickness.

In these series of experiments to determine the effect of repetitive exposures, initial ascent rates and first stop depth of undetected bubble formation, the ultrasonic doppler emboli detector was satisfactorily used to provide the end point necessary for evaluating these dive profiles.

The first eight dives, which were used to establish a baseline, revealed several important phenomena which were

seen continually throughout the series. 1) Each animal demonstrated an individual disposition to gas emboli production. During the six month period of the goat study, one animal routinely appeared to be more susceptible to bubble formation than other animals on the same profile. 2) Decompression on the same decompression profile did sometimes produce different bubble profiles from dive to dive in the same animal. This simply demonstrated the large potential for variation in response both in the individual as well as between individuals. This quality is well-known in the population of human divers.

Two significant characteristics of presently used decompression profiles have been established which appear to predispose bubble formation. Fast initial ascent rates (i.e., 60 fpm) and Haldanian type, or large, first decompression steps predisposed bubble formation as detected with an ultrasonic Doppler emboli detector.

VI. Dive Profiles

OUTLINE OF DIVE, AND GRAPHS

DIVE NR.	DATE	
90-001	@ 20 Jan 75	Standard US Navy
90-002	21 Jan 75	"
90-003	23 Jan 75	
90-004	24 Jan 75	
90-005	27 Jan 75	
90-006	28 Jan 75	
90-007	29 Jan 75	
90-008	30 Jan 75	
90-009	03 Feb 75	
ROA changed to 30 fpm		Staged decompression
TTD; same as USN 60 minutes 40 seconds		
90-010	04 Feb 75	Linear ascent
TTD: 65:00		
90-011	06 Feb 75	Linear ascent
90-012	10 Feb 75	Staged decompression
TTD: 65:20		
90-013	12 Feb 75	Linear ascent
TTD: 65:00		
90-014	05 Mar 75	Staged decompression
TTD:100:00 pluse		
90-015	07 Mar 75	Staged decompression
TTD: L 100:00 pluse		
90-016	11 Mar 75	Staged decompression

90-016	11 Mar 75	Staged decompression
TTD:100:00 pluse		
90-017	12 Mar 75	Staged decompression
TTD:100:00 pluse		
90-018	17 Mar 75	Staged decompression
TTD:100:00 pluse		
90-019	19 Mar 75	Staged decompression
TTD:100:00 pluse		
90-020	21 Mar 75	Staged decompression
TTD:100:00 pluse		
90-021	07 Apr 75	Staged decompression
TTD:100:00 pluse		
90-022	09 Apr 75	Staged decompression
TTD: 95:25		
90-024	16 Apr 75	Staged decompression
TTD: 62:40		
90-025	05 May 75	Staged decompression
TTD: 62:40		
90-026	07 May 75	Staged decompression
TTD:62:40		
90-027	09 May 75	Staged decompression
TTD: 62:40		
90-028	14 May 75	Staged decompression
TTD: 73:20		
90-029	16 May 75	Staged decompression
TTD: 82:00		

90-030	19 May 75	Linear Ascent
TTD: 62:40		
90-033	17 June 75	Staged decompression
TTD: 86:00		
90-034	18 June 75	Staged decompression
TTD: 81:00		
90-035	19 June 75	Staged decompression
TTD: 93:00		
90-036	20 June 75	Linear ascent
TTD: 65:20		
90-037	21 June 75	Linear ascent
TTD: 70:00		
90-038	22 June 75	Linear ascent
TTD: 70:00		
90-039	23 June 75	Linear ascent
TTD: 80:00		
90-040	24 June 75	Linear ascent
TTD: 80:20		
90-041	27 June 75	Linear ascent
TTD: 71:40		
90-042	27 June 75	Linear ascent
TTD: 71:40		
90-043	30 June 75	Linear ascent
TTD: 80:00		
90-044	30 June 75	Linear ascent
TTD: 80:00		

90-045	02 July 75	Linear ascent
TTD: 127:00		
90-046	02 July 75	Linear ascent
TTD: 127:00		

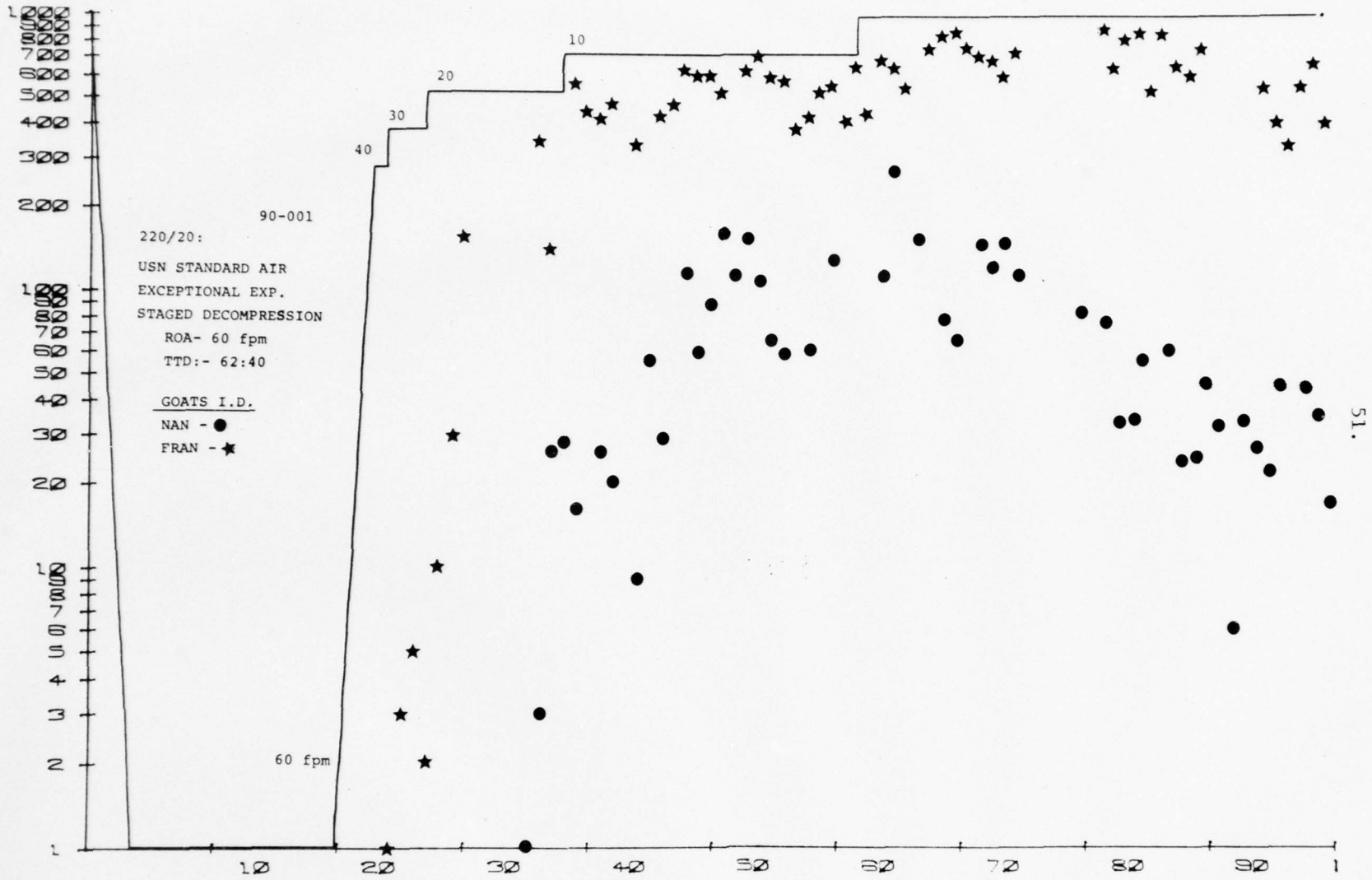
90-001
220/20:
USN STANDARD AIR
EXCEPTIONAL EXP.
STAGED DECOMPRESSION
ROA- 60 fpm
TTD:- 62:40
GOATS I.D.
NAN -
FRAN -
60 fpm
10
20
30
40
10
20
30
40
50
60
70
80
90

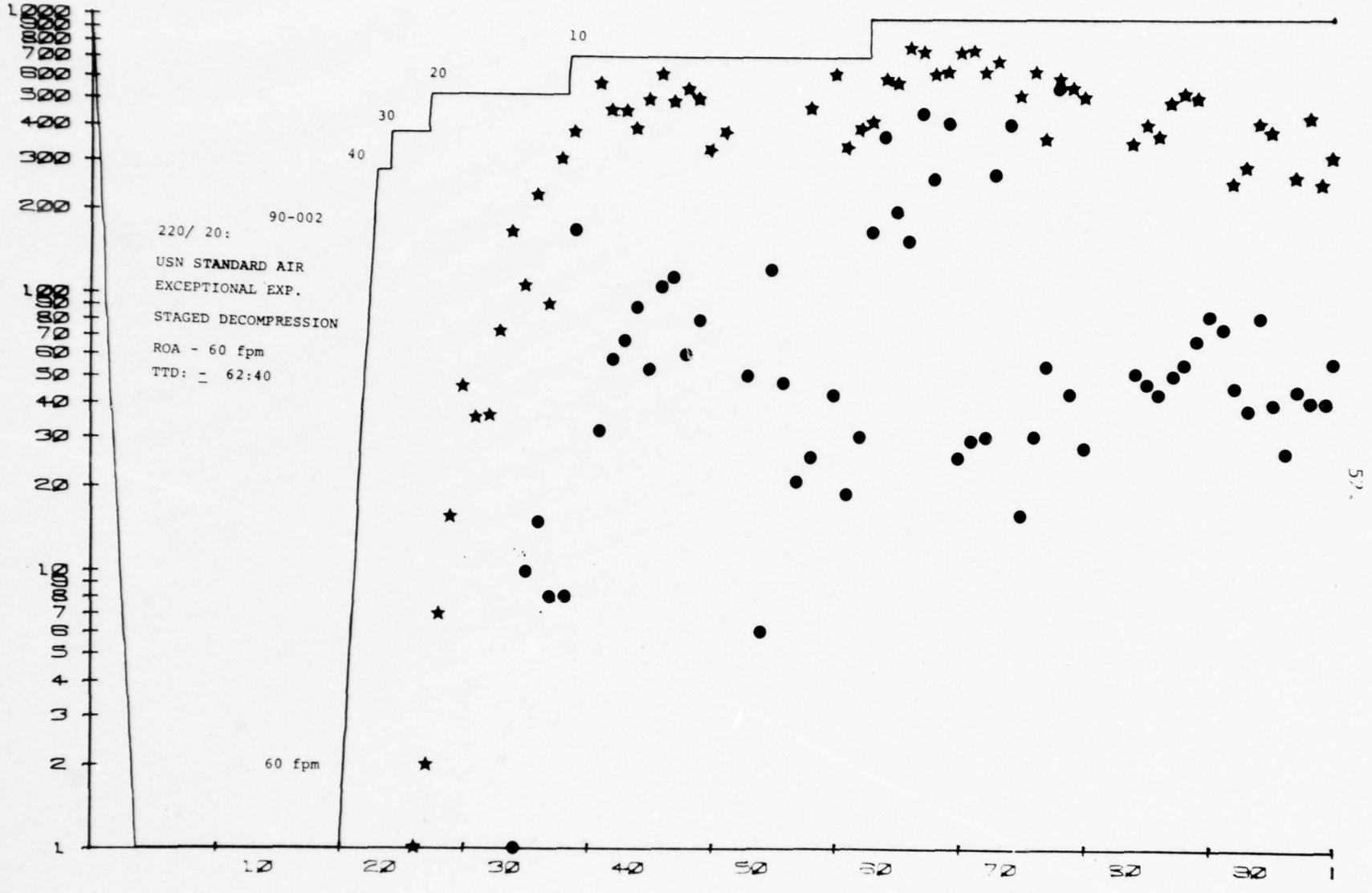
90-002
220/ 20:
USN STANDARD AIR
EXCEPTIONAL EXP.
STAGED DECOMPRESSION
ROA - 60 fpm
TTD: ~ 62:40
60 fpm
10
20
30
40
1000
900
800
700
600
500
400
300
200
100
90
80
70
60
50
40
30
20
10
9
8
7
6
5
4
3
2
1
10
20
30
40
50
60
70
80
90
1

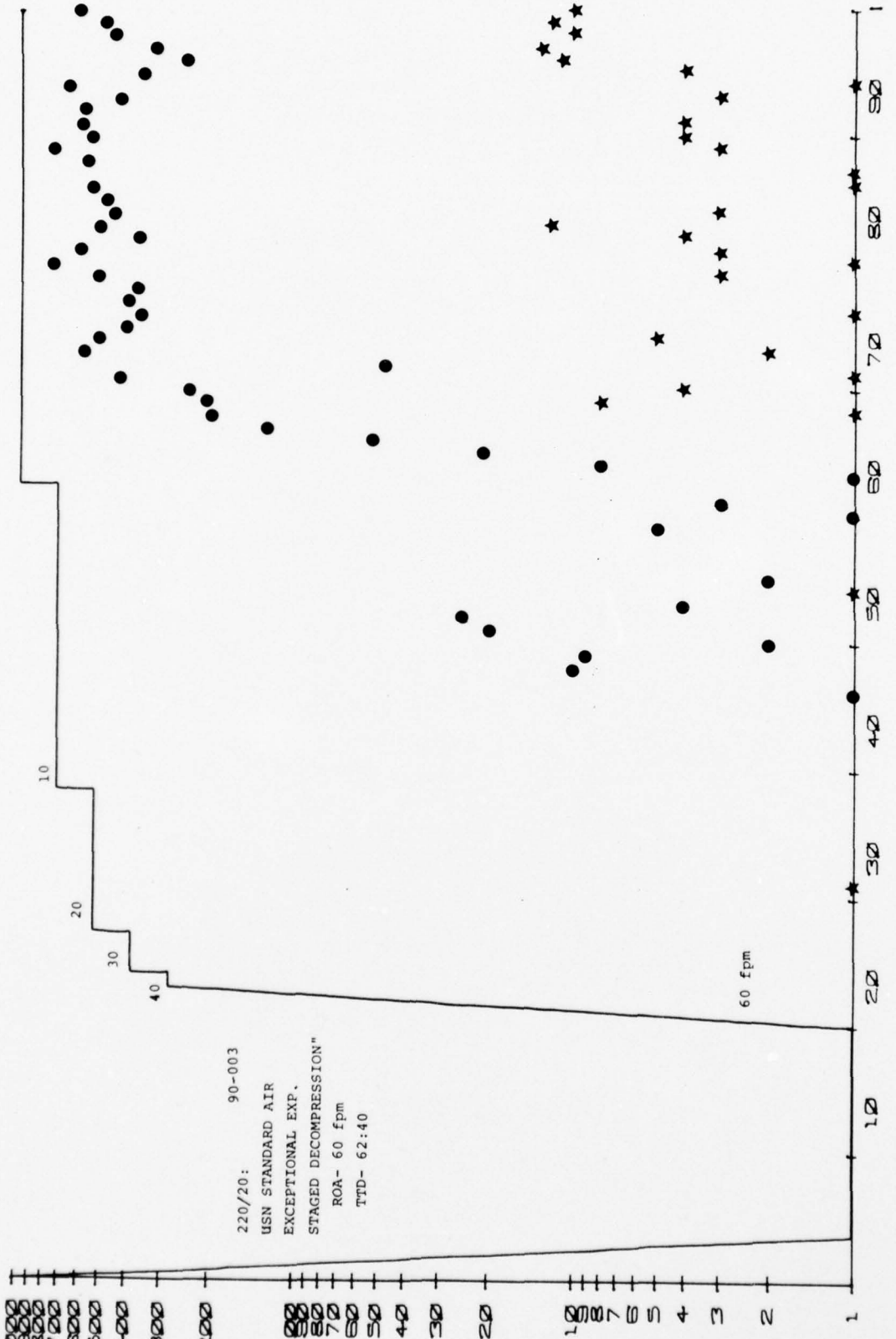
220/20: 90-003
USN STANDARD AIR
EXCEPTIONAL EXP.
STAGED DECOMPRESSION"
ROA- 60 fpm
TTD- 62:40
60 fpm
10
20
30
40
1000
900
800
700
600
500
400
300
200
100
90
80
70
60
50
40
30
20
10
7
6
5
4
3
2
1
10
20
30
40
50
60
70
80
90
1

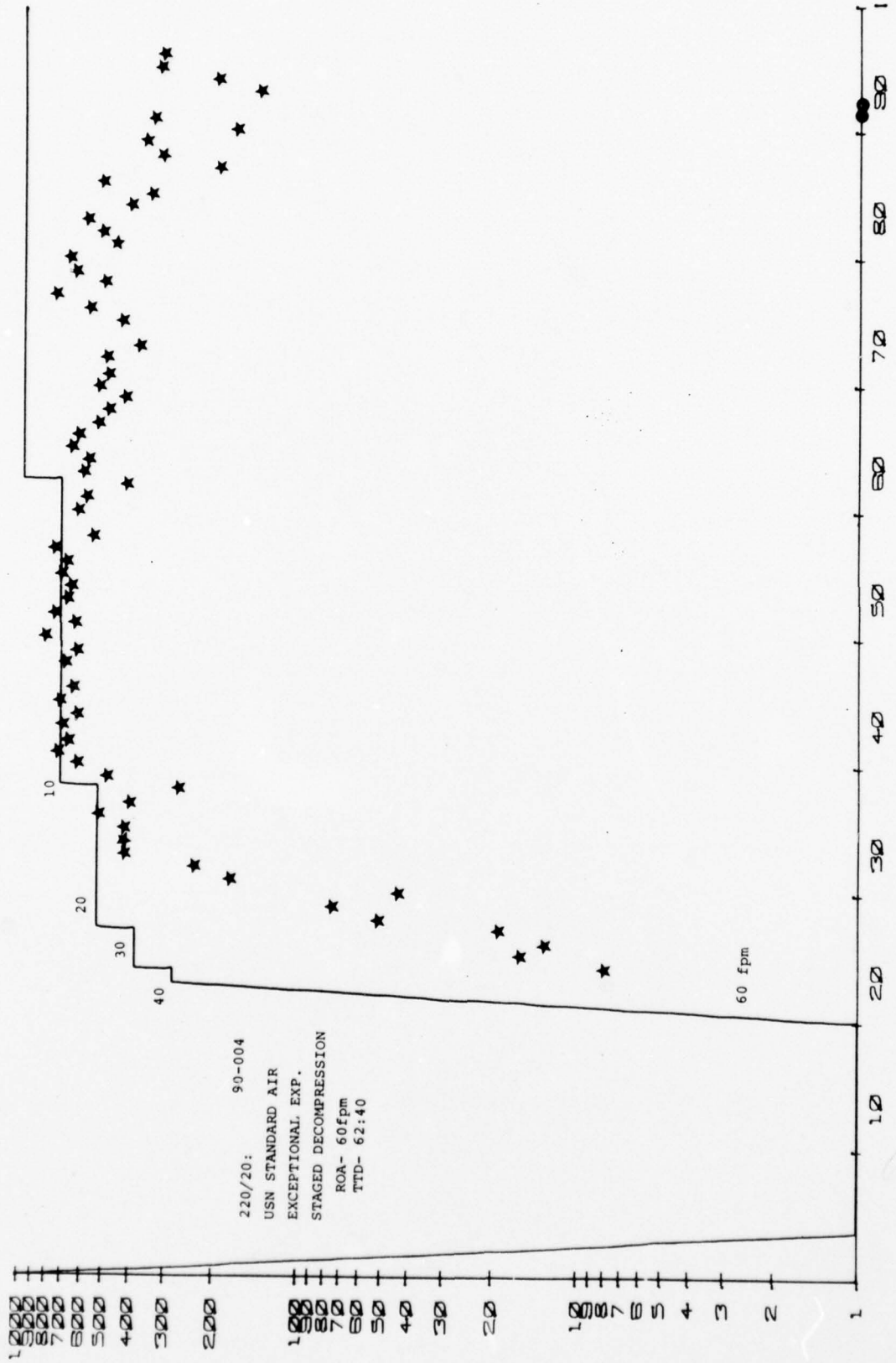
220/20: 90-004
USN STANDARD AIR
EXCEPTIONAL EXP.
STAGED DECOMPRESSION
ROA- 60fpm
TTD- 62:40
60 fpm
10
20
30
40
10
20
30
40
50
60
70
80
90
100
200
300
400
500
600
700
800
900
1000
2
3
4
5
6
7
8
9
10
20
30
40
50
60
70
80
90
1

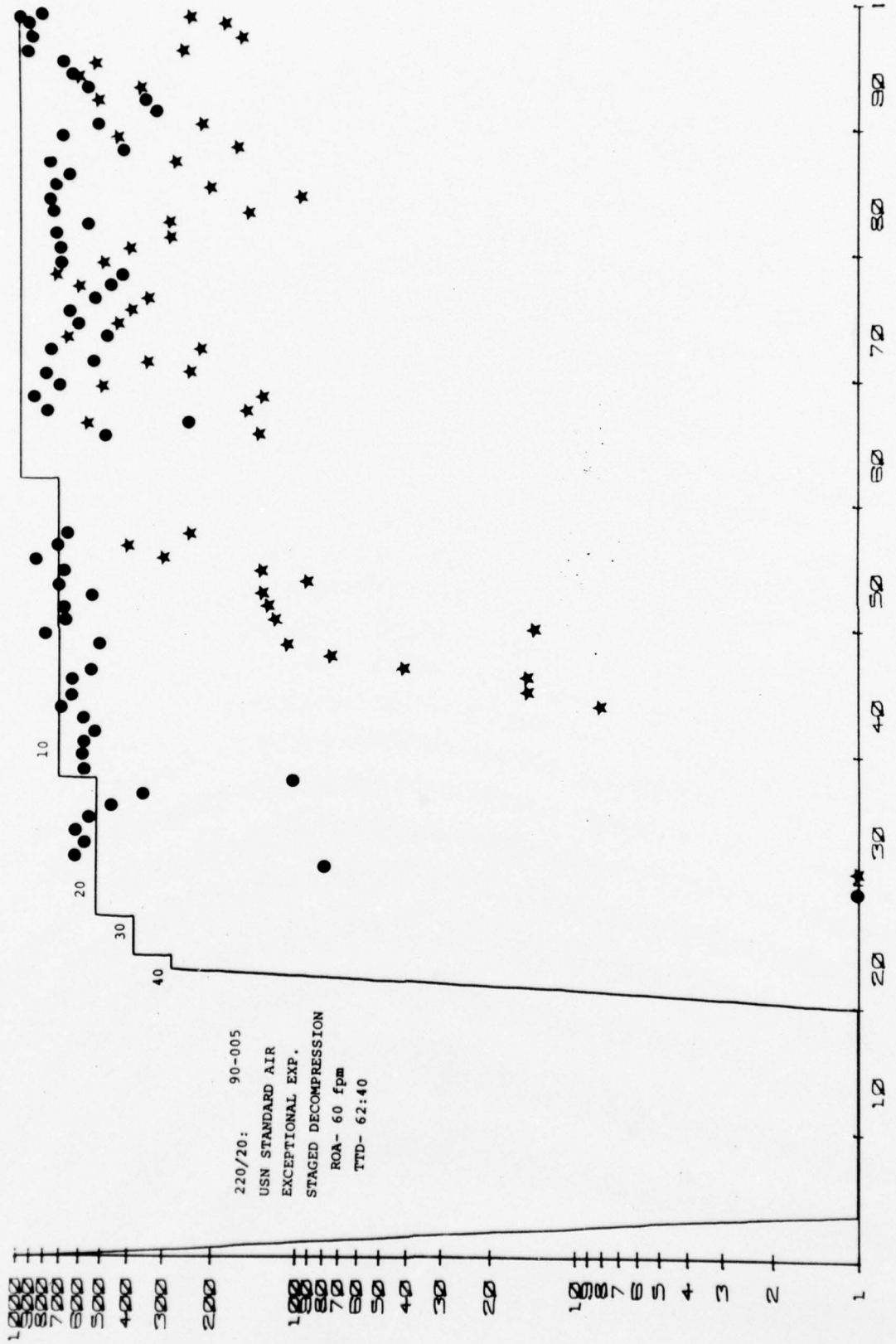
220/20: 90-005
USN STANDARD AIR
EXCEPTIONAL EXP.
STAGED DECOMPRESSION
ROA- 60 fpm
TTD- 62:40
10
20
30
40

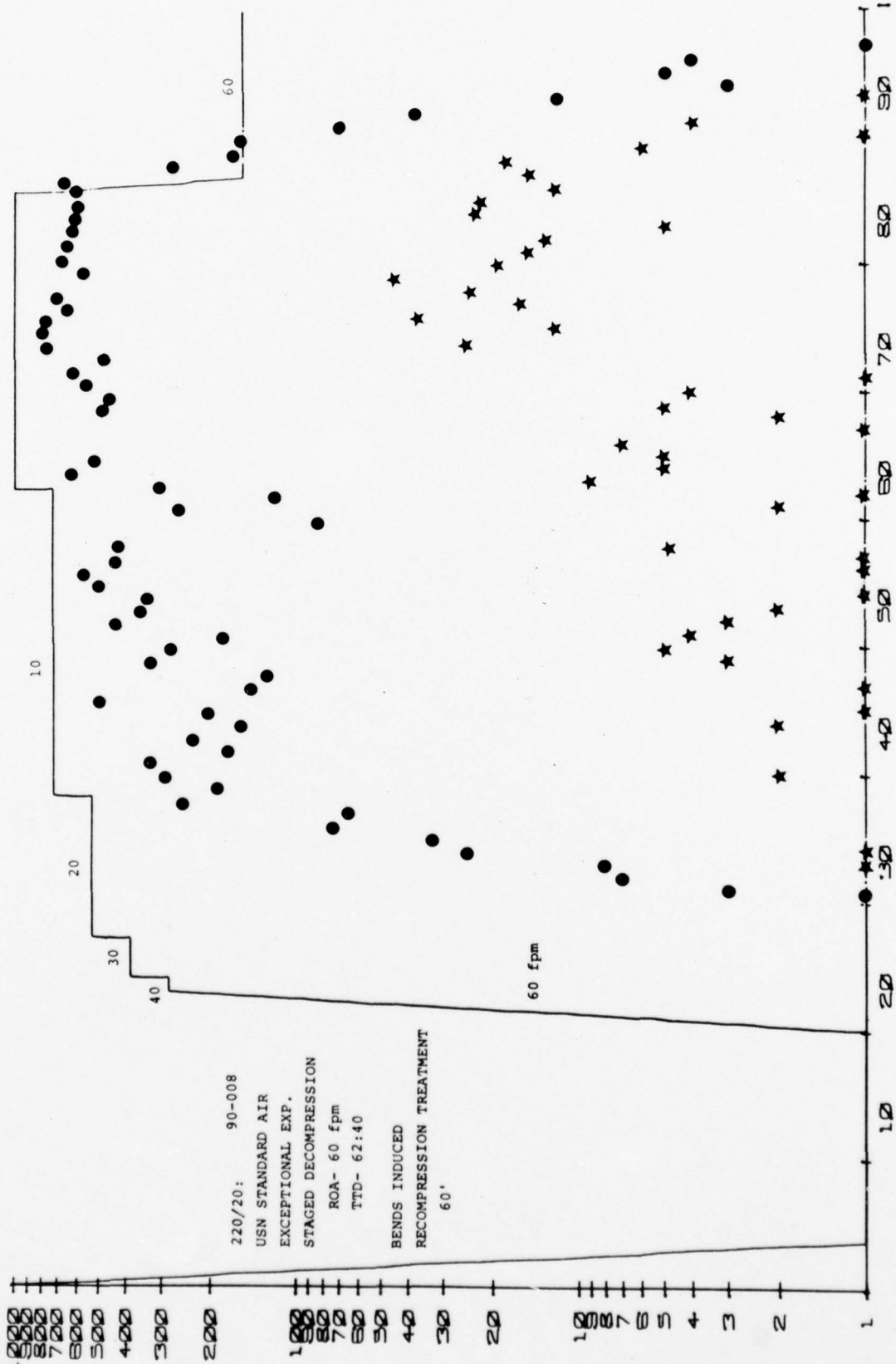
220/20: 90-008
USN STANDARD AIR
EXCEPTIONAL EXP.
STAGED DECOMPRESSION
ROA- 60 fpm
TTD- 62:40
BENDS INDUCED
RECOMPRESSION TREATMENT
60'
60 fpm
10
20
30
40
60

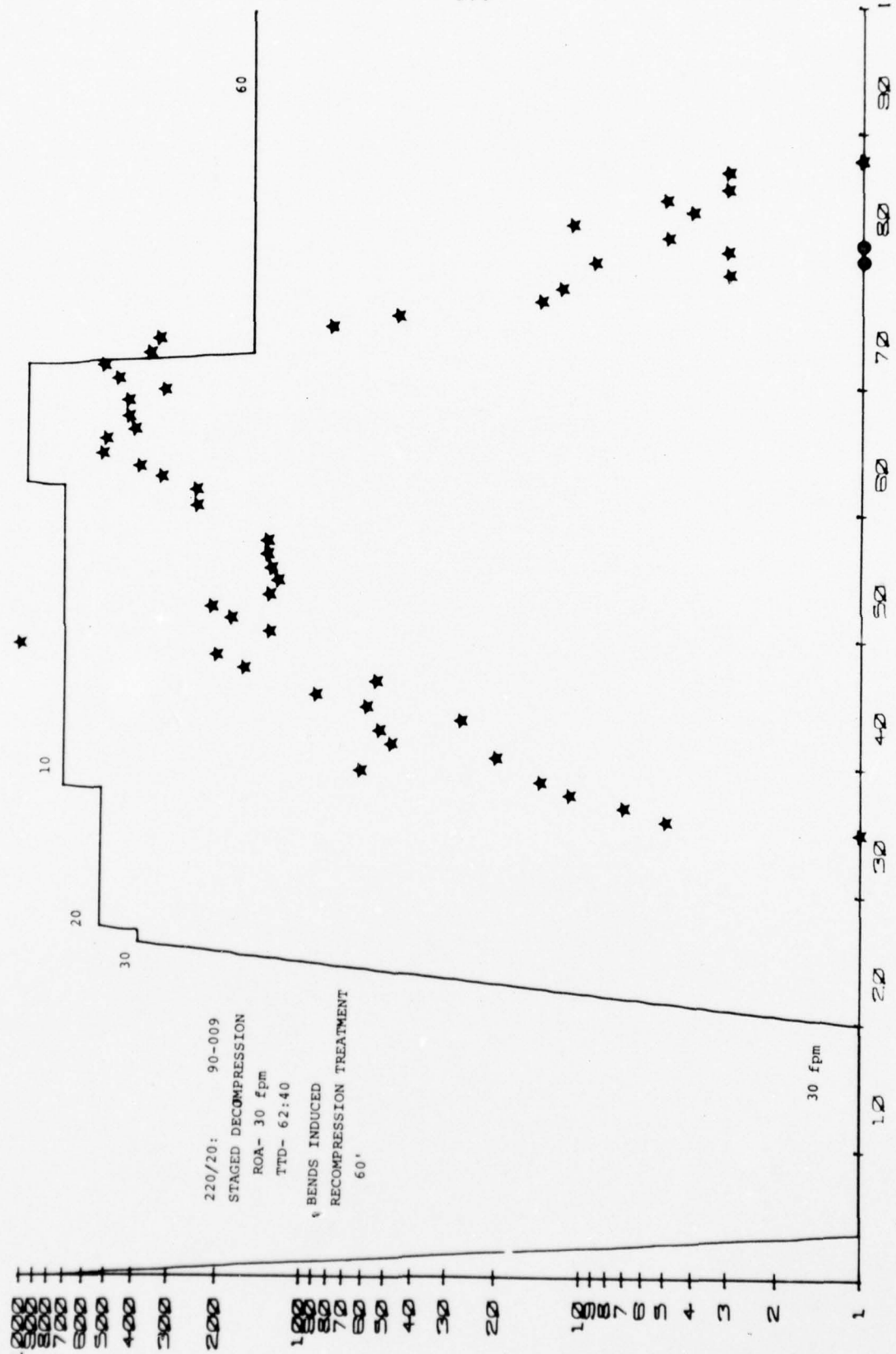
220/20: 90-009
STAGED DECOMPRESSION
ROA- 30 fpm
TTD- 62:40
BENDS INDUCED
RECOMPRESSION TREATMENT
60'
30 fpm

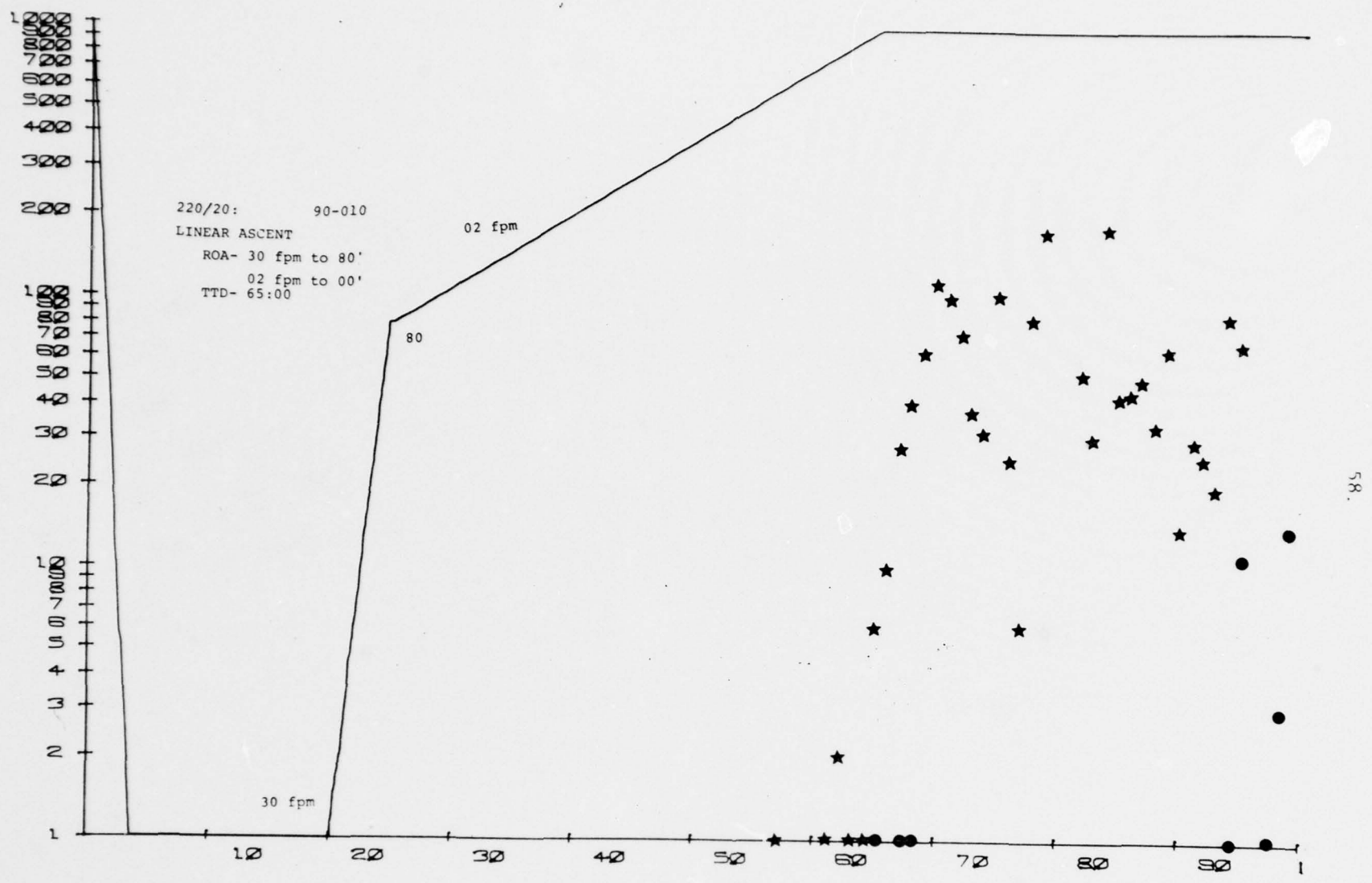
220/20: 90-010
LINEAR ASCENT
ROA- 30 fpm to 80'
02 fpm to 00'
TTD- 65:00
02 fpm
80
30 fpm

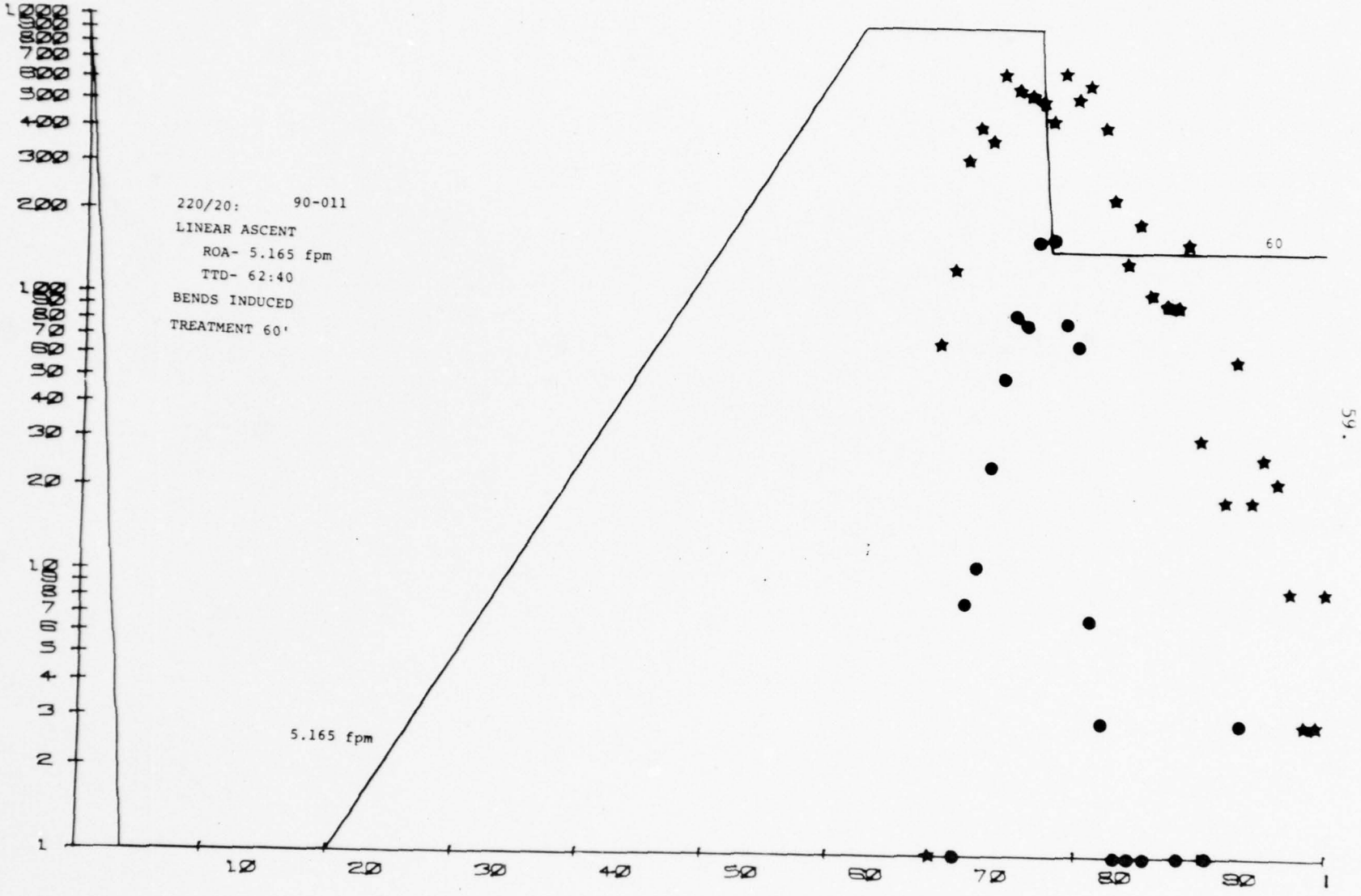
220/20: 90-011
LINEAR ASCENT
ROA- 5.165 fpm
TTD- 62:40
BENDS INDUCED
TREATMENT 60'
5.165 fpm
60
59.

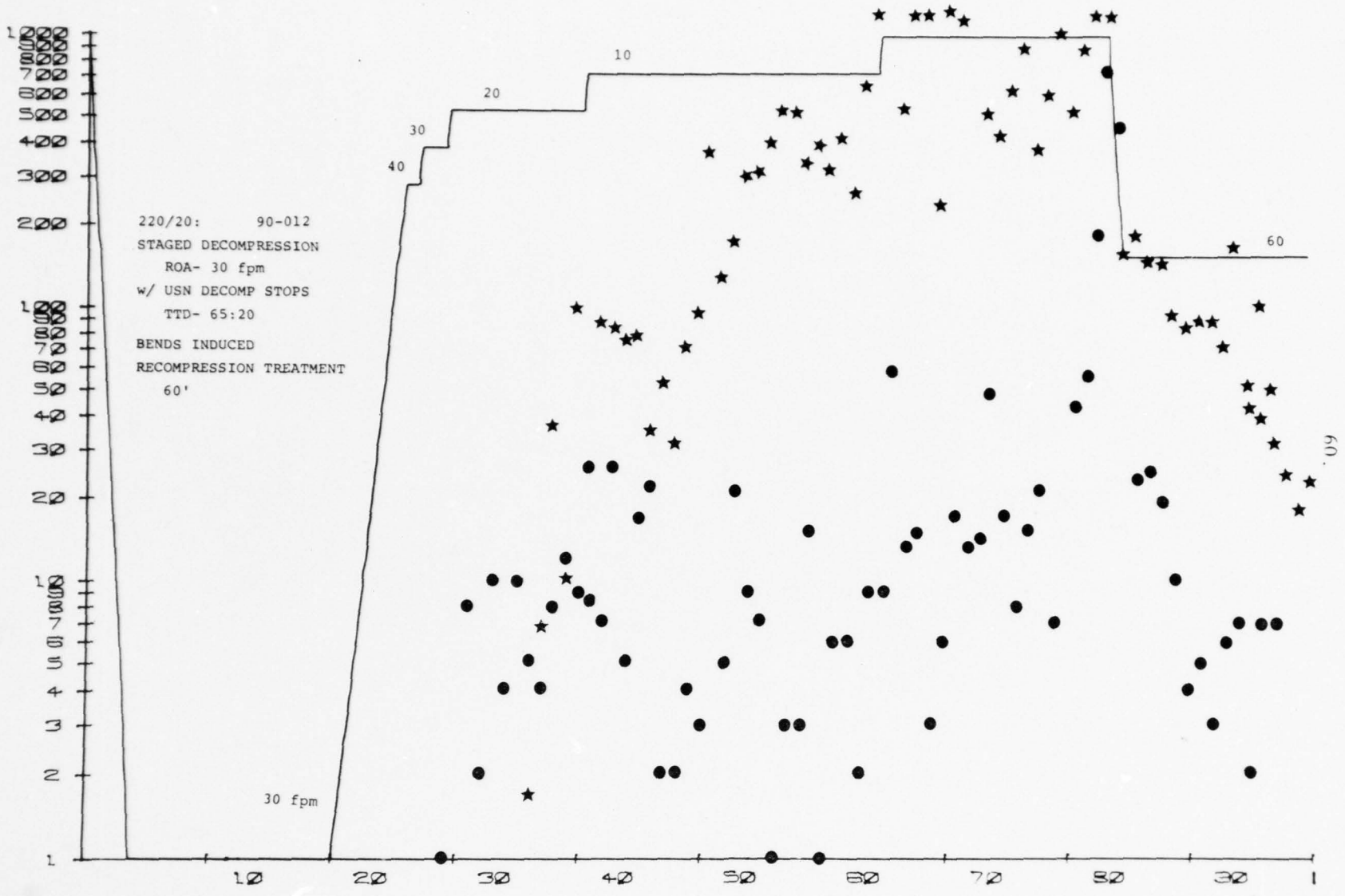
220/20: 90-012
STAGED DECOMPRESSION
ROA- 30 fpm
w/ USN DECOMP STOPS
TTD- 65:20
BENDS INDUCED
RECOMPRESSION TREATMENT
60'
30 fpm
10
20
30
40
60
1000
500
800
700
600
500
400
300
200
100
50
80
70
60
50
40
30
20
10
9
8
7
6
5
4
3
2
1
10
20
30
40
50
60
70
80
90
1
09

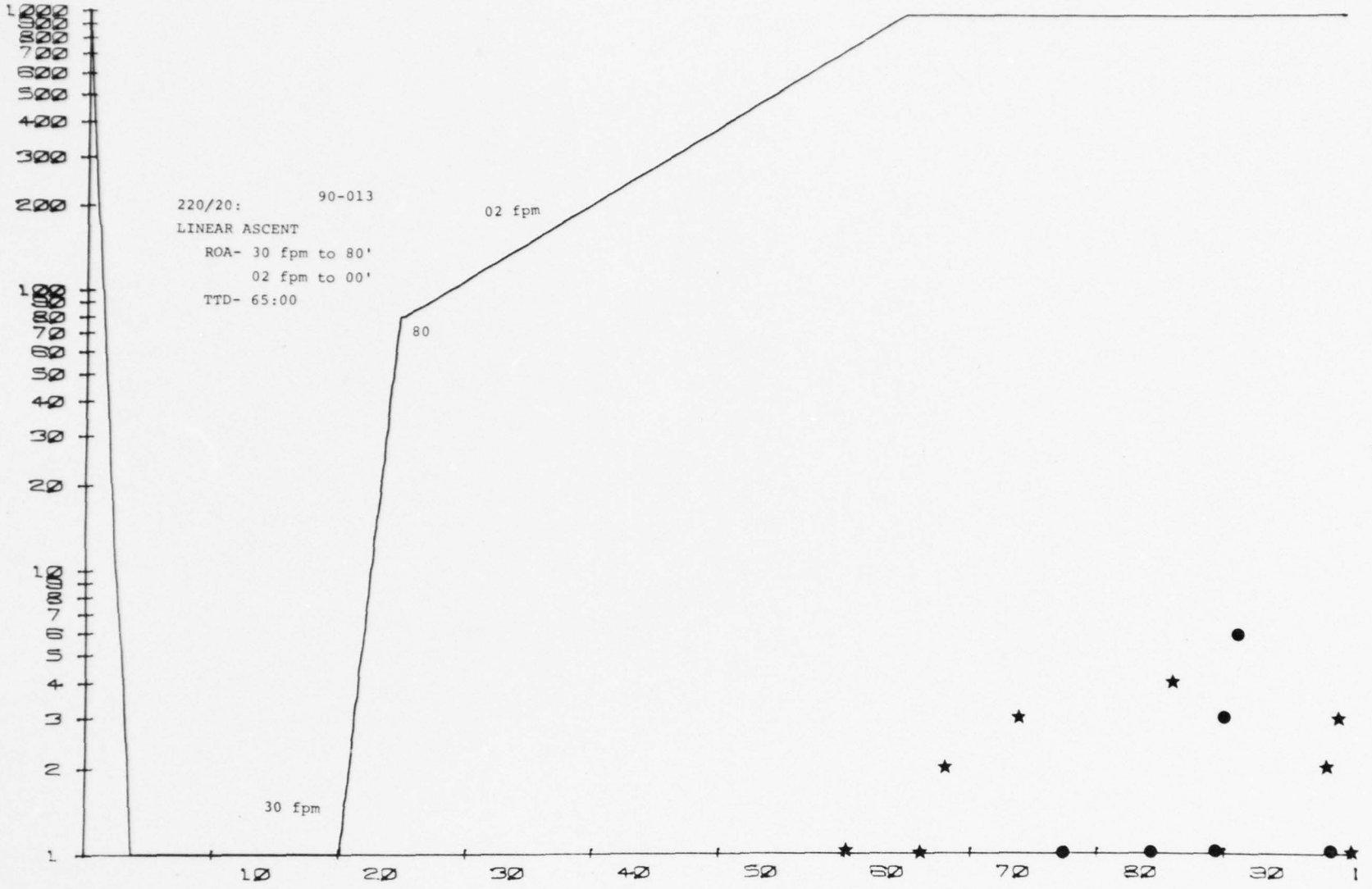
220/20:
90-013
LINEAR ASCENT
ROA- 30 fpm to 80'
02 fpm to 00'
TTD- 65:00
02 fpm
80
30 fpm
1
2
3
4
5
6
7
8
9
10
20
30
40
50
60
70
80
90
100
200
300
400
500
600
700
800
900
1000
10
20
30
40
50
60
70
80
90
1

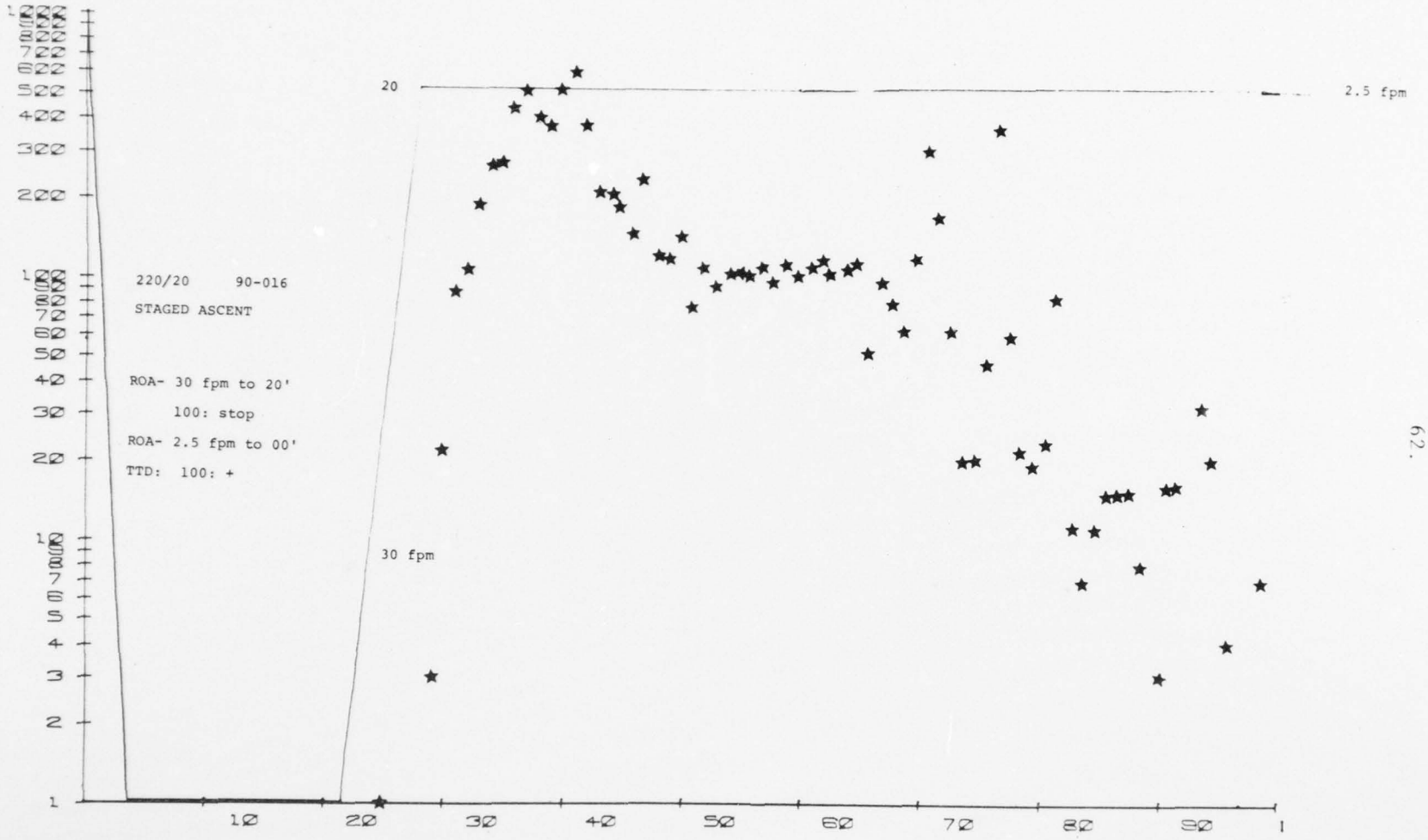
220/20 90-016
STAGED ASCENT
ROA- 30 fpm to 20'
100: stop
ROA- 2.5 fpm to 00'
TTD: 100: +
20
2.5 fpm
30 fpm
1Ø
2Ø
3Ø
4Ø
5Ø
6Ø
7Ø
8Ø
9Ø

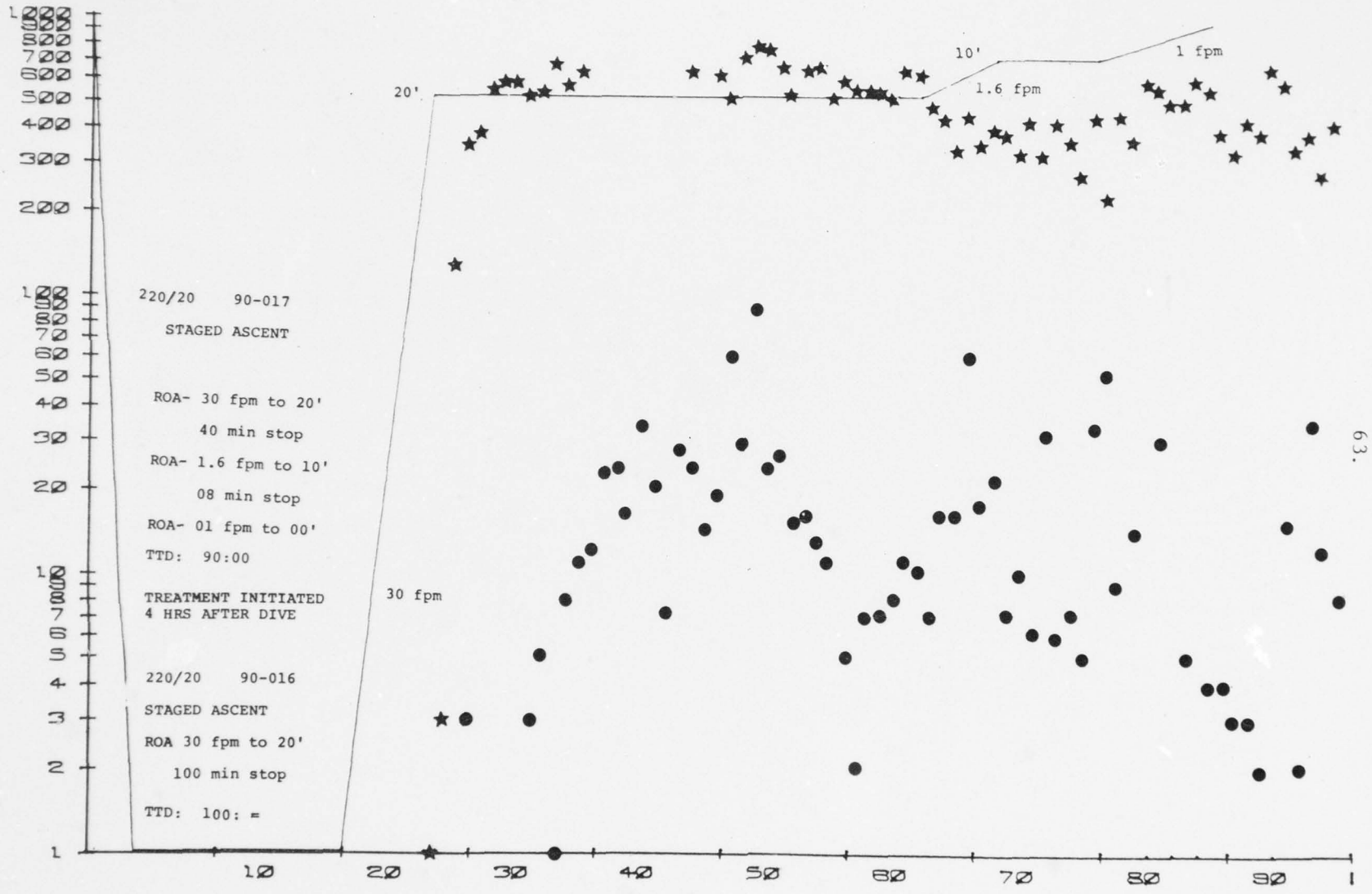
220/20 90-017
STAGED ASCENT
ROA- 30 fpm to 20'
40 min stop
ROA- 1.6 fpm to 10'
08 min stop
ROA- 01 fpm to 00'
TTD: 90:00
TREATMENT INITIATED
4 HRS AFTER DIVE
220/20 90-016
STAGED ASCENT
ROA 30 fpm to 20'
100 min stop
TTD: 100: =
20'
10'
1 fpm
1.6 fpm
30 fpm

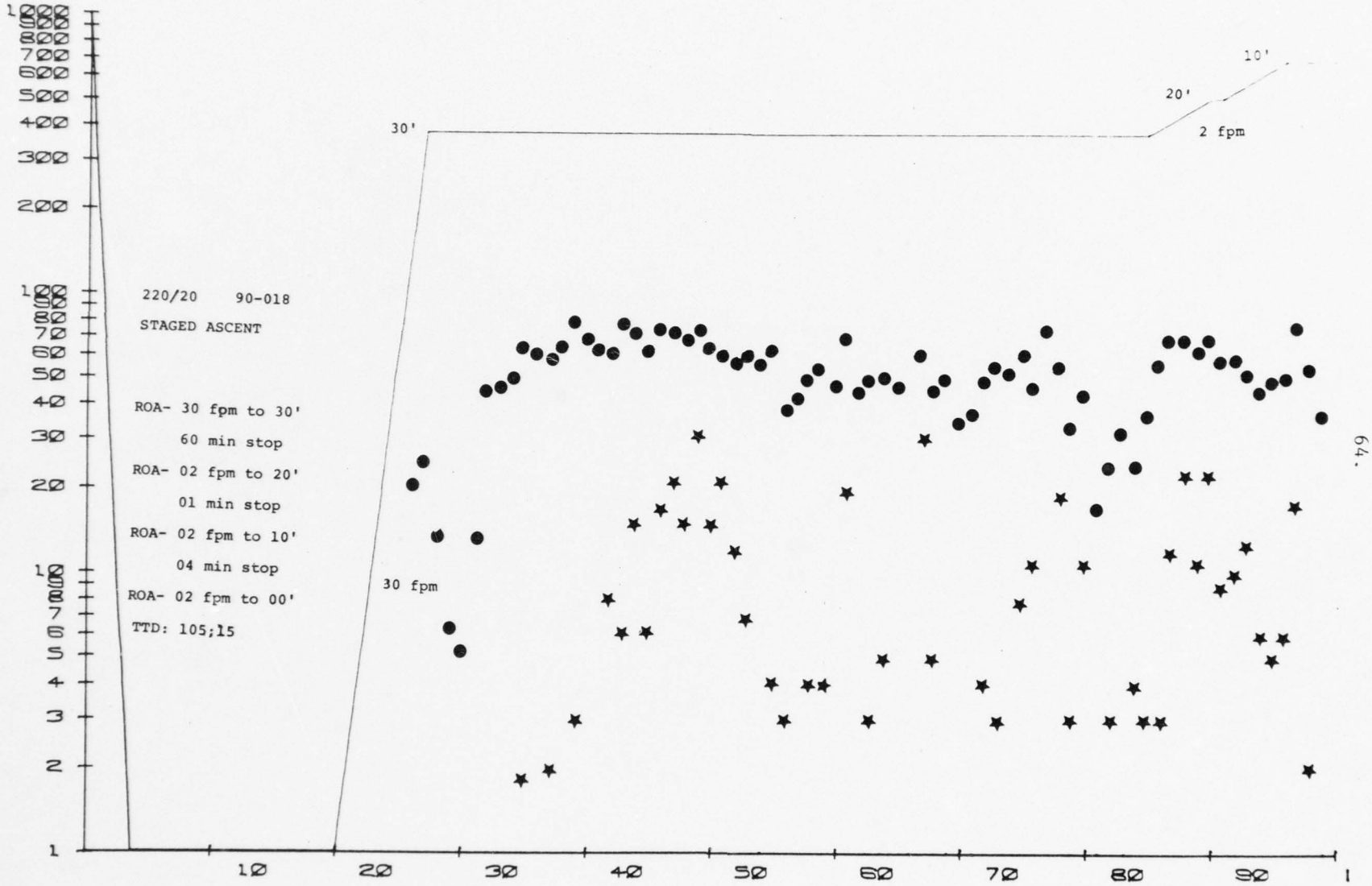
220/20 90-018
STAGED ASCENT
ROA- 30 fpm to 30'
60 min stop
ROA- 02 fpm to 20'
01 min stop
ROA- 02 fpm to 10'
04 min stop
ROA- 02 fpm to 00'
TTD: 105;15
30'
20'
10'
2 fpm
30 fpm
64.

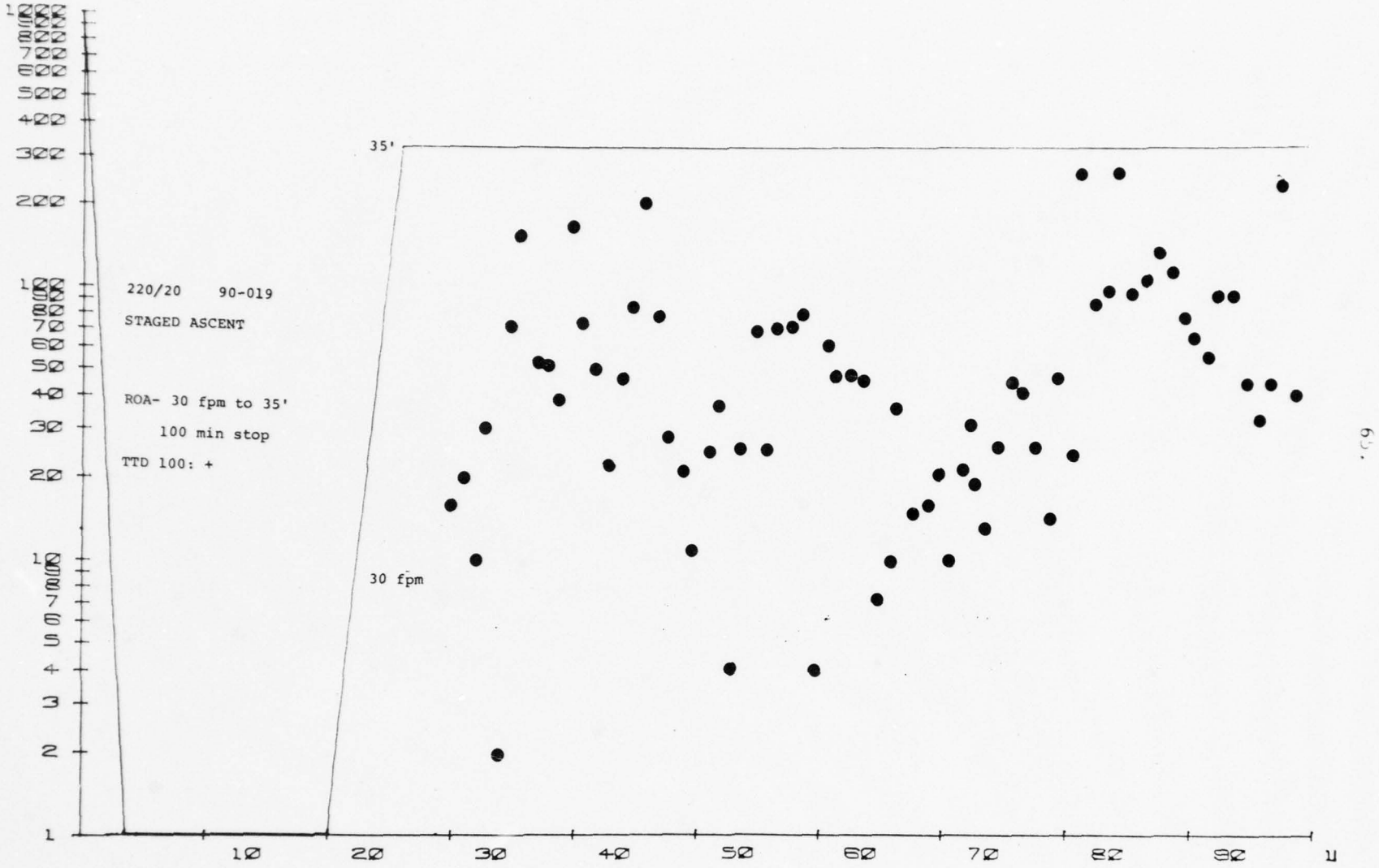
220/20 90-019
STAGED ASCENT
ROA- 30 fpm to 35'
100 min stop
TTD 100: +
35'
30 fpm
1
2
3
4
5
6
7
8
9
10
20
30
40
50
60
70
80
90
100
200
300
400
500
600
700
800
900
1000

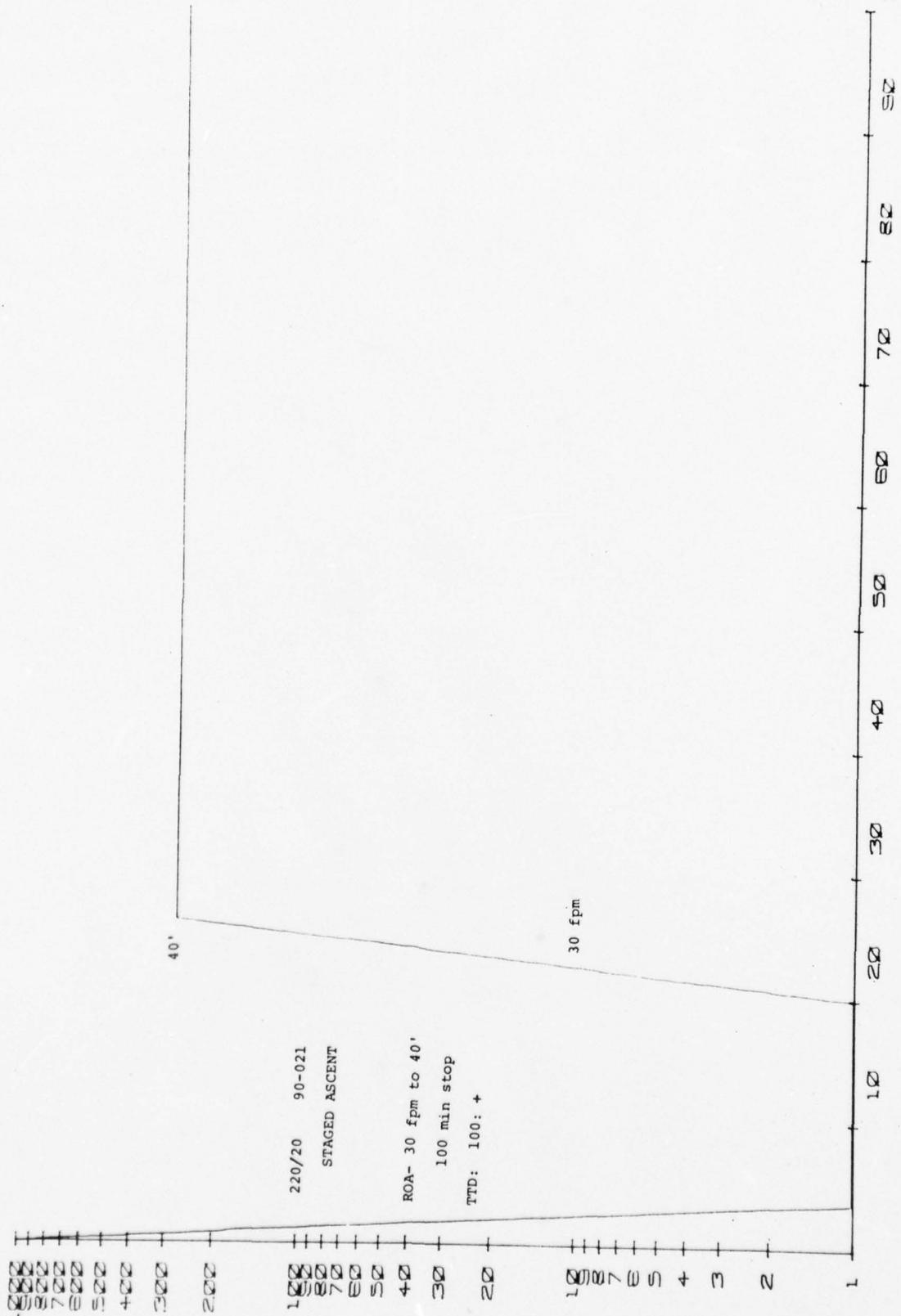
40'
30 fpm
220/20 90-021
STAGED ASCENT
ROA- 30 fpm to 40'
100 min stop
TTD: 100: +
10
20
30
40
50
60
70
80
90
100
1
2
3
4
5
6
7
8
9
10
20
30
40
50
60
70
80
90
100
110
120
130
140
150
160
170
180
190
200
210
220

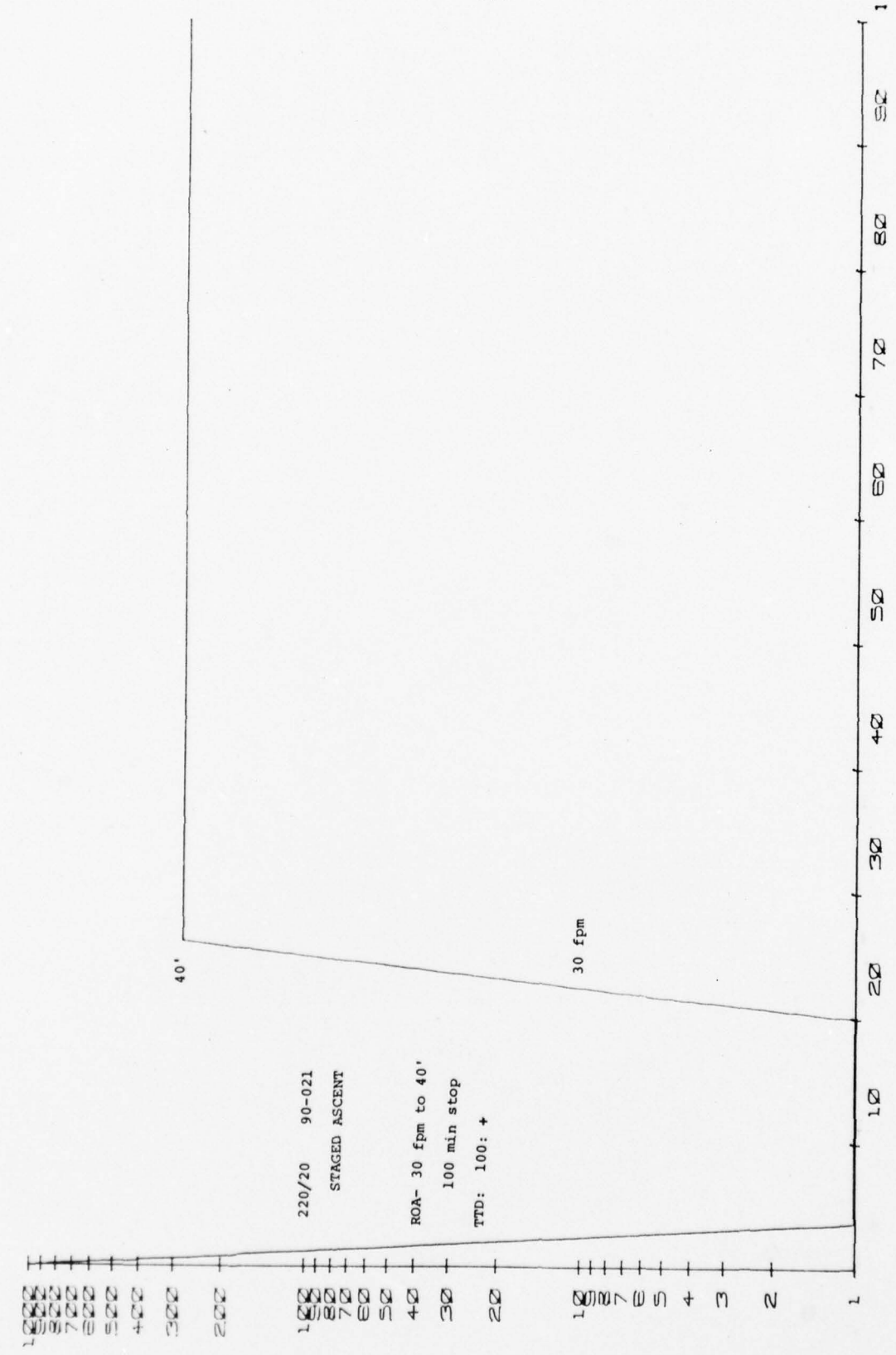
40'
30 fpm
220/20 90-021
STAGED ASCENT
ROA- 30 fpm to 40'
100 min stop
TTD: 100: +

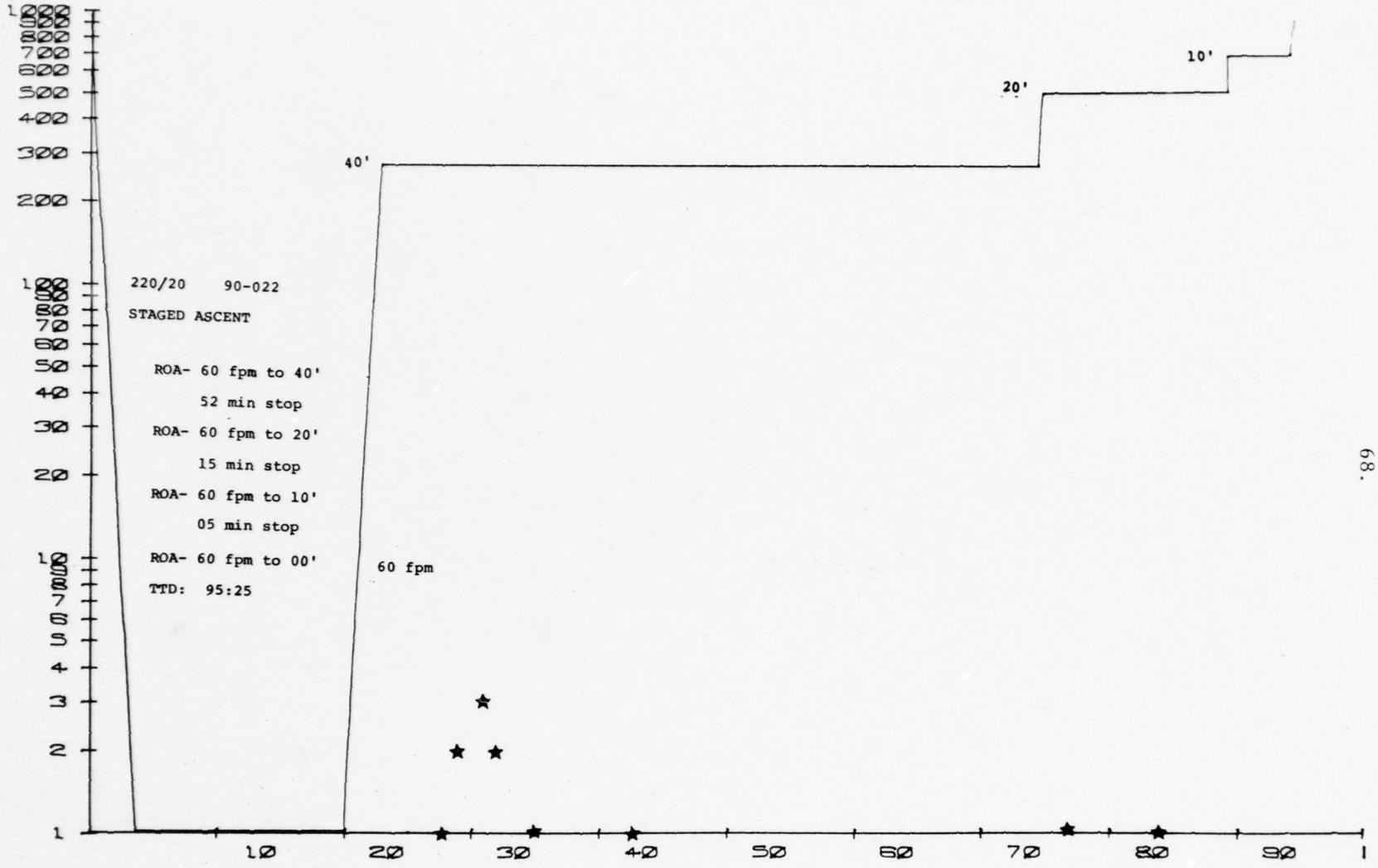
220/20 90-022
STAGED ASCENT
ROA- 60 fpm to 40'
52 min stop
ROA- 60 fpm to 20'
15 min stop
ROA- 60 fpm to 10'
05 min stop
ROA- 60 fpm to 00'
TTD: 95:25
60 fpm
40'
20'
10'
1000
900
800
700
600
500
400
300
200
100
90
80
70
60
50
40
30
20
10
9
8
7
6
5
4
3
2
1
10
20
30
40
50
60
70
80
90
1

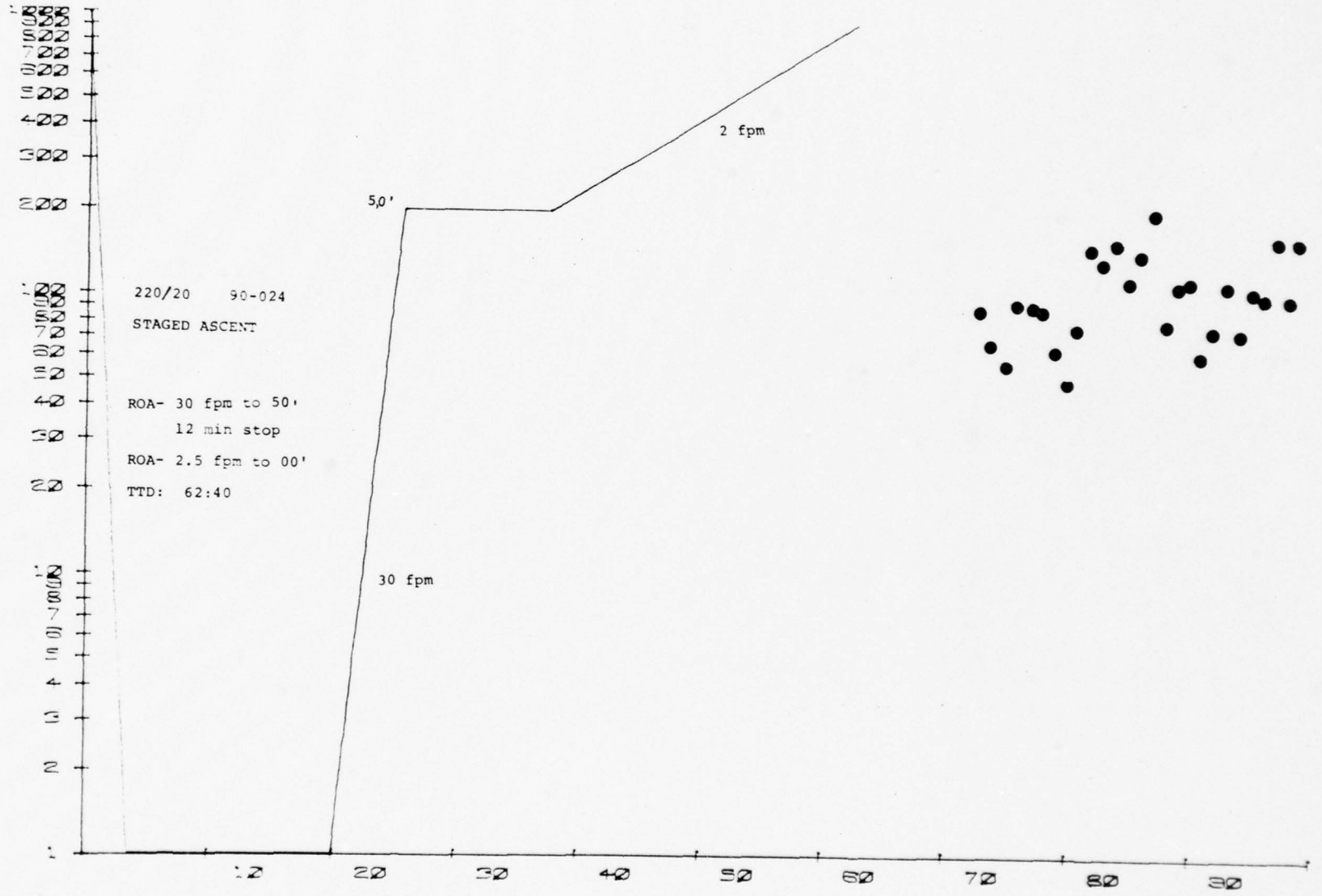
220/20 90-024
STAGED ASCENT
ROA- 30 fpm to 50'
12 min stop
ROA- 2.5 fpm to 00'
TTD: 62:40
5,0'
2 fpm
30 fpm
10
20
30
40
50
60
70
80
90

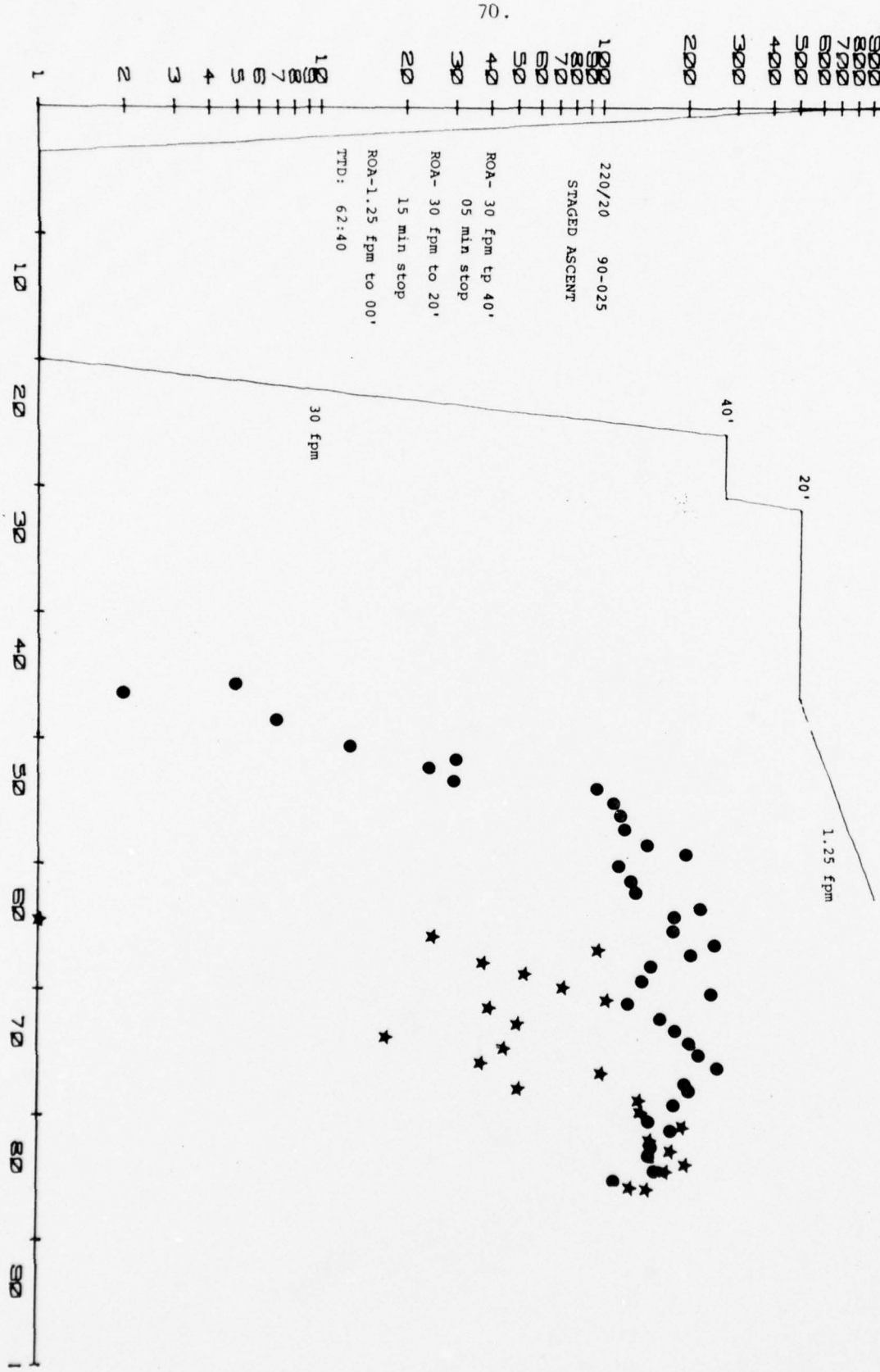
220/20 90-025
STAGED ASCENT
ROA- 30 fpm tp 40'
05 min stop
ROA- 30 fpm to 20'
15 min stop
ROA-1.25 fpm to 00'
TTD: 62:40
40'
20'
1.25 fpm
30 fpm

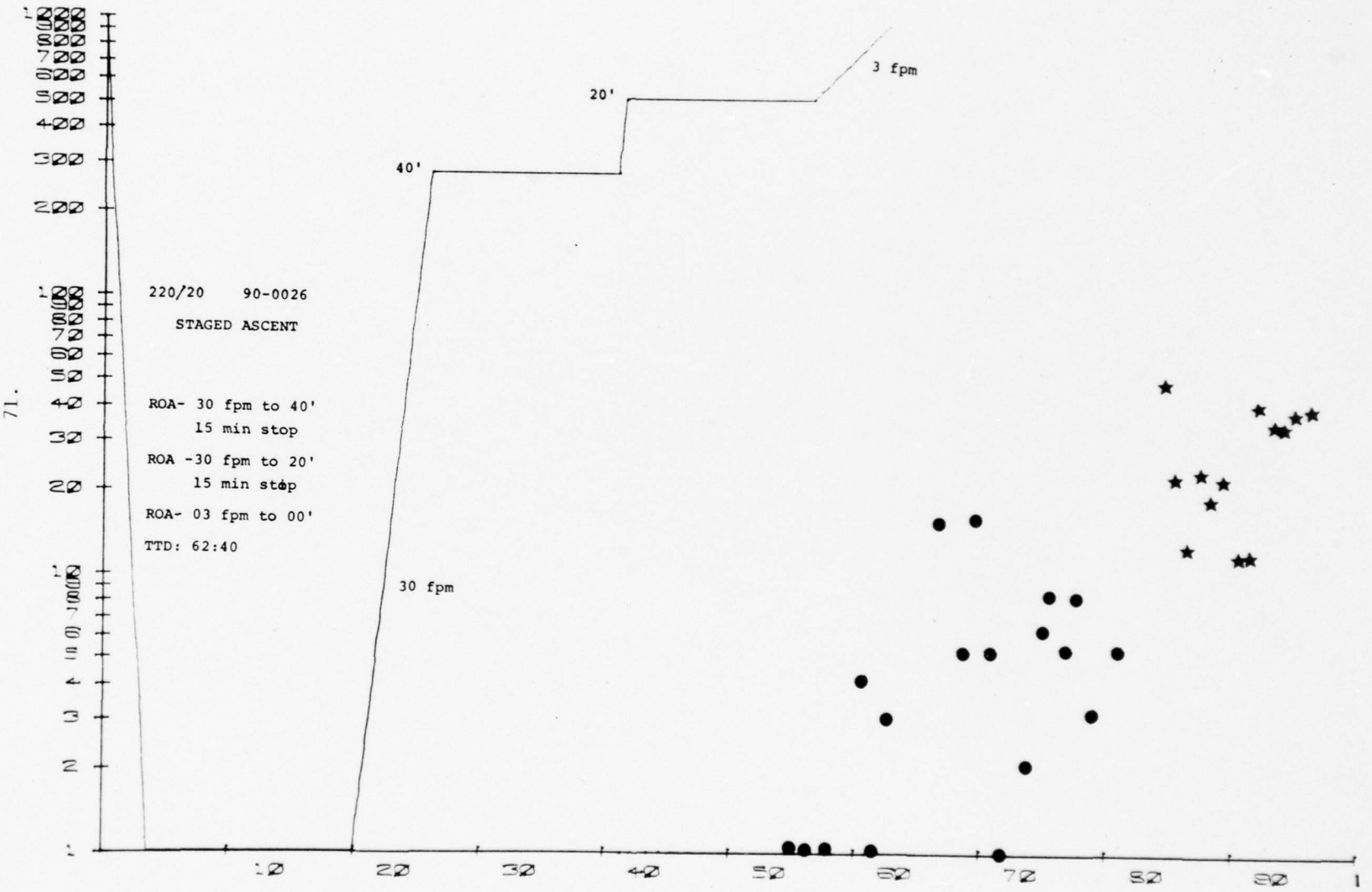
220/20 90-0026
STAGED ASCENT
ROA- 30 fpm to 40'
15 min stop
ROA -30 fpm to 20'
15 min stop
ROA- 03 fpm to 00'
TTD: 62:40
40'
20'
3 fpm
30 fpm

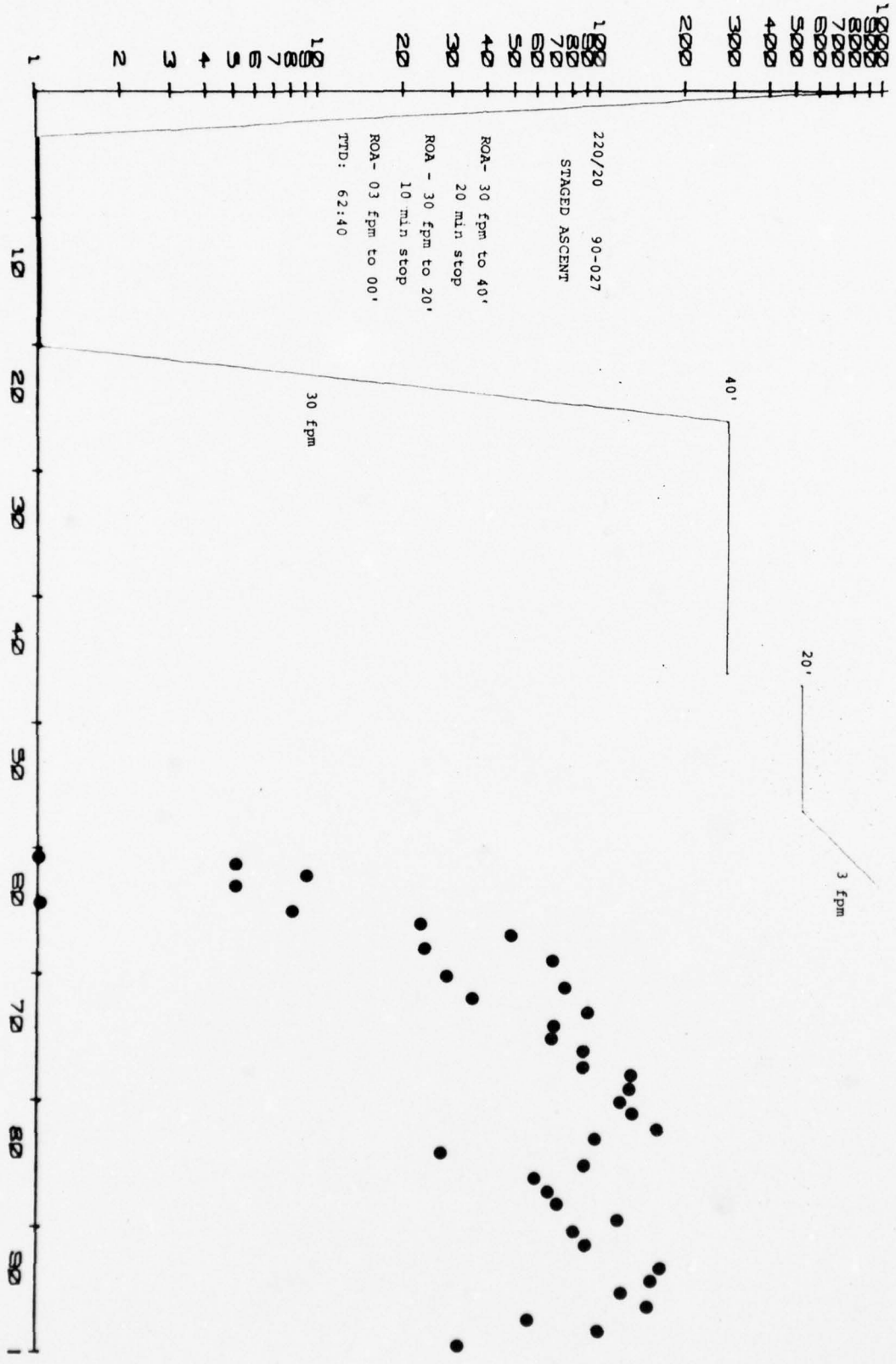
220/20 90-027
STAGED ASCENT
ROA- 30 fpm to 40'
20 min stop
ROA - 30 fpm to 20'
10 min stop
ROA- 03 fpm to 00'
TTD: 62:40
40'
20'
30 fpm
3 fpm

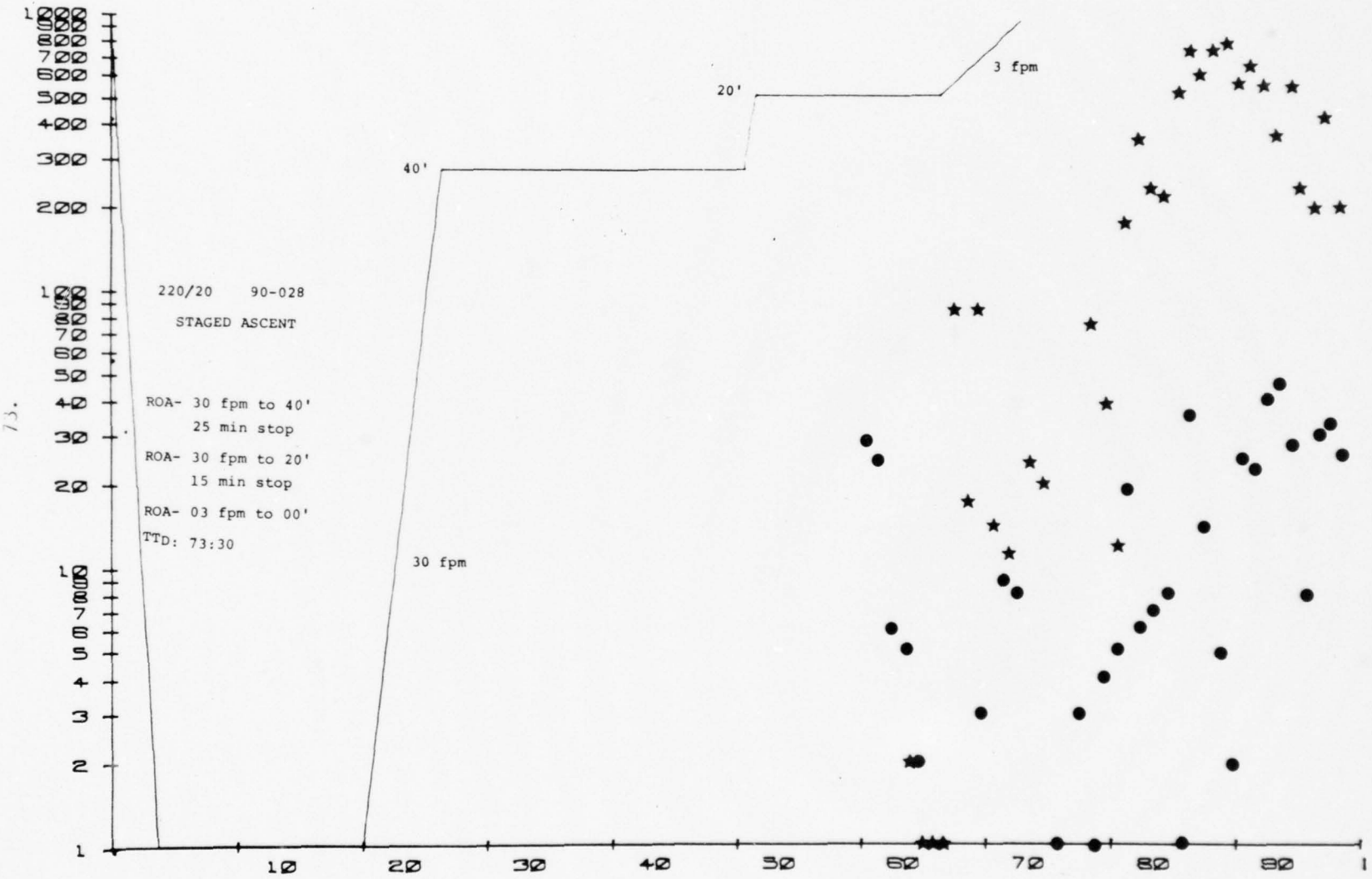
220/20 90-028
STAGED ASCENT
ROA- 30 fpm to 40'
25 min stop
ROA- 30 fpm to 20'
15 min stop
ROA- 03 fpm to 00'
TTD: 73:30
40'
20'
3 fpm
30 fpm
1000
900
800
700
600
500
400
300
200
100
90
80
70
60
50
40
30
20
10
9
8
7
6
5
4
3
2
1
10
20
30
40
50
60
70
80
90
1

73.

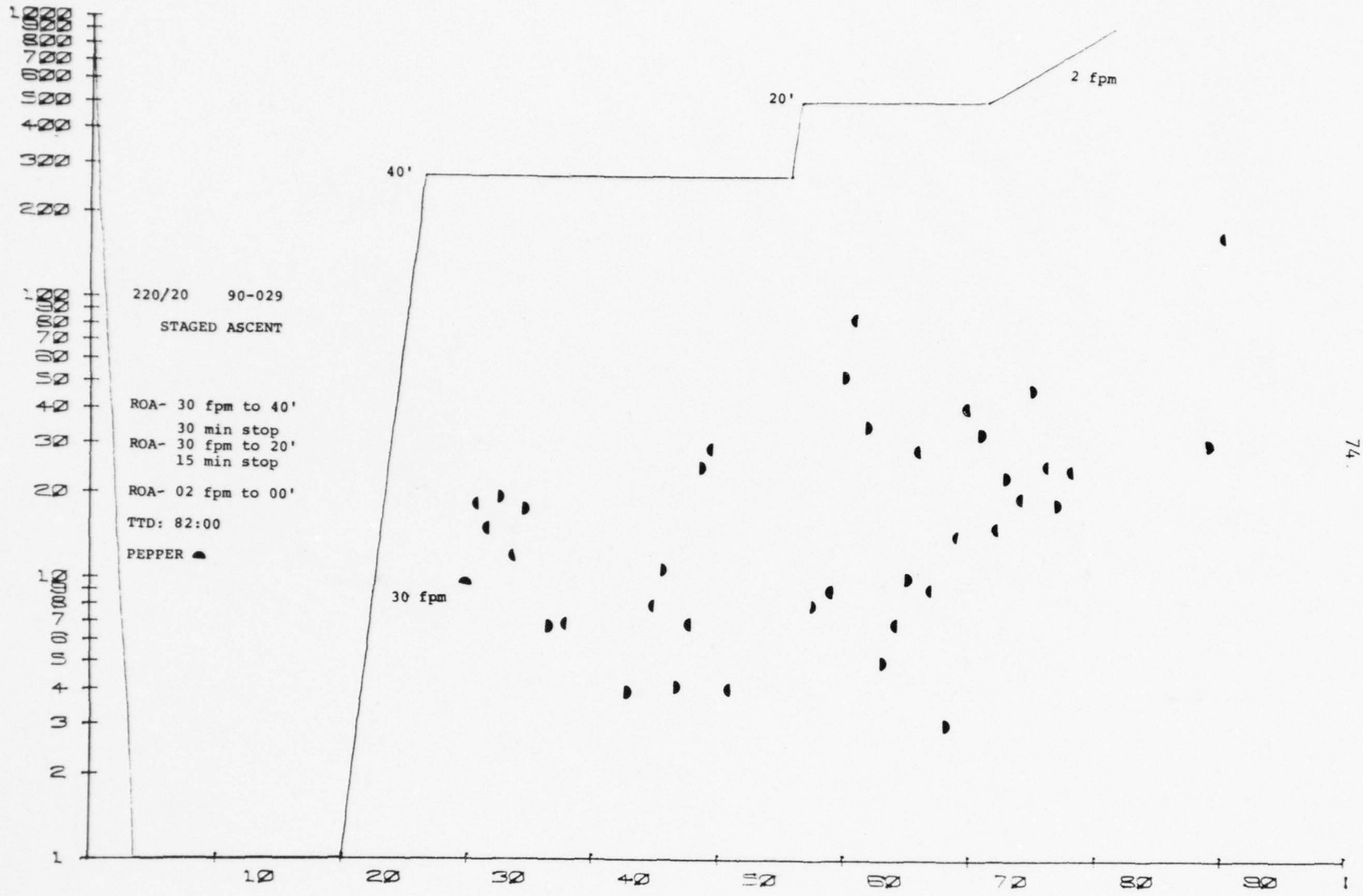
220/20 90-029
STAGED ASCENT
ROA- 30 fpm to 40'
30 min stop
ROA- 30 fpm to 20'
15 min stop
ROA- 02 fpm to 00'
TTD: 82:00
PEPPER
40'
20'
2 fpm
30 fpm
74

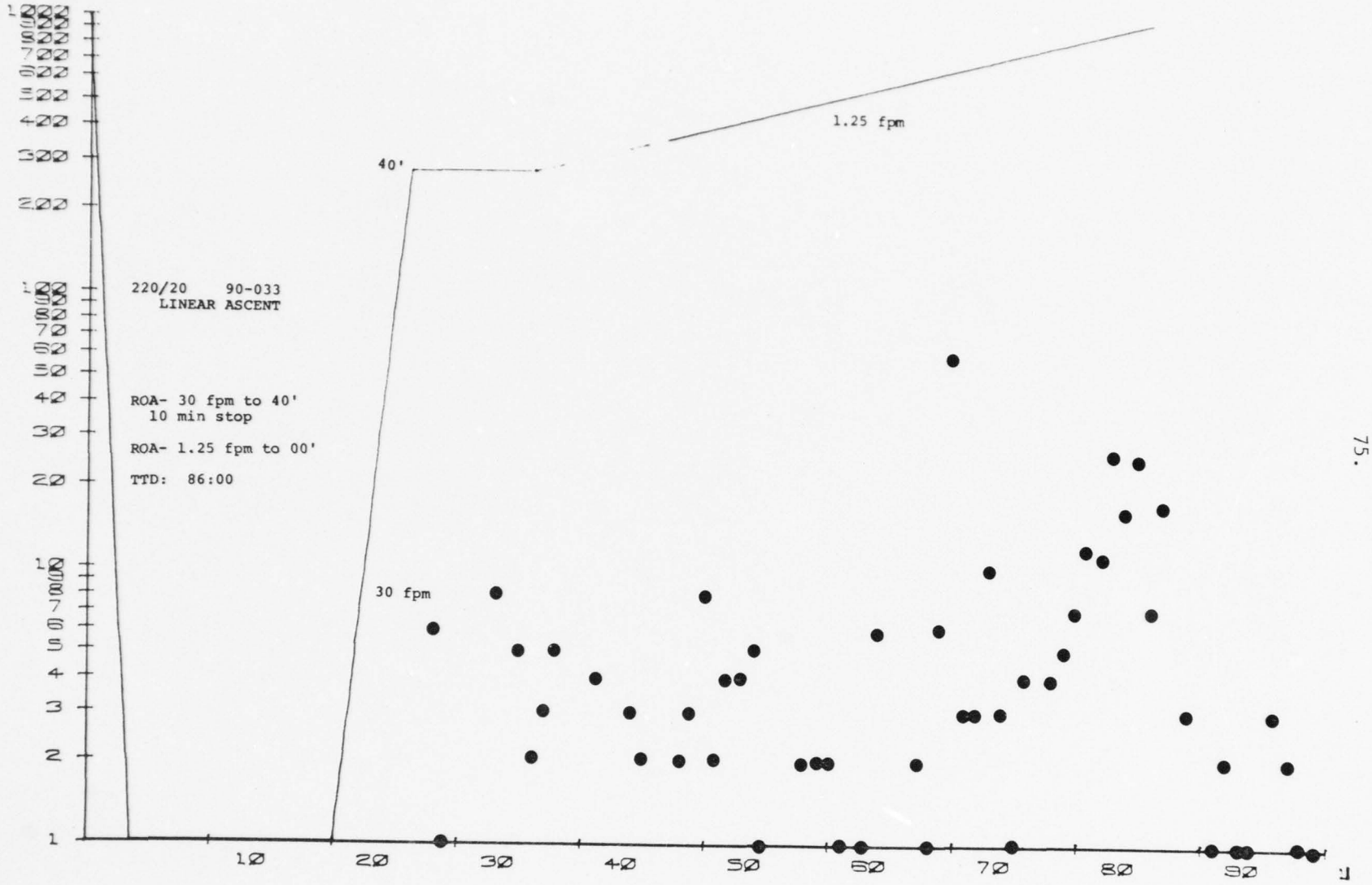
220/20 90-033
LINEAR ASCENT
ROA- 30 fpm to 40'
10 min stop
ROA- 1.25 fpm to 00'
TTD: 86:00
40'
30 fpm
1.25 fpm
1
2
3
4
5
6
7
8
9
10
20
30
40
50
60
70
80
90

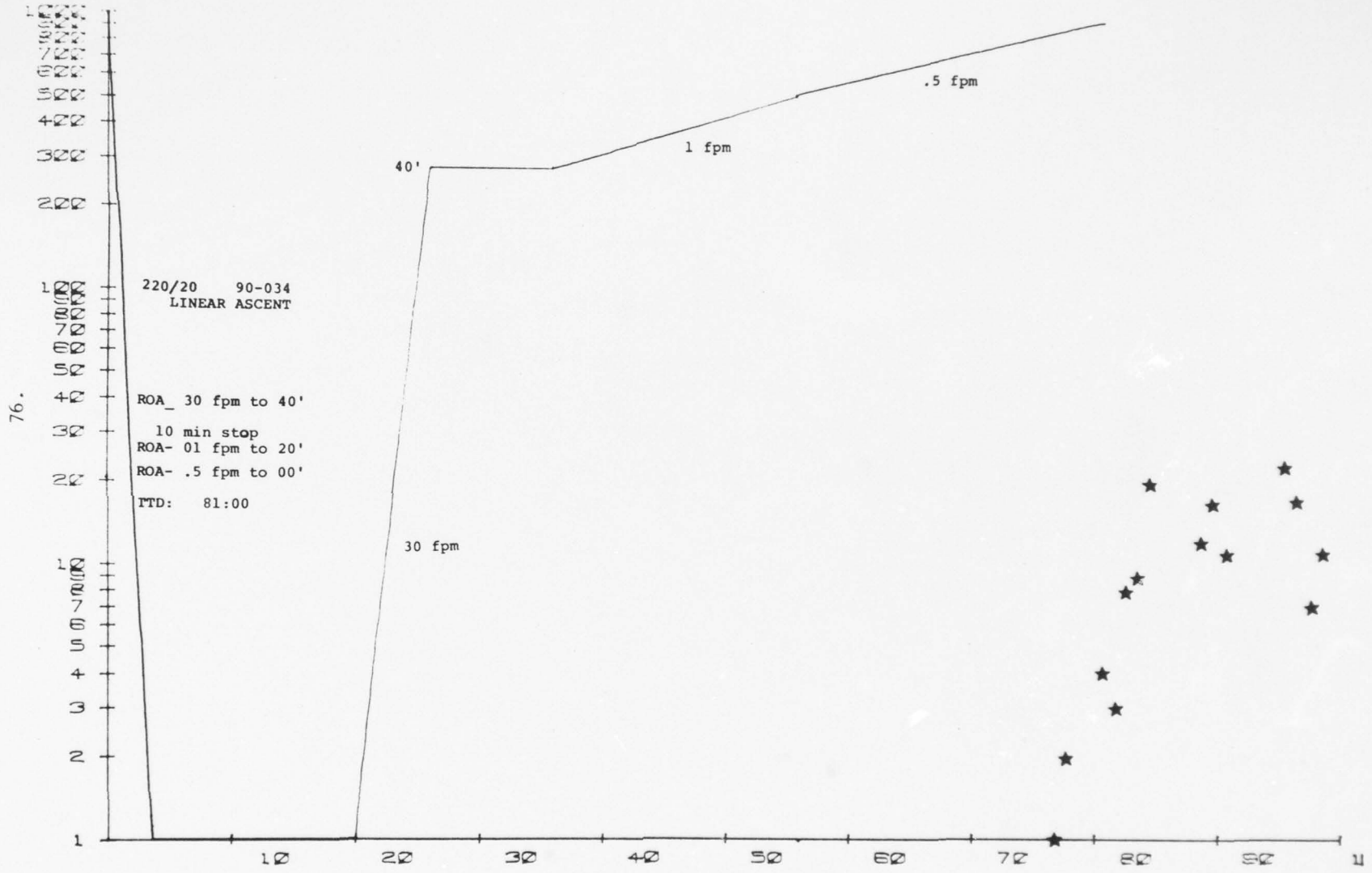
76.
220/20 90-034
LINEAR ASCENT
ROA_ 30 fpm to 40'
10 min stop
ROA- 01 fpm to 20'
ROA- .5 fpm to 00'
ITD: 81:00
40'
30 fpm
1 fpm
.5 fpm
1
2
3
4
5
6
7
10
20
30
40
50
60
70
80
90

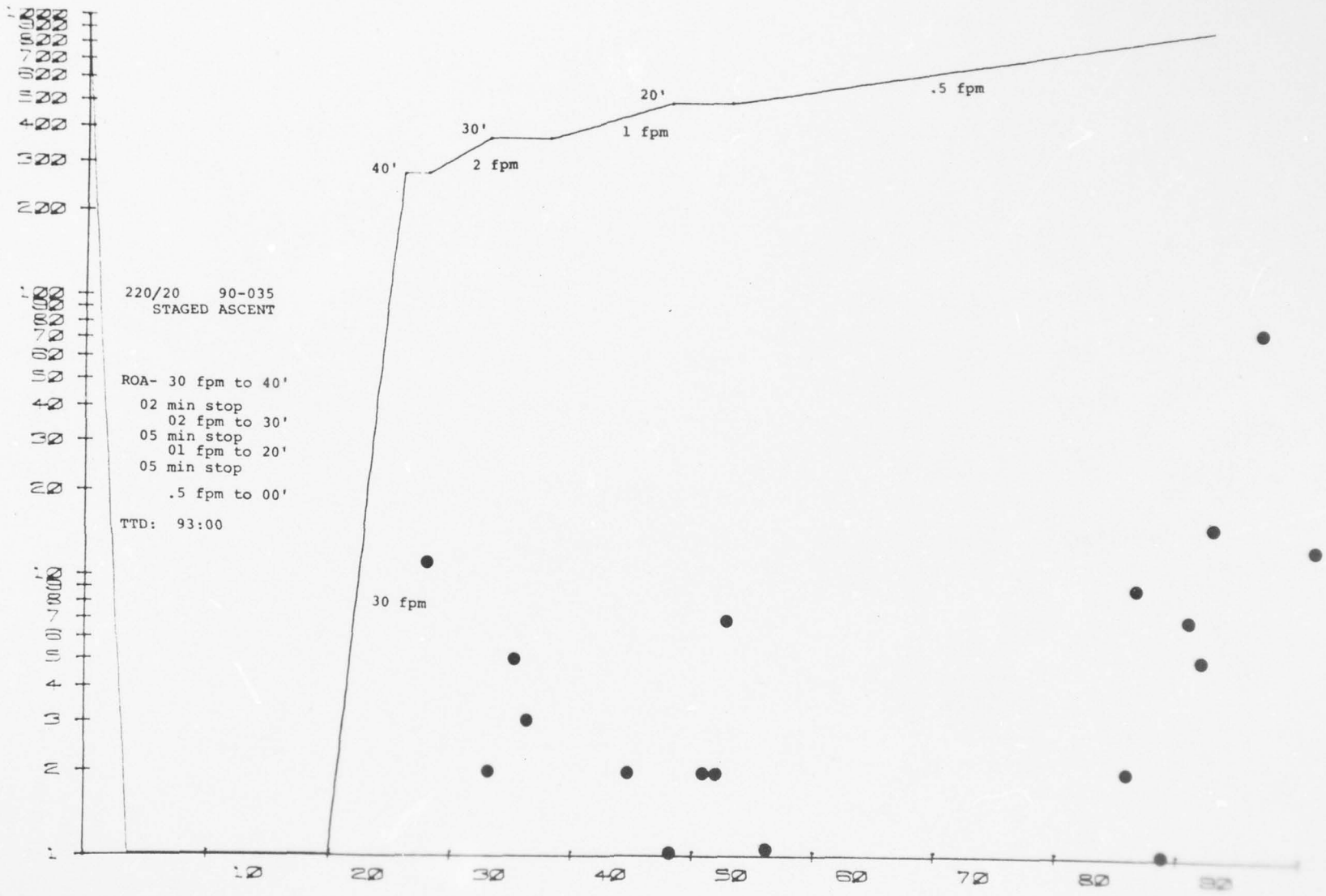
220/20 90-035
STAGED ASCENT
ROA- 30 fpm to 40'
02 min stop
02 fpm to 30'
05 min stop
01 fpm to 20'
05 min stop
.5 fpm to 00'
TTD: 93:00
40'
30'
20'
2 fpm
1 fpm
.5 fpm
30 fpm
10
20
30
40
50
60
70
80

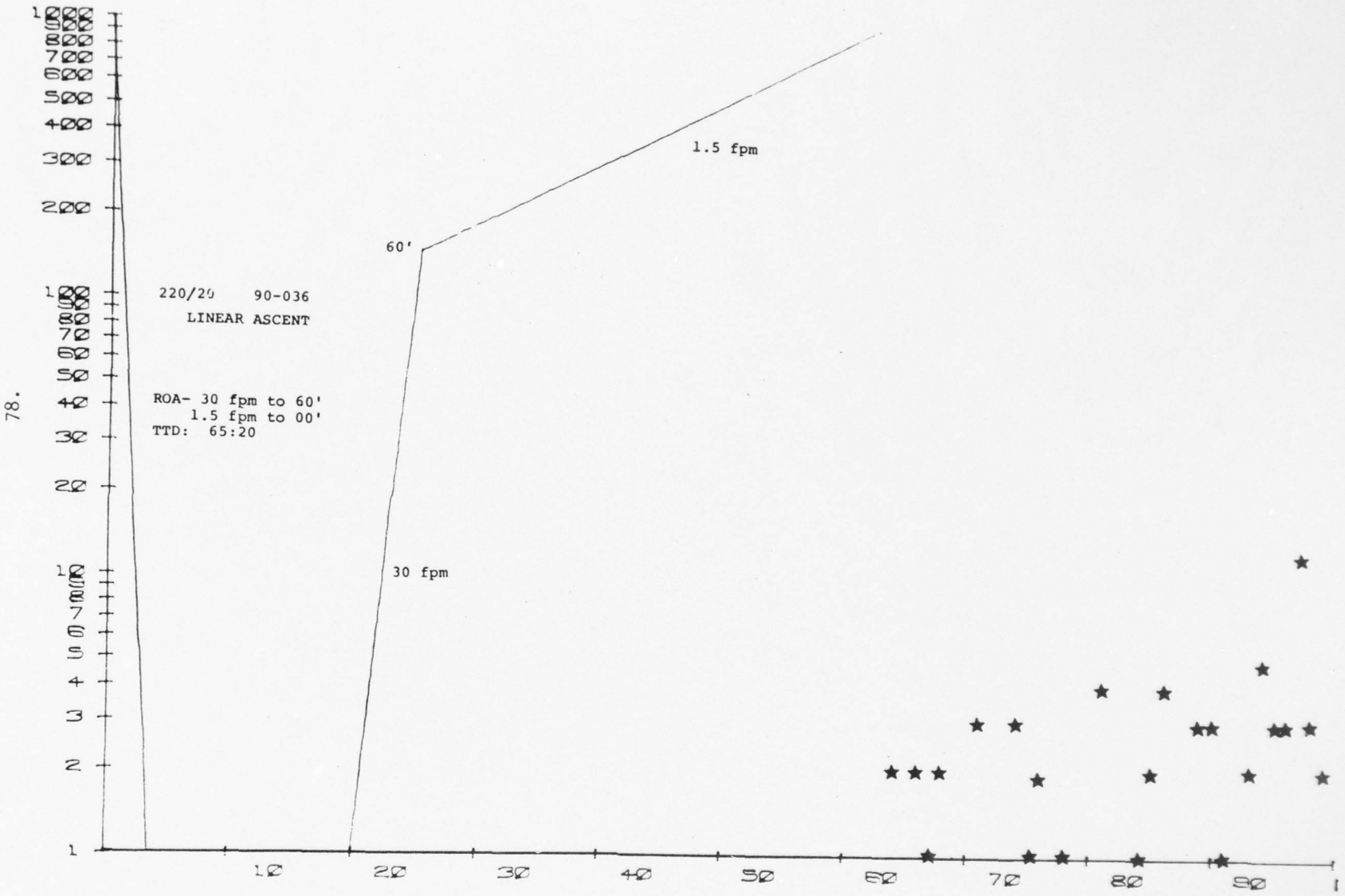
78.
220/20 90-036
LINEAR ASCENT
ROA- 30 fpm to 60'
1.5 fpm to 00'
TTD: 65:20
60'
1.5 fpm
30 fpm

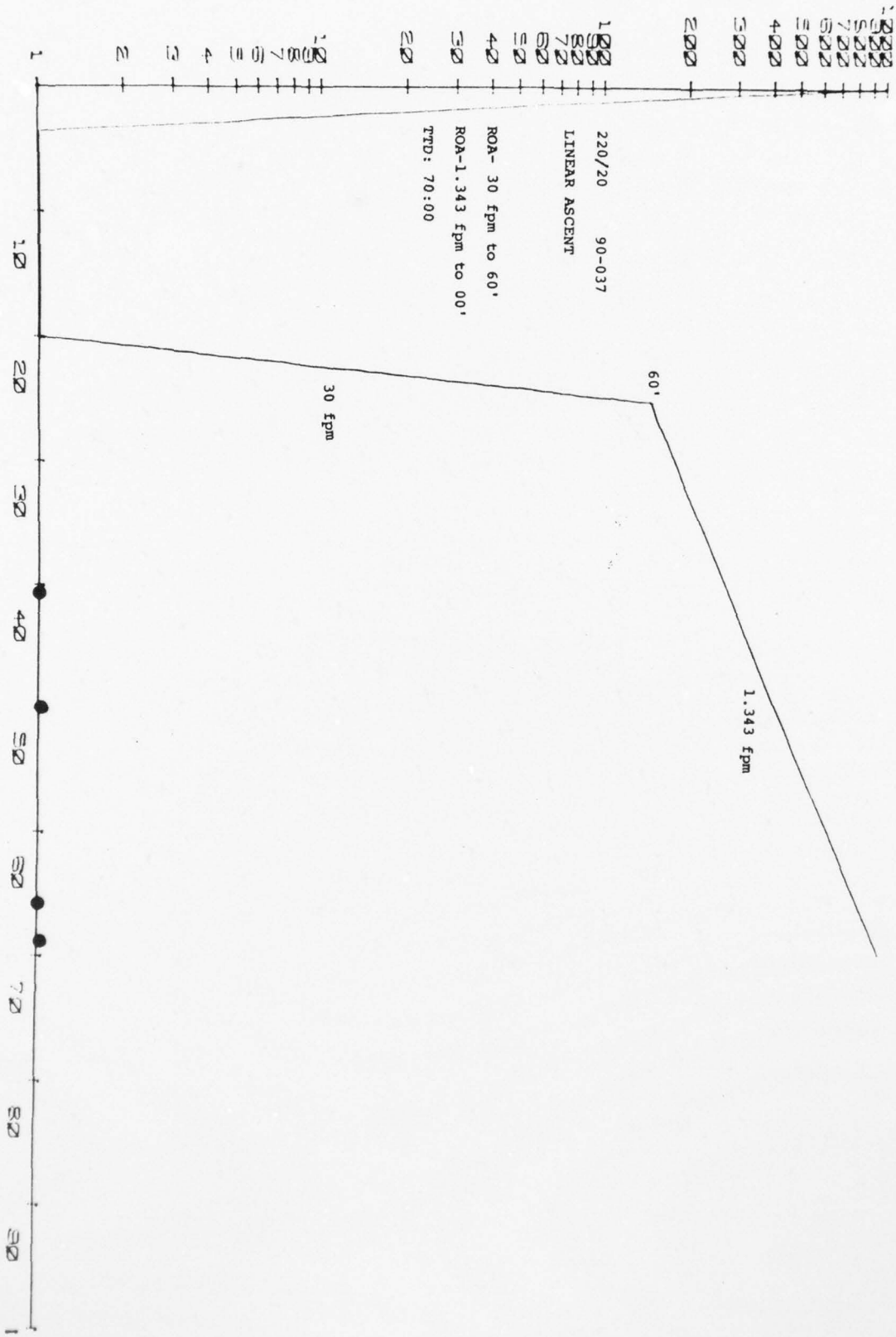
220/20 90-037
LINEAR ASCENT
ROA- 30 fpm to 60'
ROA-1.343 fpm to 00'
TTD: 70:00
60'
30 fpm
1.343 fpm

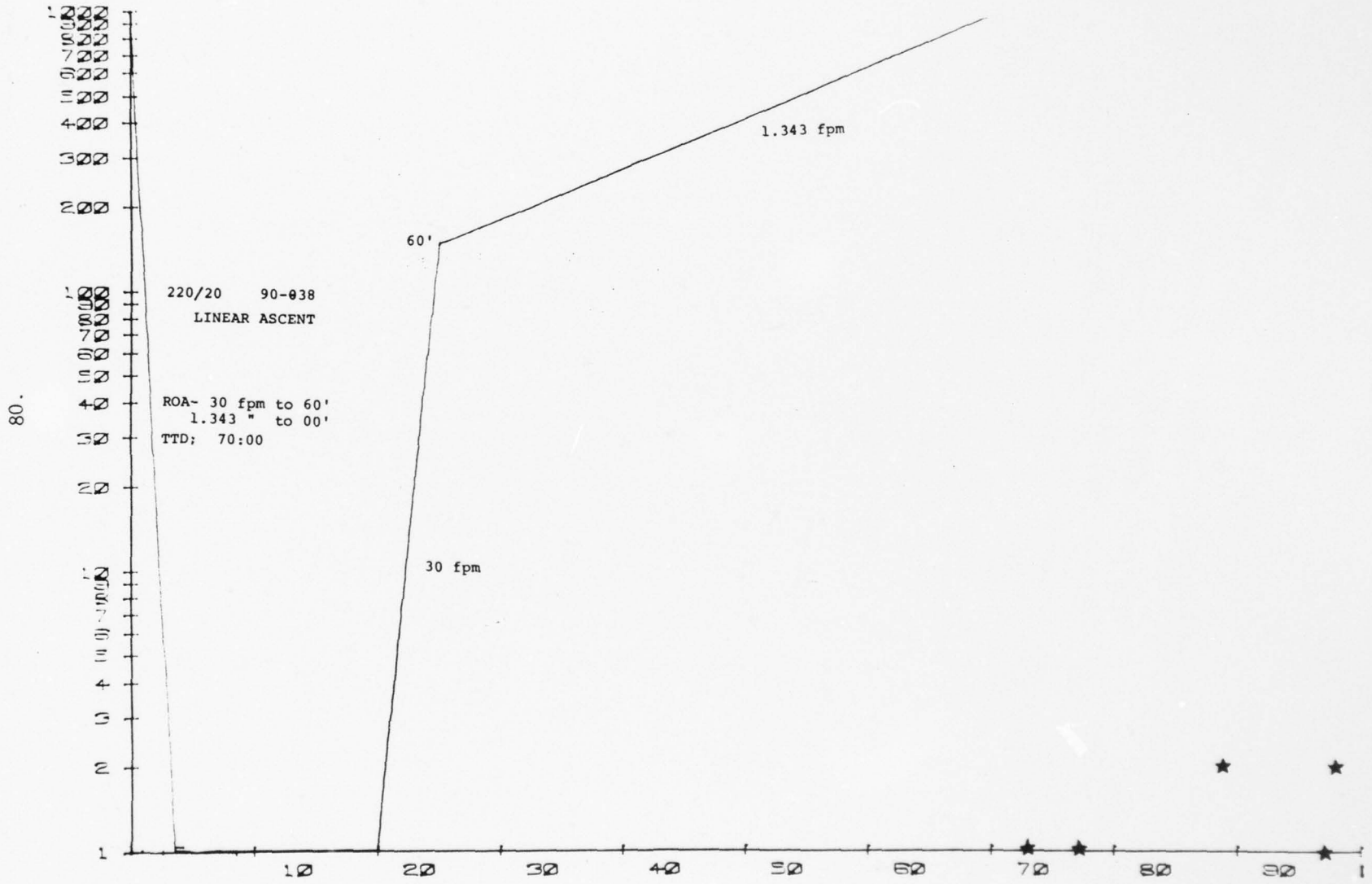
220/20 90-038
LINEAR ASCENT
ROA~ 30 fpm to 60'
1.343 " to 00'
TTD; 70:00
60'
1.343 fpm
30 fpm
10
20
30
40
50
60
70
80
90

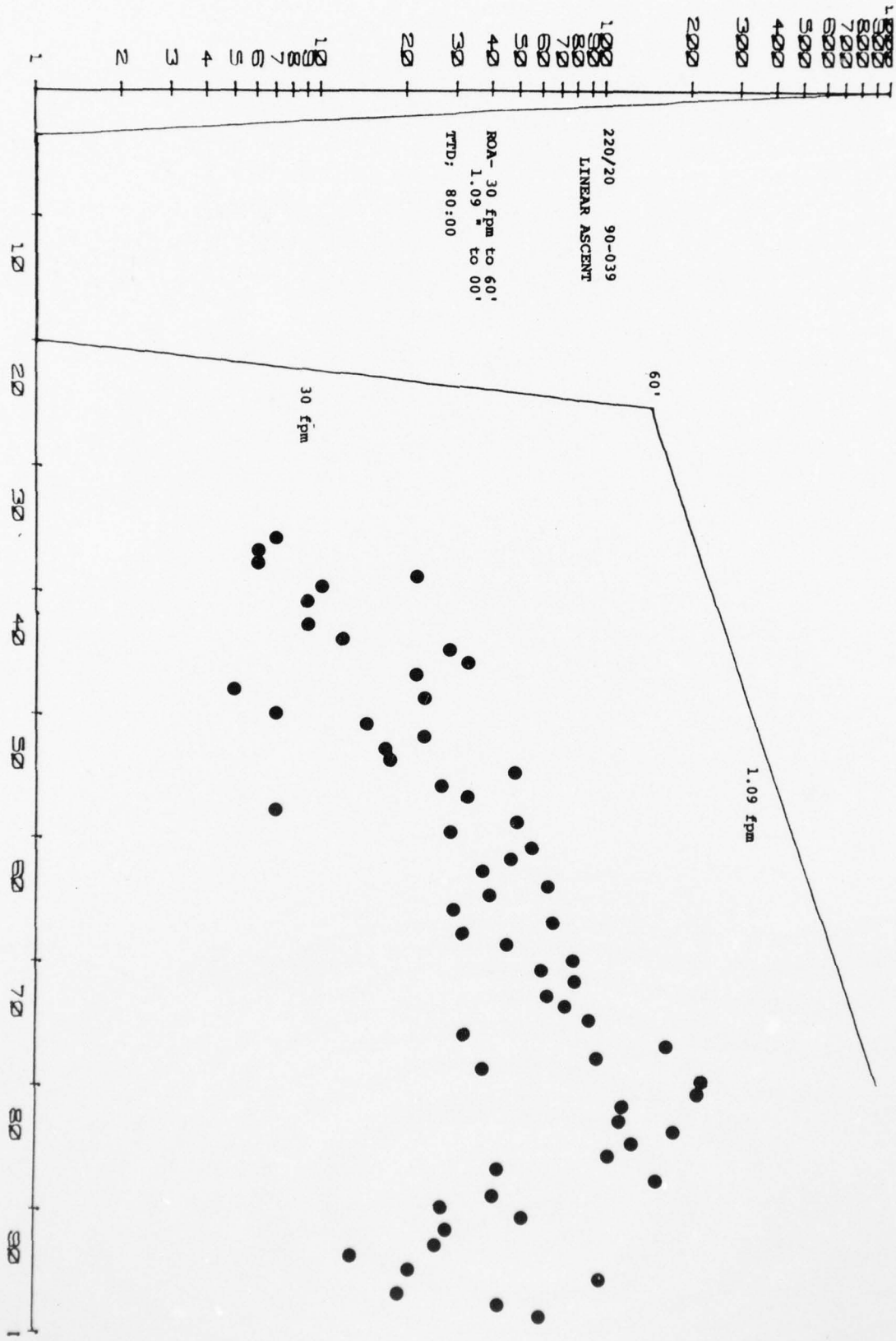
220/20 90-039
LINEAR ASCENT
ROA- 30 fpm to 60'
1.09 " to 00'
TTD; 80:00
60'
30 fpm
1.09 fpm

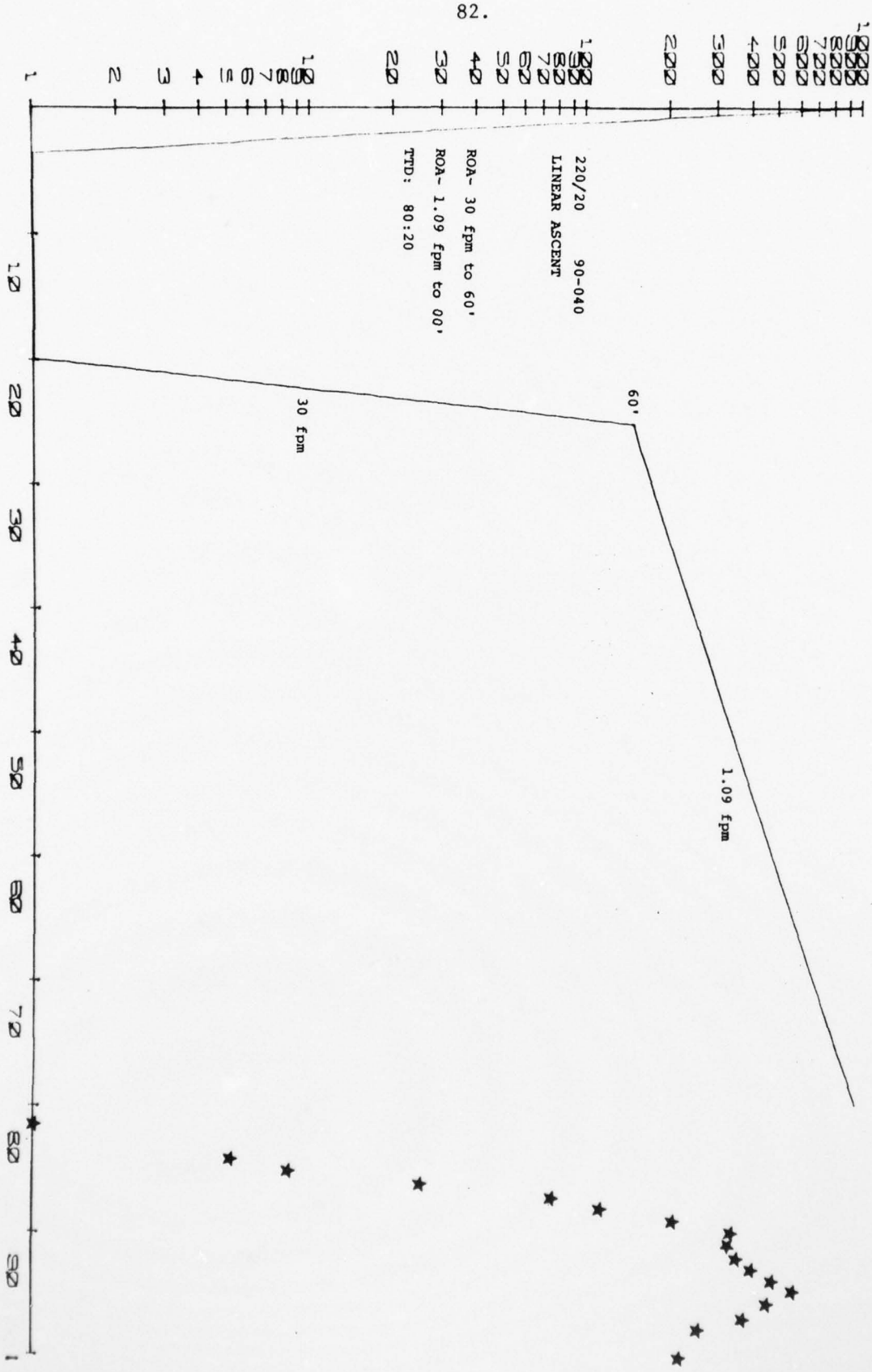
220/20 90-040
LINEAR ASCENT
ROA- 30 fpm to 60'
ROA- 1.09 fpm to 00'
TTD: 80:20
30 fpm
60'
1.09 fpm

Section II

Instrumentation Development

Hyperbaric Decompression Bloodflow Monitoring

- - - Prepared for the Virginia Mason Research Center
under VMRC Contract No. N00014-69-6-0402

- - - By D.P. Haugen and E.O. Belcher

- - - APL-UW 7609

- - - June 1976

TABLE OF CONTENTS

ABSTRACT

Methods have been developed for detecting and counting emboli that occur in the bloodstream as a result of decompression. Ultrasonic Doppler-shift techniques are used to monitor the bloodflow *in vivo*. Quasi-matched filter processing is used to detect the emboli signals, which are contained in a generally noisy background.

INTRODUCTION

This report summarizes the three-year collaboration between this Laboratory and the Virginia Mason Research Center (VMRC) to develop and apply improved techniques of monitoring bloodflow *in vivo* to detect the presence of abnormal gas emboli. This program has been supported by a year-to-year subcontract with VMRC. That support has been augmented by Laboratory sponsorship of a graduate student working directly on the project as a Research Assistant.

Our role has been to provide technical assistance in the areas of ultrasonic bloodflow monitoring and related signal processing--with the ultimate objective of improving the techniques used to detect the presence and assess the significance of abnormal emboli occurring in the bloodstream because of decompression.

The collaborative effort has been a rather flexible one. General goals and objectives were defined in a proposal at the beginning of each year. These were then pursued as much as possible according to plan, but not at the expense of ignoring new problems or special needs that evolved during the course of the research. This approach has been rewarding in that critical, short-term needs could be immediately addressed and promising new ideas investigated promptly.

The work began in 1972 and continued through September 1975 when support from the Naval Medical Research and Development Command through the Office of Naval Research to VMRC for instrumentation development ceased. During that period, several devices and techniques were developed to aid in the detection and quantification of emboli in the bloodstream of both animals and humans, and a better understanding of embolis signals was achieved.

Of special interest is the development of an "emboli counter," wherein we have attempted to produce, relatively inexpensively, a capability for real-time detection and assessment of abnormal emboli. The

result is an analog "quasi" matched-filter signal processor which detects and counts emboli signals based on the narrowband energy content of the signals relative to the broadband background noise level. The counter is proving useful for both real-time and post-experiment evaluation of the time-course of emboli formation. This is particularly true when the signals are obtained from sensors implanted on major vessels in animals, and thus have a high signal-to-noise ratio. However, there are wide variations in signal-to-noise ratio and overall signal amplitude that the instrument cannot accommodate. It is clear that significant improvements can be achieved in the emboli counter by implementing adaptive techniques to adjust the system gain and detection threshold according to the character of the incoming signal and noise. We are seeking support to continue development of this device.

The following sections of the report address, in turn, the following areas of the development work: (1) the ultrasonic bloodflow monitor, (2) the transducer probes, (3) signal modeling and analysis, and (4) the emboli counter. The numerous straightforward engineering tasks accomplished to support the main research activities are not included. Conclusions and recommended directions for additional development activities are provided in the last section.

ULTRASONIC BLOODFLOW MONITOR

Introduction

Gas emboli in the bloodstream present large acoustical discontinuities to propagating sound, and can be readily detected with ultrasonic detectors. Three approaches to ultrasonic detection are:

(1) Attenuation measurements using through-transmission techniques

(2) Echo amplitude measurements, using both cw and pulsed transmissions

(3) Doppler-shift techniques, both cw and pulsed.

The first two methods are capable of detecting gas emboli in both blood and tissues; however they provide only amplitude information and suffer generally from low signal-to-noise ratios. The Doppler-shift technique, on the other hand, provides simultaneous amplitude and frequency discrimination.

Detection of Doppler-shifted Signals

For a moving reflector and a stationary transmitter and receiver, the Doppler shift is related to the transmitted frequency by the equation

$$\omega_d = \omega' - \omega_o \simeq \frac{2\,V\,\omega_o\,\cos\theta}{c} \quad , \qquad (1)$$

where ω' is the received angular frequency, ω_o is the transmitted angular frequency, V is the reflector velocity, c is the velocity of sound in the medium of interest, and θ is the angle between the incident sound wave and the direction of the reflector motion.

Detection of Doppler-shifted signals can be done in several ways. Two easily implemented approaches, square-law envelope demodulation and frequency conversion by mixing, are depicted in Figures 1 and 2, respectively. For the case of simultaneous scattering from multiple emboli, these two techniques yield different results. To demonstrate, assume that the return signal is comprised of the sum of the returns from N independent emboli. In this case, ignoring phase shifts, the received signal is

$$S(t) = \sum_{i=1}^{N} B_i \cos(\omega_o + \omega_{d_i})t \quad , \tag{2}$$

where B_i characterizes the amplitude of the return from the i^{th} emboli and will generally be a function of emboli size, type, and location in the sound beam, ω_o is the transmitted frequency, and ω_{d_i} is the Doppler shift arising from the relative velocity of the i^{th} target.

For square-law amplitude demodulation, the processed signal is

$$S_1(t) = \frac{K^2}{2}\left\{A^2 + \sum_{i=1}^{N} B_i^{\,2} + 2\sum_{i=1}^{N} AB_i \cos(\Delta\omega + \omega_{d_i})t \right. \tag{3}$$

$$\left. + \sum_{i=1}^{N}\sum_{j=1}^{N} B_i B_j \cos(\omega_{d_i} - \omega_{d_j})t \right\} \quad i \neq j \quad ,$$

while for the frequency conversion process it is

$$S_2(t) = \frac{k^2}{2} \sum_{i=1}^{N} AB_i \cos(\Delta\omega - \omega_{d_i})t \quad , \tag{4}$$

where $\Delta\omega = \omega_o - \omega_r$ and ω_r is the receiver reference frequency.

When only a single embolus is involved, both methods yield merely a frequency-shifted version of the transmitted signal. However, when more than one embolus is present simultaneously, square-law demodulation produces a signal spectrum that includes the difference frequencies of the various pairs of emboli in addition to the normal Doppler-shifted frequencies.

Note that if $\Delta\omega = 0$, the positive and negative flow velocities will be indistinguishable in the signal spectrum. Consequently, to observe an "unfolded" spectrum or to distinguish flow direction using the above technique, $\Delta\omega$ must be made sufficiently high for the maximum negative velocity scatterer to produce a positive Doppler frequency.

Doppler Bloodflow Monitor

The Doppler bloodflow monitoring instrumentation available to us at the beginning of the research program did not provide reasonably high-quality signals, even for aural monitoring purposes. To obtain improved signals, we developed a new instrument employing a mixer to convert the signals to either a baseband (i.e., $\omega_r = \omega_o$) for aural monitoring, or to a low-frequency carrier ($\omega_r \neq \omega_o$) for spectral analysis. This is a simple, low-cost device employing cw transmissions at 5 MHz. The transmitter uses a crystal-controlled oscillator with a buffer amplifier to drive the transmitting transducer. In our application, the

AD-A062 441 VIRGINIA MASON RESEARCH CENTER SEATTLE WASH F/G 6/19
HYPERBARIC DECOMPRESSION BY MEANS OF BUBBLE DETECTION.(U)
APR 78 K H SMITH, L STAYTON N00014-69-C-0402
UNCLASSIFIED NL

2 OF 2
AD
A062441

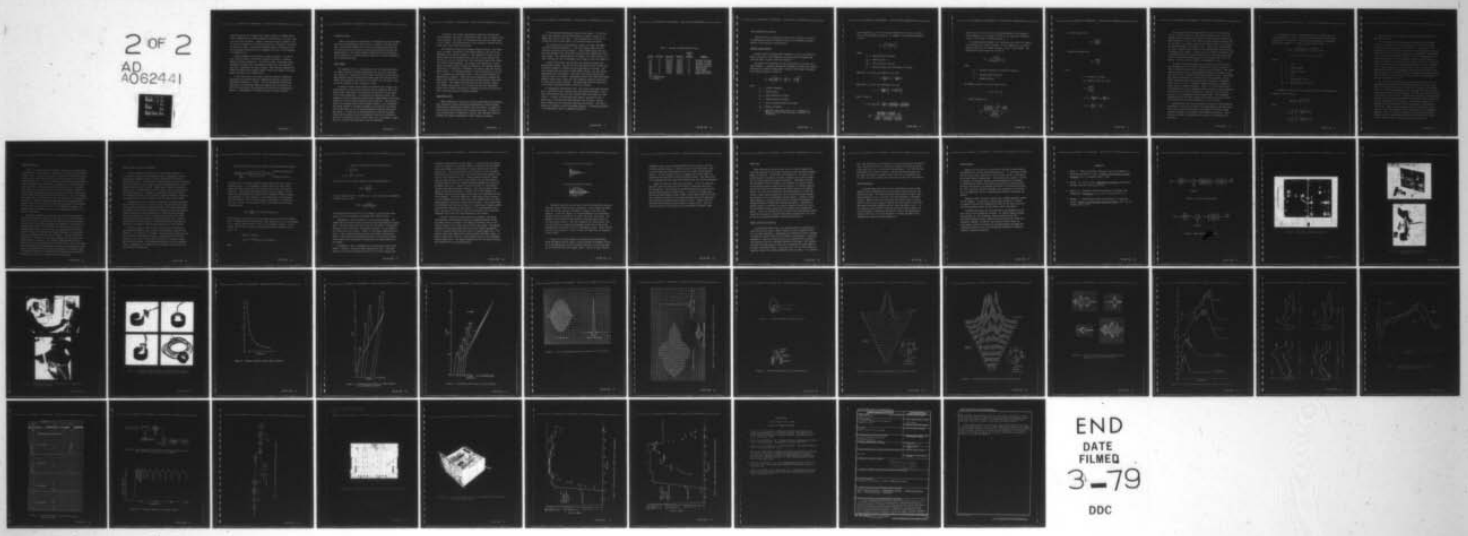

END
DATE
FILMED
3-79
DDC

optimum frequency for maximizing the signal strength is somewhat above 2 MHz, depending on the average absorption coefficient of the tissue and the size of the transducer. However, because the signal strength is not critical and beamwidth is inversely proportional to frequency, we decided to operate at 5 MHz. This provides adequate signal strength and, with the transducers described below, a beamwidth less than 1 cm in diameter at a depth of 5 cm.

A block diagram of the receiver is shown in Figure 3. In the direct and filter modes, the receiver reference frequency is obtained directly from the transmitter. In the filter mode, a high-pass filter eliminates the high-level, low-frequency signals that are associated with heart, breathing, and subject motion. This filtering enhances the audible interpretation of emboli signals, which occur mainly in the frequency band above a few hundred hertz.

In the 10-kHz mode, an external oscillator provides a reference frequency 10 kHz removed from the transmitted frequency to place the zero-Doppler frequency at 10 kHz. A 40-dB, 500-Hz wide notch filter centered at 10 kHz prevents high-level signals from zero-velocity reflectors and scatterers from saturating the receiver and recording apparatus. A photograph of the Doppler monitor is shown in Figure 4.

TRANSDUCER PROBES

Probes for noninvasive monitoring of the pulmonary artery in humans, and cuffs for implanting on major vessels in animals, have been developed. Both devices support two crystals for transmitting energy into the blood vessel and receiving the energy backscattered from acoustic discontinuities. The designs optimize beam patterns and focusing for signal enhancement, consistent with the physical constraints imposed by the intended application.

Chest Probes

The pulmonary artery is the preferred site for monitoring because all emboli entering the venous bloodstream from the entire body must pass through it. Monitoring of the brachial and femoral veins produces much improved signal-to-noise ratios because heart and lung motion are absent and the vessels are closer to the surface, but, of course, indicates the condition of only one limb at a time.

To obtain the most useful signals for detection and counting, the vessel should be located in the far-field of the transducer with a reasonably small angle between the direction of blood flow and the direction of sound propagation. In monitoring the pulmonary artery, this condition is most conveniently obtained with a probe mounted on the chest surface left of the sternal border near the fourth rib. This location results in a nominal probe-to-vessel depth of about 4 or 5 centimeters. The signal strength is strongly dependent on the position and orientation of the probe, as well as on the anatomy and physical attitude of the subject. In addition, as mentioned before, motion of the heart, lungs, and the subject, as well as movement of the probes relative to the skin or underlying tissue, produce high-level, low-frequency signals which are reflected from interfaces near the transducer.

To minimize this problem and provide a method for routine long-term monitoring, the special, chest-mounted probe shown in Figures 5 and 6 was developed. The probe is stabilized on the chest with tape and/or elastic straps. The adjustable arm is then trained to ensonify the desired vessel and locked into position.

The transducer elements are identical square crystals, 0.25 centimeter in length, and mounted in the plastic holder at the end of the adjustable arm as shown in Figure 5. The transducer elements are air-backed except on the periphery where they are in direct contact with the plastic, and are covered with a thin coating of acrylic for electrical isolation and protection. The elements are separated by 2 centimeters and angled slightly toward one another so as to produce maximum sensitivity at a depth of 5 centimeters, the typical depth for the pulmonary artery. The transducer material is PZT-4 resonated at 5 MHz and the size-frequency relationship yields a 3-dB far-field beamwidth of approximately 4 degrees. These units have significantly improved the quality and consistency of data obtained over that possible using hand-held probes. Good signals have been obtained from subjects inside a test chamber over periods of 4 to 6 hours with the only requirement placed on the subjects being that of assuming essentially the same posture as when the probe was initially adjusted.

Implantable Cuffs

Emboli monitoring of animals is usually accomplished using implantable transducers because they provide high-quality, reliable signals. Unfortunately, commercially available units are subject to severe corrosion problems and generally do not operate very long. To obtain at least several months of operation, a special cuff transducer mount was designed for surgical implantment on major vessels in animals.

The design proceeded through essentially two phases. In the first phase, the transducer crystals were mounted on opposite sides of a C-shaped cuff machined from nylon. A self-locking insert closed the "C" to hold the cuff in place after it was inserted around the vessel.

The second design was motivated by a desire to reduce the number of crystal assemblies required. In the first design, each cuff contained the necessary pair of crystals. In the second design, the crystals were mounted in the insert that closed the cuff, rather than in the main portion. This approach permits one insert to be used with any size cuff, reducing the cost of providing a wide range of sizes (see Figure 7).

In both cuff designs, the crystals were originally sealed with a polyurethane coating. Four of the first type and one of the second were eventually implanted in animals with varying degrees of success. One unit operated well for almost 5 months before failing. One unit failed immediately after implantation. The other three units operated satisfactorily from 1 to 2 months. Inspection of these units after post-mortem removal revealed that in four cases the transducer crystals and electrical leads were severely corroded. The polyurethane had not bonded well to the nylon, permitting fluids to attack the crystals.

In subsequently manufactured units, the crystals have been protected with a sprayed-on acrylic coating rather than with polyurethane. Two of these units operated well for over 6 months before the animals were sacrificed. A third, while providing poor signals, operated for over 4 months and is not believed to have suffered from corrosion. Several more of these units are currently being used successfully. The acrylic coating has obviously solved the leakage problems. The operating history of the implantable cuffs is summarized in Table I.

Table I. History of implantable cuff use.

Design	Coating*	Implanted	Removed	Useful Life (months)	Comments
1st	P	10/31/73	5/8/74	4	Severely corroded
1st	P	1/9/74	5/9/74	>1	Severely corroded
1st	P	1/14/74	4/8/74	<1	Severely corroded
2nd	P	1/21/74	3/5/74	1	Severely corroded
1st	P	4/10/74	5/23/74	0	Broken leads
2nd	A	1/5/75	8/15/75	>4	Poor signals
2nd	A	1/5/75	9/20/75	>6	Animal sacrificed
2nd	A	1/7/75	9/30/75	>6	Animal sacrificed

*P = polyurethane
A = acrylic

SIGNAL MODELING AND ANALYSIS

Both theoretical and empirical studies were conducted to assist in interpreting the emboli and bloodflow data and in designing automated methods of detecting and counting emboli.

Computer-aided Analyses

Several computer programs were formulated to assist our studies of emboli scattering. These programs are based on the developments published by Devin, Kinster, Nishi and Zemanek.[1-4]

One method of determining the size of gas emboli is by their resonant frequency. A computer program was developed to examine the resonant frequencies of bubbles ranging from 1 micron to 100 microns in diameter. The resonant frequency is given by

$$f_o = \frac{1}{2\pi R}\left[\frac{3\gamma R}{\rho_L \epsilon}\left(1 + \frac{2\alpha}{P_o R}\left(1 - \frac{\epsilon}{3\gamma}\right)\right)\right]^{\frac{1}{2}},$$

where

f_o = resonant frequency

R = bubble radius

P_o = static pressure in liquid

α = surface tension of liquid

γ = ratio of specific heats of the gas

ρ_L = density of liquid

ϵ = parameter that varies from 1 to γ, depending on whether the bubbles are isothermic, adiabatic, or in between.

In this equation, f_o is not an explicit function of R since ε is a function of both frequency and radius. To compute ε the following expression is used:

$$\phi = \left(\frac{\pi f \rho_g C_p}{K} \right)^{\frac{1}{2}} ,$$

where

f = insonification frequency

ρ_g = density of gas

C_p = heat capacity of the gas

K = thermal conductivity coefficient of the gas.

When $2\phi R \geq 5$ we have the adiabatic case, and

$$\varepsilon = 1 + \frac{3(\gamma-1)}{2\phi R} \left(1 + \frac{3(\gamma-1)}{2\phi R} \right).$$

When $2\phi R \leq 2$ we have the isothermal case, and

$$\varepsilon = \gamma - \frac{(2\phi R)^4}{1890} \left(1 - \frac{2.1(\gamma-1)^2}{\gamma} \right).$$

When $2 < 2\phi R < 5$,

$$\varepsilon = (1 + \delta_{th}^2) \left[1 + \frac{3(\gamma-1)}{2\phi R} \cdot \frac{\sinh(2\phi R) - \sin(2\phi R)}{\cosh(2\phi R) - \cos(2\phi R)} \right] .$$

$$\delta_{th} = \frac{\frac{\sinh(2\phi R) + \sin(2\phi R)}{\cosh(2\phi R) - \cos(2\phi R)} - \frac{1}{\phi R}}{\frac{2\phi R}{3(\gamma-1)} + \frac{\sinh(2\phi R) - \sin(2\phi R)}{\cosh(2\phi R) - \cos(2\phi R)}} .$$

To find f_o vs R, we used a routine employing parabolic interpolation which converged to an accuracy of ±0.16% in less than five iterations. A plot of the results is shown in Figure 8.

A second program determines the scattering cross section of bubbles as a function of (1) bubble diameter, (2) gas composition, (3) ensonification frequency, (4) ambient pressure, and (5) liquid medium. The expression for scattering cross section is

$$\sigma_s = \frac{\pi R_o^2}{(1-(f_o/f)^2)^2 + \delta^2} ,$$

where

f_o = resonant frequency for bubble of radius R_o

f = insonification frequency

δ = damping constant.

The damping constant is a sum of three terms:

$$\delta = \delta_1 + \delta_2 + \delta_3 .$$

1. Thermal damping term

$$\delta_1 = \frac{\left(\frac{16\ Fg}{9(\gamma-1)^2 f_o} - 3\right)^{\frac{1}{2}} - \frac{3\delta-1}{3(\delta-1)}}{\frac{8\ Fg}{9(\gamma-1)^2 f_o} - 2} ,$$

2. Viscous damping term

$$\delta_2 = \frac{8\pi\mu f_o \alpha}{3\gamma P_o g} \quad ,$$

3. Radiation damping term

$$\delta_3 = \frac{2\pi f_o R}{C_2} \quad ,$$

where

μ = viscosity of liquid

C_2 = speed of sound in liquid

$$F = \frac{3\gamma P_o \phi^2}{4\pi^2 \rho_L f_o}$$

$$\alpha = 1 + \frac{3(\gamma-1)}{2\phi R}\left(1 + \frac{3(\gamma-1)}{2\phi R}\right)$$

$$g = 1 + \frac{2\sigma}{P_o R}\left(1 - \frac{\alpha}{3\sigma}\right) \quad .$$

The results computed for oxygen bubbles in water (Figures 9 and 10) are in general agreement with other published results. Note the dependence of scattering cross section on ensonification frequency and bubble diameter. The fact that bubbles scatter significant energy only at, and above, the resonant frequency may afford a means of classifying the scattering bubbles according to size. For instance, transmission of short, broadband energy pulses into the medium would excite resonant scattering in the bubbles. A small array of calibrated transducers and/or frequency-selective filters could be used to sense the energy scattered in different frequency bands and thus determine the size of the bubbles. This possibility should be investigated *in vitro*.

In order to be able to efficiently quantify and classify emboli, the characteristics of the emboli signals must be known in detail so that a matched filter or digital correlator can be designed. Many emboli signals, especially those from implanted transducers, originate in the near-field of the transducers giving them special features. The problem was studied theoretically to investigate the characteristics of the emboli signals resulting from the particular transducer instruments being used in our work. A computer program was written to compute the power spectra of idealized signals. Figures 11 and 12 show the time and frequency plots of an idealized bubble ensonified in the transducer's far-field and near-field, respectively. Note that in each case the response is in a relatively narrow frequency band. This narrowband characteristic of the bubble signal makes feasible the type of narrowband matched-filter detector discussed in a later section.

Another program was used to determine the relative sound pressures generated by a scatterer located in the volume common to the two transducer beams. These results allow us to determine the emboli signal response envelopes to be expected from different transducers. These response envelopes are important in the design of a matched-filter processor.

To compute the relative sound pressures, first consider the circular transducer of radius a vibrating in simple harmonic motion shown in Figure 13. The pressure at $P(r,\theta)$ can be expressed as an integral of all area elements, $ds = \sigma d\sigma d\psi$, over the entire surface.

$$P(r,\theta) = \frac{j\rho c k\, U_o}{2\pi} \int_0^a \int_0^{2\pi} \frac{\sigma\, e^{j(wt-kr^1)}}{r^1}\, d\sigma d\psi$$

$$r^1 = (r^2 + \sigma^2 - 2r\sigma \sin\theta \cos\psi)^{\frac{1}{2}} ,$$

where

j = $\sqrt{-1}$

ρ = medium density

c = velocity of sound

k = $2\pi/\lambda$

λ = wavelength of sound

U_o = peak transducer velocity.

To find the relative pressure magnitude $|\underline{P}|$ the above expression is reduced to the following:

$$|\underline{P}(r,\theta)| = \sqrt{I_1^{\,2} + I_2^{\,2}}$$

where

$$I_1 = \int_0^a \int_0^{2\pi} \frac{\sigma \cos Kr^1}{r^1}\, d\sigma d\psi$$

$$I_2 = \int_0^a \int_0^{2\pi} \frac{\sigma \sin Kr^1}{r^1}\, d\sigma d\psi \quad .$$

These integrals have no analytic solution and must be solved by numerical analysis.

Next, the geometry of the transducer assembly must be included. Consider, for instance, the first design of the cuff used for animal implantment discussed earlier in this report. In these units, the transducers were separated by 180° around the circumference of the cuff, and tilted at 45° so that their fields were perpendicular, intersecting at the flow axis as indicated in Figure 14. This configuration was approximated theoretically by assuming the diameter of the transducer crystal was equal to the average of the length and width of the crystals used. To account for the relative pressure magnitude at the receiving crystal due to a particle in the ensonified region, a point by point product was formed of the superimposed relative magnitudes which serve as the acoustic gain functions of the two individual transducer crystals. This was done over a region large enough to include all significant portions of the pressure field.

The results of this process are shown in Figures 15 and 16. The amplitude of the envelope of the scattered signal is shown as a function of the distance off-axis that a bubble is assumed to pass through the cuff. For the small-diameter cuff, the ensonified region is mainly within the near-field of the transducer. For the larger cuff, the region is primarily in the far-field. The amplitude envelopes are asymmetrical because as a scatterer passes through the ensonified region its distance from the transducer crystals changes. The scatterer actually cuts through each transducer pattern at an oblique angle to the pattern's center line. Bubble signals obtained with these transducers during *in vitro* studies show good qualitative agreement with the theoretical mappings. Figure 17 shows some examples of bubble signal envelopes obtained using the small-diameter cuff. These envelopes are similar to those shown in Figure 16 for various distances off-axis.

Spectral Analysis

There is a marked change in the power spectrum of bloodflow during the heart cycle. More energy is contained in the high velocity regions during systole. An important question is whether the emboli power spectrum is of the same type and has the same time variation as the normal bloodflow spectrum. If not, any differences that exist might be exploitable in designing emboli detection instrumentation. Signals obtained from a goat were investigated with this question in mind. The bloodflow signals were separated into four sets by dividing the heart cycle into four phases beginning with the initiation of systole. Power spectra were then computed for each of the four phases. Figure 18 indicates the progression from high-velocity flow to low-velocity flow through the heart cycle. Figure 19 compares normal flow to flow containing many emboli. Note that the envelope of the heavily embolized flow generally has the same spectral shape, but is 5 to 10 dB higher in power. The spectra shown are smoothed results of the averaged spectra for 10 consecutive heart beats.

The largest difference in spectra shape for normal and bubbled flow occurs in the first quarter of the heart cycle. This is shown in Figure 20 in which the spectrum for the bubbled flow has been shifted down by 10 dB. Note that the bubbled flow contains a larger amount of high-frequency energy. The fact that the spectra for the two flows generally have similar time variations is consistent with the theory that the bubbles are uniformly distributed throughout the blood, and moving in synchronism with the fluid transport. However, noticeable exceptions, as indicated in Figure 20, may imply that at least a part of the theory is incorrect. For instance, perhaps bubbles move at velocities that are determined in part by their size. If so, this would be highly important in interpreting the signals for quantification purposes in designing bubble detection instrumentation. Additional work is required to broaden the experimental base and extend the analytical results before such a relationship could be generalized.

EMBOLI SIGNAL DETECTION AND COUNTING

A carrier frequency of 5 MHz results in bloodflow signals of 0 to 10 kHz, within the audio-frequency range. Consequently, on-line monitoring of bloodflow signals to detect the presence of emboli is usually done aurally. The results are highly subjective, and the listener must self-filter the noisy signal to detect the characteristic "chirp" caused by the presence of emboli. Experienced listeners can achieve a useful degree of interpretation of these signals, but even their results are highly qualitative. Meaningful, quantitative analysis of blood-borne emboli by listening to the audible signals is difficult and possible only during low emboli formation rates and stable signal levels.

Continuous, real-time assessment of emboli that includes determination of such factors as size, speed, density, and certain physical properties would significantly improve the ability to interpret the changes occurring in the bloodstream and their relationship to the physiological changes taking place during decompression. Work toward this end has been done by others in the past, including coarse analysis of emboli signal spectra and determination of emboli formation rates. However, such work has not been extensive, and signal processing techniques optimized for this specific purpose apparently have not been employed.

The basic problem is that of extracting the signal caused by an embolus from interfering noise caused by other acoustic reflectors and scatterers. The solution is to employ a filtering process that will suppress the noise and enhance the signal. An optimum filter for this operation is one that, in some sense, optimizes the process of detecting the desired signals. The information required to build an optimum filter is contained in the statistics of the signal and the noise, and the correlation between them.

The idealized filter system is shown in the following block diagram,

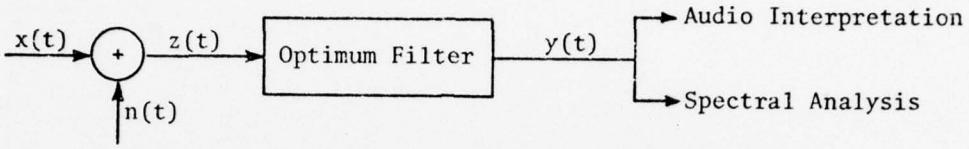

in which x(t) is the signal caused by moving emboli and n(t) is the interfering noise. It is reasonable to assume that for at least short periods the emboli moving past the monitoring point have a Poisson distribution. The Poisson distribution implies that the number of occurrences in nonoverlapping time intervals are independent random variables. The probability of one occurrence is thus proportional to the length of the time interval. With the Poisson process assumption, the emboli signals, x(t), become a pulse sequence with a random amplitude and random occurrence times:

$$x(t) = \sum_{k=-\infty}^{\infty} A_k F(t-t_k) \cos [2\pi f_k (t-t_k)]$$

where $A_k F(t-t_k) \cos [2\pi f_k (t-t_k)]$ is the signal received from the k^{th} embolus. A_k is a random variable describing the signal amplitude, $F(\ )$ is the envelope, t_k is a Poisson random variable, and f_k is the Doppler frequency. The expected value of x(t), $E[x(t)]$, and the auto-correlation function of x(t), $K_{xx}(\tau)$, are

$$E[x(t)] = \lambda \cdot E[A] \cdot g$$

$$K_{xx}(\tau) = \lambda \cdot E[A^2] \cdot K_{ss}(\tau) + (\lambda \cdot E[A] \cdot g)^2 \ ,$$

where

λ = parameter characterizing the Poisson process

$$g = \int_{-\infty}^{\infty} s(t)dt$$

$$K_{ss}(\tau) = \int_{-\infty}^{\infty} s(t+\tau)s(t)dt \ .$$

The solution for the transfer function of the optimum filter is

$$H(f) = \frac{K_{xz}(f)}{K_{zz}(f)} \ .$$

If the interfering noise is assumed to be a zero mean process independent of emboli signals, then

$$H(f) = \frac{K_{xx}(f)}{K_{xx}(f) + K_{nn}(f)} \ .$$

If the power spectral densities of the signal, $K_{xx}(f)$, and the noise, $K_{nn}(f)$, could be determined, the optimum filter could be built.

Unfortunately, the above model is not directly applicable. The signal and noise characteristics are not the stationary processes assumed above. They vary within the heart cycle and also depend on the monitoring point, probe orientation, and subject's anatomy. No two subjects will produce the same signals. Because of this highly complicated situation, a truly optimum filtering process would require matching the filter to each particular monitoring situation, and would also involve time-variable filter parameters to account for the nonstationarity of the signals.

Development of such a capability was far beyond the scope of this effort. Instead, a relatively modest approach was taken. The first step was to increase the signal-to-noise ratio by capitalizing on the

narrowband characteristics of the signals. As shown earlier in Figures 11 and 12, signals from individual emboli are typically several hundred hertz wide compared to a bandwidth of several thousand hertz for the overall flow. The signal-to-noise ratio, therefore, can be increased by dividing the spectrum of the overall flow into several adjacent channels of a few hundred hertz each. Signal amplitude detection thresholds set above the noise level in each channel will be more sensitive to emboli signals than will a single detection threshold set above the broadband noise level. Figure 21 shows the output of a four-channel prototype processor using this principle. Note how the emboli signals appear in the separate channels. Figure 22 is a block diagram of a 15-channel emboli detector/counter system built for laboratory use early in the program. The system employed 15 single-stage filters covering a total bandwidth of 8 kHz. Good results were obtained from this device when reasonably high-quality signals were available. The relative channel thresholds were adjusted to reflect the noise-level frequency dependence generally observed for most subjects. For each monitoring situation, the gain of the overall system was adjusted to set the pre-dive background noise level just below detection in any channel.

A second, improved detector/counter was developed. The filter characteristics were improved by using two-stage Butterworth filters. An optimum filter is matched to the signal of interest--that is, the impulse response of the filter will be that of the signal. The impulse response of a two-stage Butterworth filter more closely approximates that of an embolus signal than does that of a single-stage filter. Because the two-stage response more closely matches the bubble signal, it gives a larger peak output for a given bubble than will the corresponding one-stage filter. The impulse responses of the two types of filters are illustrated in the following sketch.

one-stage filter impulse response

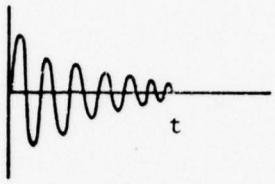

two-stage filter impulse response

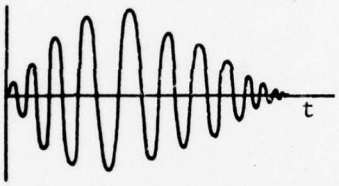

Additional improvements were made in the filter bandwidths and spacing, and in post-detection signal processing. In both human and animal data, the average spectral noise power is higher at the lower frequencies. In the new counter, the filter bandwidths were consequently narrower at the low frequencies to offset the larger noise power. The spacing of the filters was also reduced to decrease signal losses in the inter-filter notches. The total bandwidth was reduced about 4 kHz as *vena cava* flow in animals and pulmonary artery flow in man do not significantly exceed 4000 Hz on the 5-MHz Doppler system. Twelve filters span the 4-kHz bandwidth. Figure 23 shows the bandwidths and placement of the filters.

Figure 24 is a block diagram of the improved detector/counter. After the Doppler-shifted signal is passed through the bandpass filters, it is envelope-detected and the estimated impulsive noise in each channel is subtracted from the averaged signal. Because of their limited

bandwidth, signals from individual bubbles will be passed in only one to three adjacent channels. Impulsive noise, on the other hand, tends to be wide-band and simultaneously raises the levels of many adjacent filters. To take advantage of this, a weighted sum of all outputs is subtracted from the output of each individual channel. Thus noise tends to be extracted from the signal while bubbles pass with little attenuation.

Figure 25 shows the counter that was built. It has two identical, parallel, detector/counter systems to permit simultaneous monitoring of two subjects. This counter is currently being used for both on-line and post-dive analysis of Doppler data. It is fully interfaced with the on-line Wang computer system at VMRC so that emboli counts are digitally recorded and plotted in real time along with other dive parameters such as pressure (depth) and gas analyses results. Figures 26 and 27 are plots made during post-dive analyses of typical dives. Note the ease with which the dive profile can be correlated with emboli count.

FUTURE WORK

Much experimental and theoretical work is needed to properly develop the potential for detecting, quantifying, and classifying abnormal emboli in bloodflow. The potential applications are, of course, much broader than just hyperbaric research, extending into clinical diagnostics and monitoring during surgical operations. Systematic research and development effort is needed to (1) determine the characteristics of the various possible emboli and noise signals, (2) develop adaptive, matched-filter processor techniques for optimum detection of abnormal emboli, (3) assess and evaluate the expected performance of these approaches using computer simulation, and (4) develop prototype hardware and software to test and demonstrate these concepts. Because of their prime importance, attention should first be focused on development of optimum noninvasive methods for detecting gas emboli. Promising approaches should be simulated on a digital computer and assessed using actual bloodflow signals which have been obtained from decompressing humans. Later, the characteristics of signals from other abnormal emboli should be investigated and general detection, quantification, and classification algorithms developed, simulated and evaluated.

Emboli Scattering Properties

To proceed systematically, it is necessary that the scattering of sound from various types of emboli (bubbles, lipids, coagulated blood, etc.) be fully understood. Experimental and theoretical work is required to formulate accurate models of the signals of these emboli. Scattering strength as a function of emboli type, size, ensonification frequency, and transducer type and orientation should be determined. For instance, resonant scattering might be useful for classifying and sizing bubbles. An ideal air bubble exhibits a scattering cross section three orders of magnitude larger than a bubble physically twice as large. It is possible,

then, that operation at one frequency will selectively enhance the signals from a particular bubble size, and swept-frequency operation may permit a wide range of sizes to be detected instantaneously. (At 5 MHz the resonant bubble size is about 1 micron.) Because blood-borne bubbles are not ideal air bubbles, resonance effects will not be as pronounced as the ideal case would indicate, but certainly they should be investigated.

Signal Processing

An optimum signal processor can take many forms and yield a wide range of results depending upon the restrictions within which the optimization was done. The effort described herein produced a small, portable instrument for use in on-line, real-time assessment of bloodflow signals. However, because of the relatively limited scope of the program, the use of large, digital computers that can provide a truly optimum signal processing capability has not been considered to date. In the long run, particularly if bloodflow and emboli signals prove to be rich in diagnostic information and directly tied to the physiological processes involved, it will be desirable to develop and apply such a comprehensive signal processing capability.

ACKNOWLEDGMENTS

Support for this work was derived mainly from ONR Contract N00014-69C-0402 with the Virginia Mason Research Center. Dr. Kent Smith of VMRC and his entire staff, especially Dr. Brian D'Aoust and Mr. Roland White, have won our special appreciation. Their enthusiastic support, scientific insight, and unlimited patience and understanding were invaluable in motivating our efforts, familiarizing us with their research needs, focusing our attention, and guiding our efforts in rewarding directions. Dr. Jon O. Jacobson, formerly with VMRC, was instrumental in involving us in the VMRC work and was a contributing collaborator throughout the project.

Graduate student research assistance was a highly important element in this program. In particular, George Huang and Edward O. Belcher (co-author) were directly responsible for much of the success achieved with the bloodflow monitor and the emboli counter development.

Invaluable assistance was also provided by the managment and support staff at this Laboratory including: Mr. Medford Hogman, program area manager; Dr. John Ehrenberg, signal processing specialist; Mr. Harvey McMichael and Mr. Elbert Pence, physicists; Mr. Keith Yett, mechanical engineer; and Messrs. Paul Sulonen, Richard Stahl and Carl Larson, electronic technicians, who painstakingly developed the techniques involved in the art of assembling implantable transducers capable of long-term operation.

REFERENCES

1. Devin, C., "Survey of thermal, radiation, and viscous damping of pulsating air bubbles in water," Journal of the Acoustical Society of America, Vol. 31 (December 1959) p. 1654.

2. Kinsler, L.E. and A.R. Frey, Fundamentals of Acoustics (John Wiley and Sons, New York, 1961) pp. 174-178.

3. Nishi, R.Y., "Ultrasonic detection of bubbles with Doppler flow transducers," Ultrasonics, Vol. 10, No. 4 (July 1972) p. 173.

4. Zemanek, J., "Beam behavior within the nearfield of a vibrating piston," Journal of the Acoustical Society of America, Vol. 49, No. 1 (January 1971) p. 181.

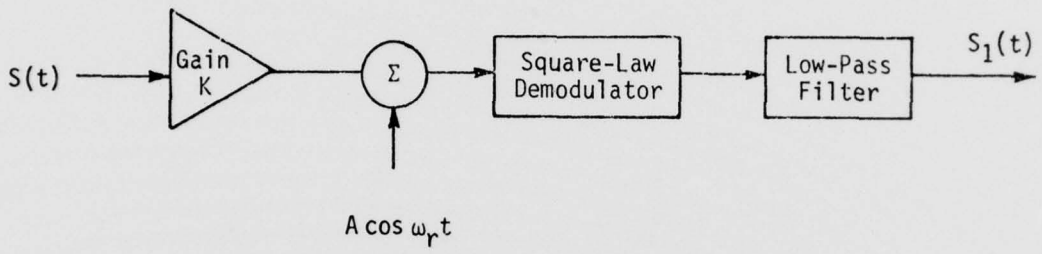

Figure 1. Square-law demodulation.

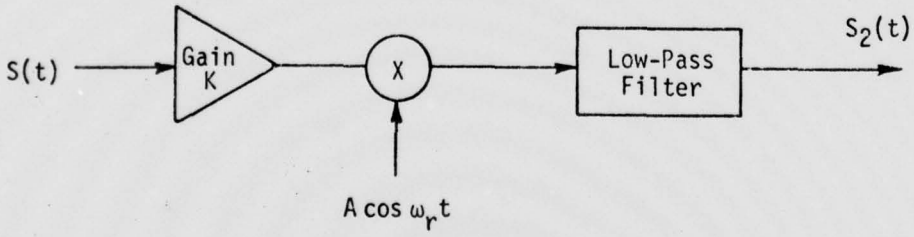

Figure 2. Mixer Frequer rsion.

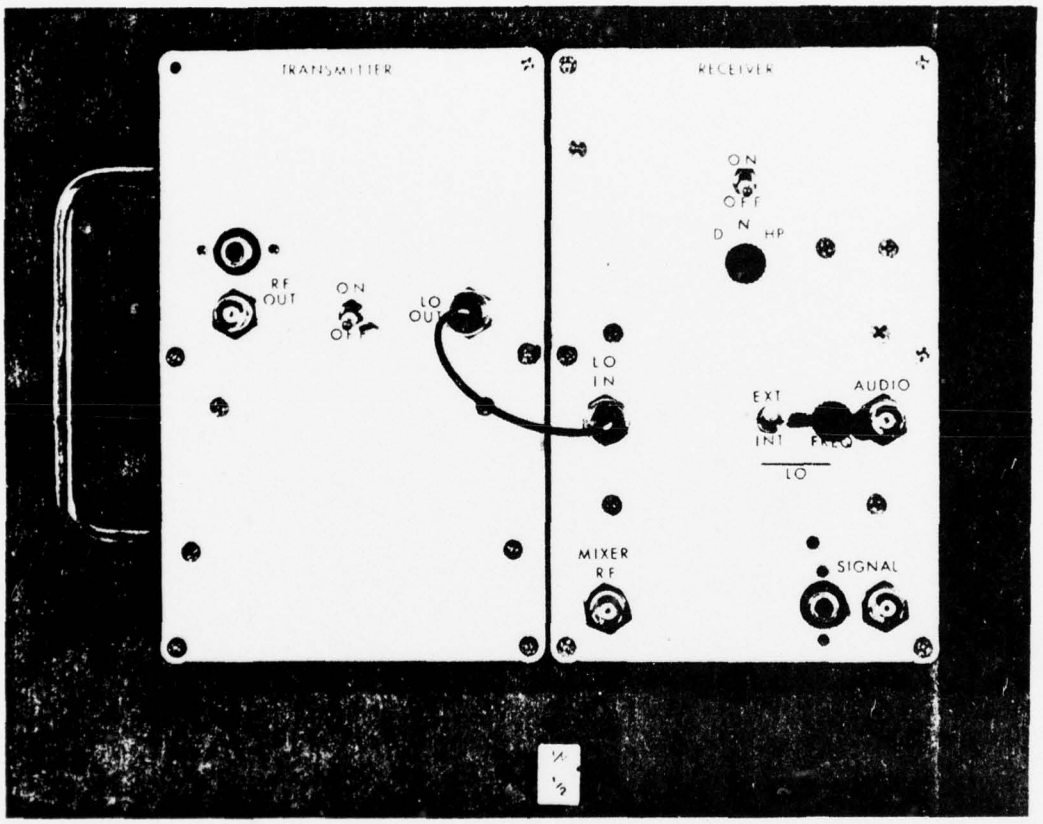

Figure 4. 5-MHz Doppler bloodflow monitor.

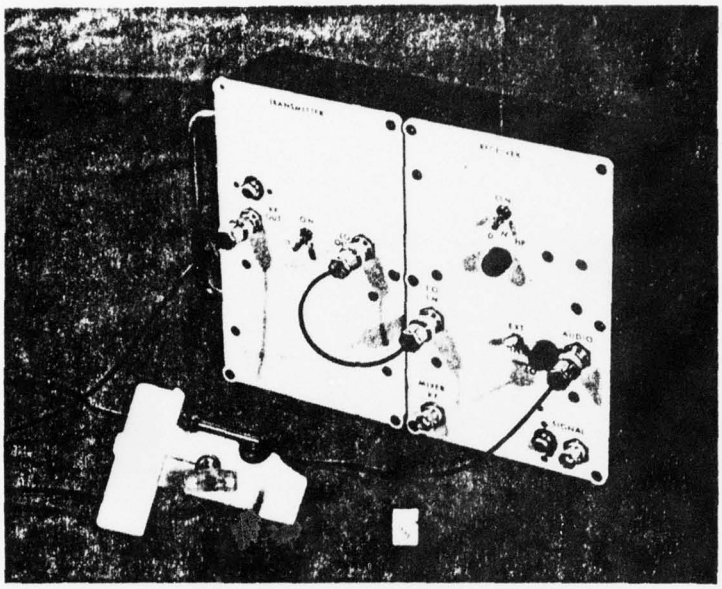

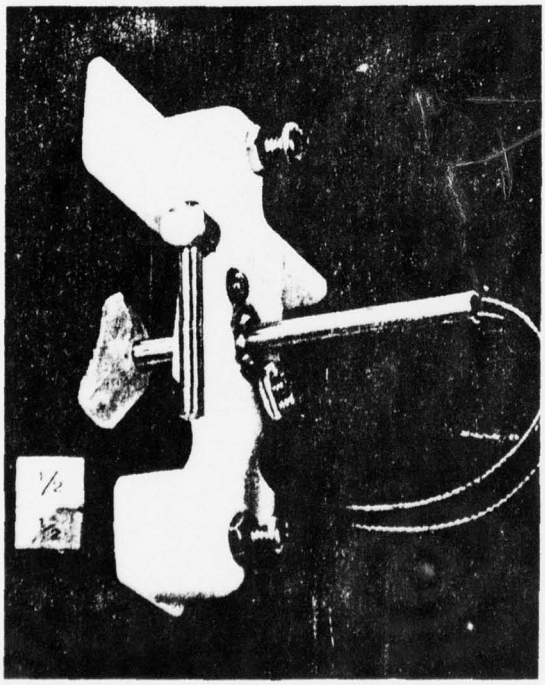

Figure 5. 5-MHz Doppler bloodflow monitor and adjustable chest probe.

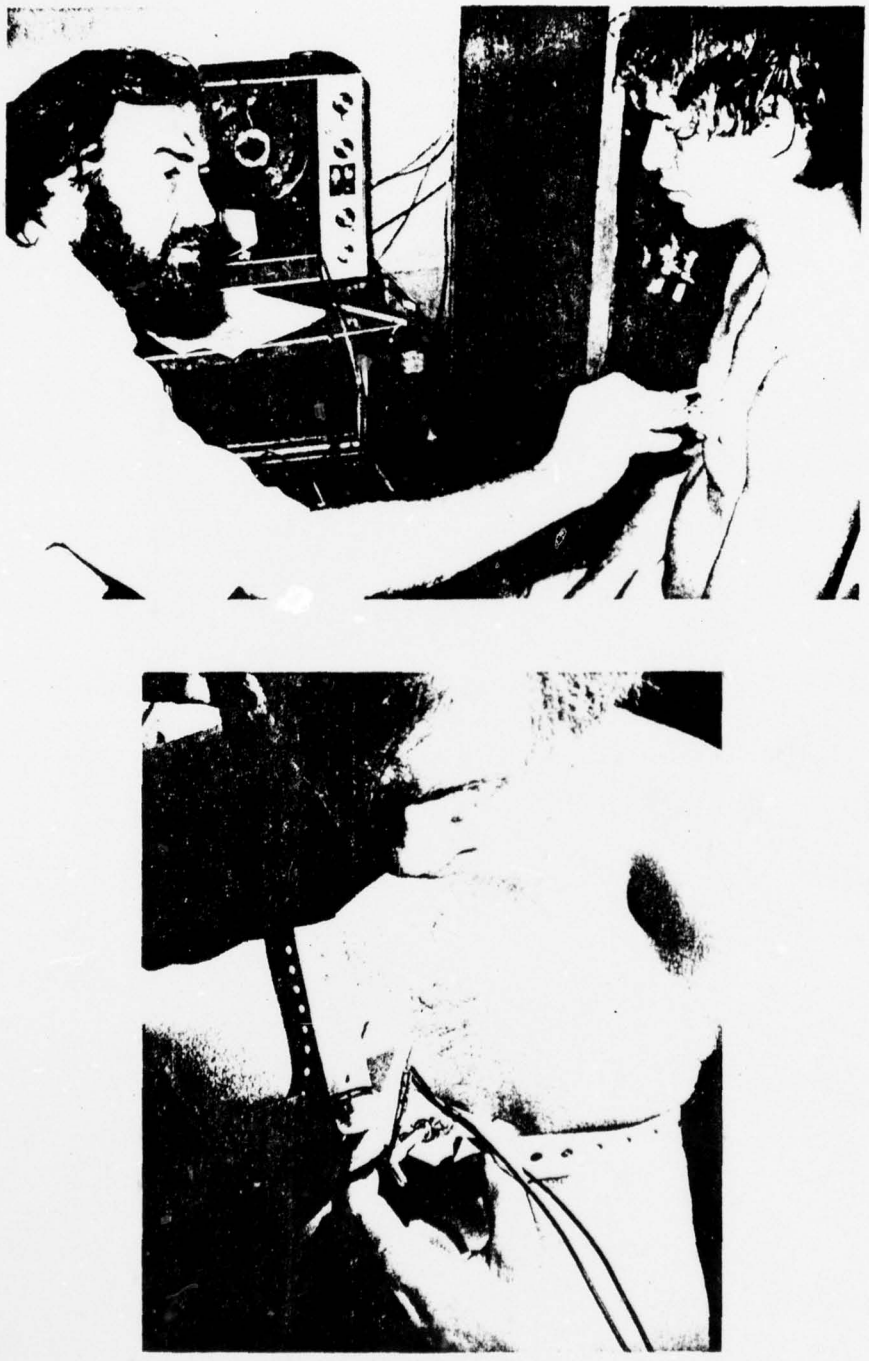

Figure 6. Adjusting chest probe on subject prior to compression in hyperbaric chamber.

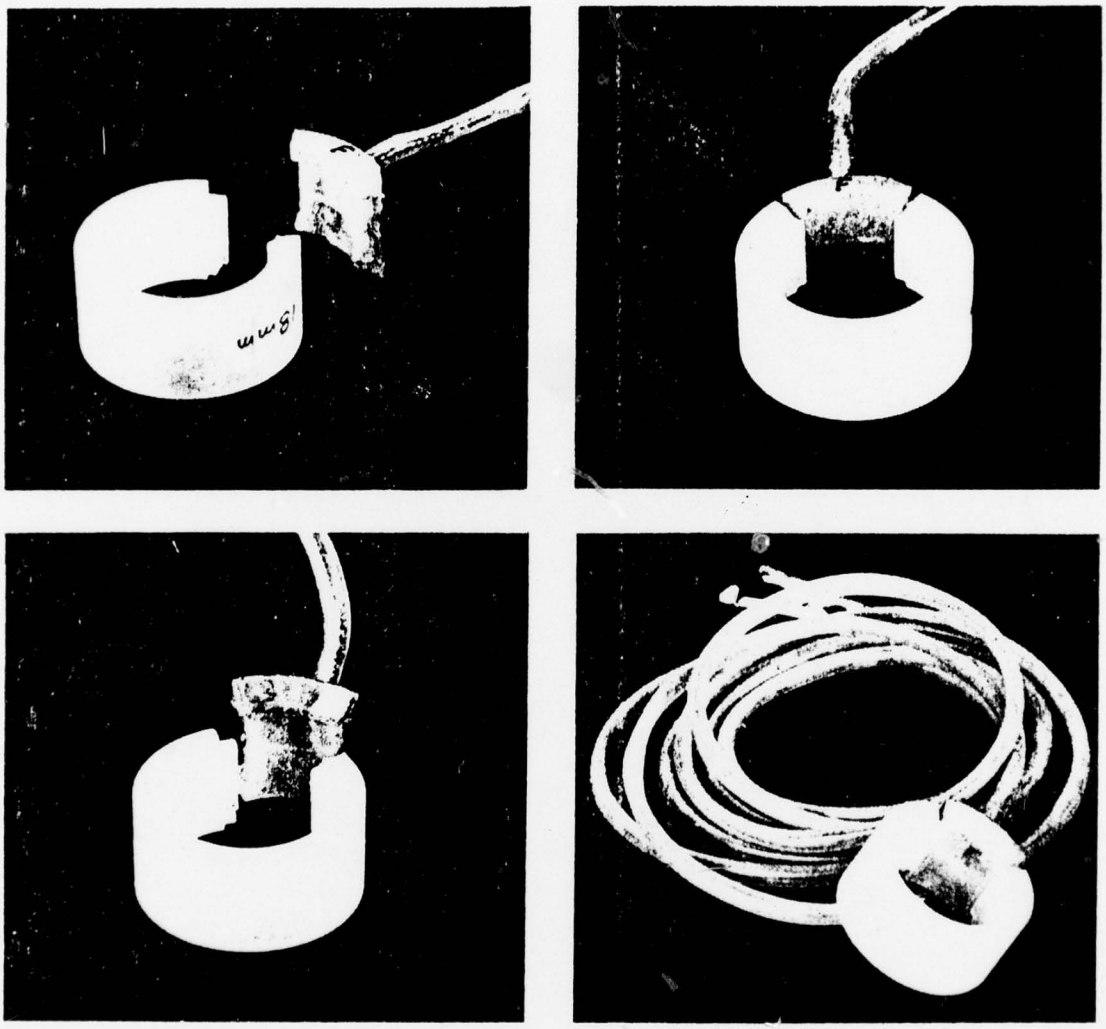

Figure 7. Implantable cuff transducer. Universal insert holding transducer crystals fits into a wide range of cuff sizes.

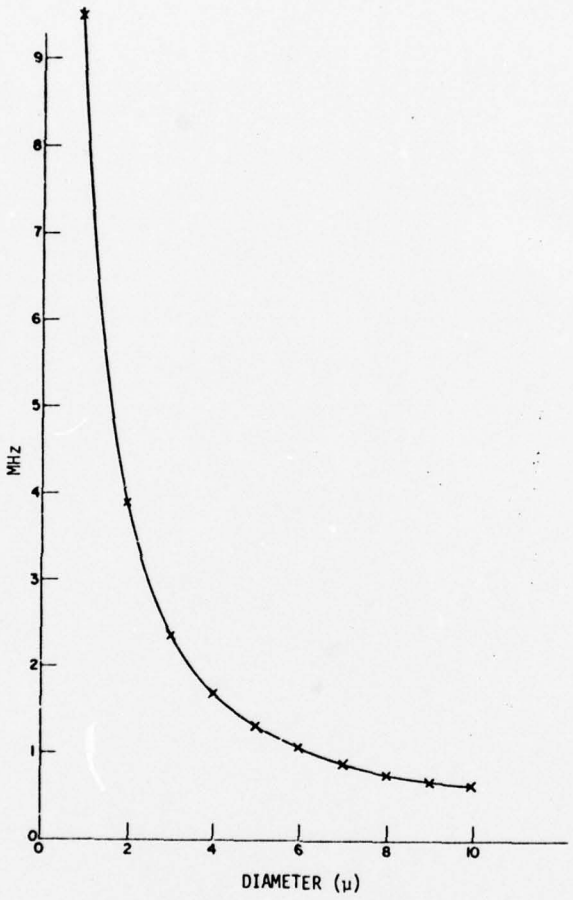

Figure 8. Resonant frequency versus embolus diameter.

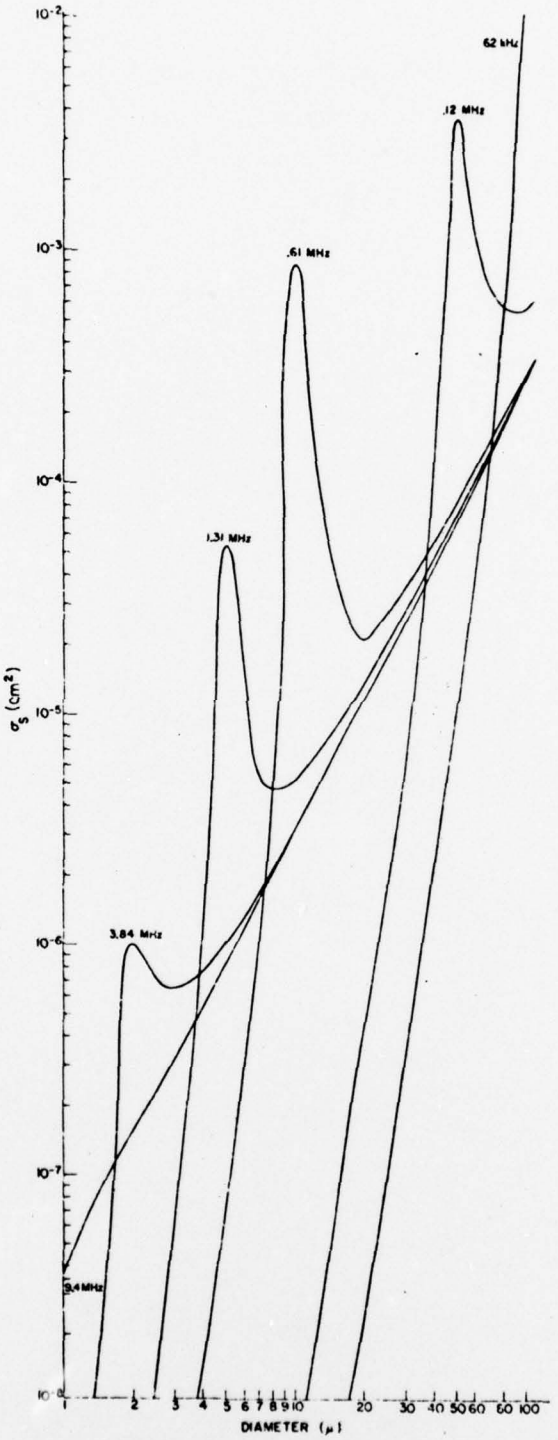

Figure 9. Scattering cross section of oxygen bubbles at one atmosphere pressure.

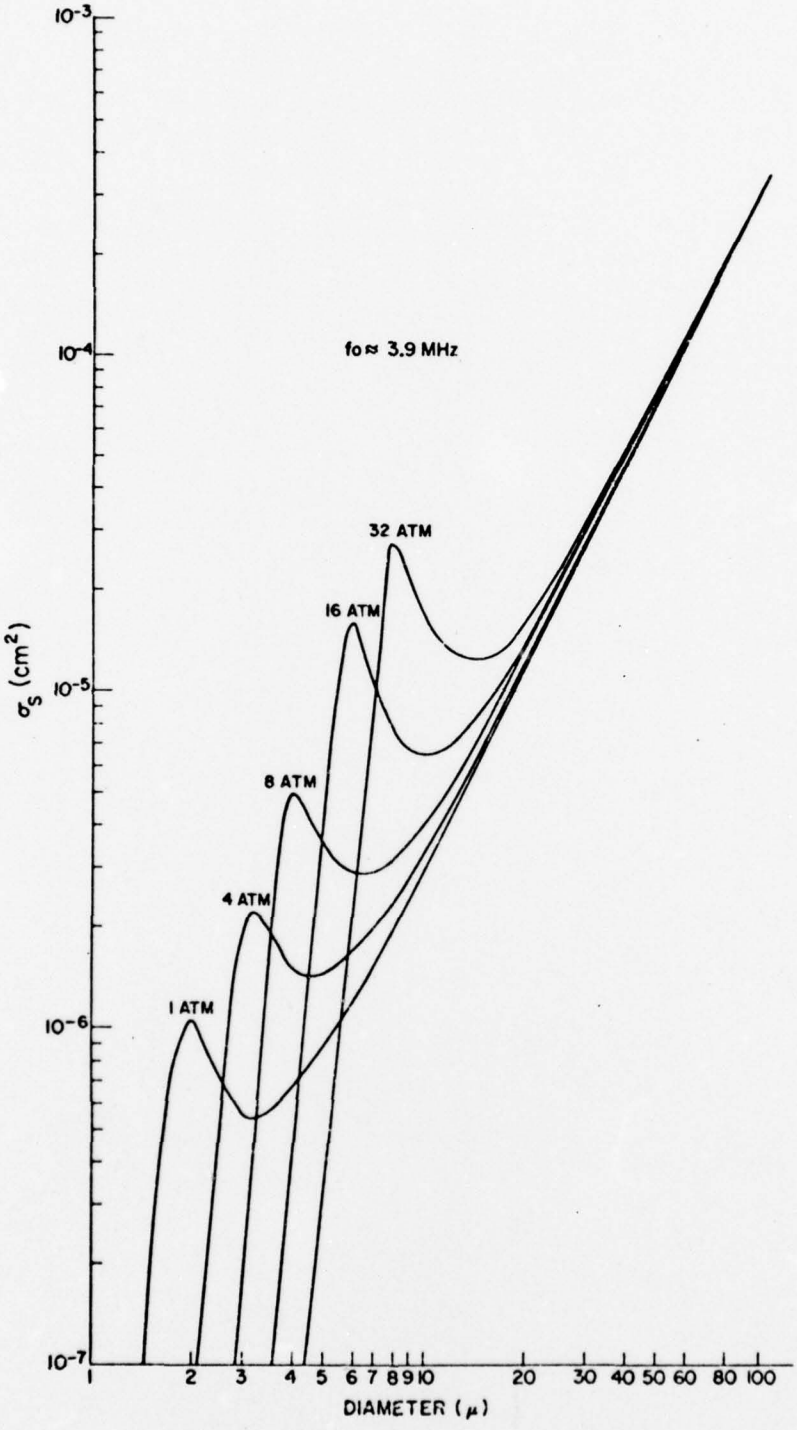

Figure 10. Scattering cross section of oxygen bubbles.

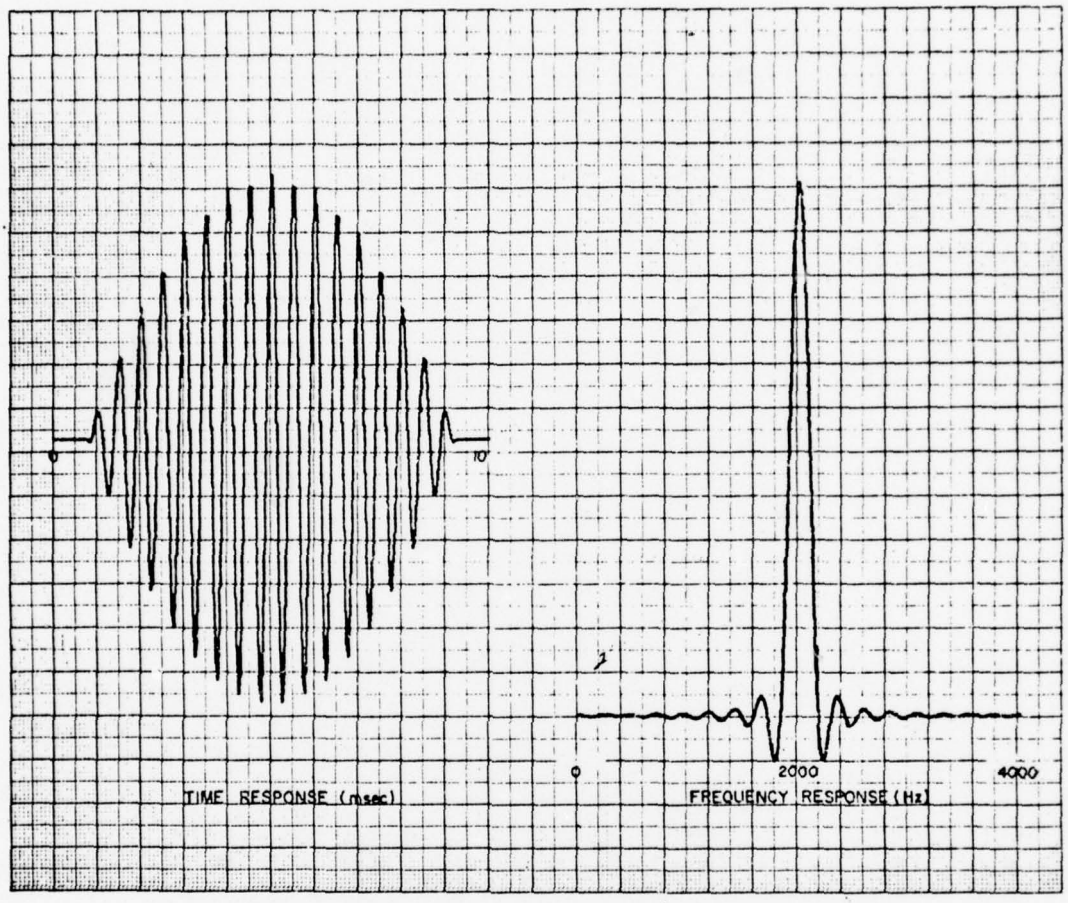

Figure 11. Time and frequency response for bubbles in the far field.

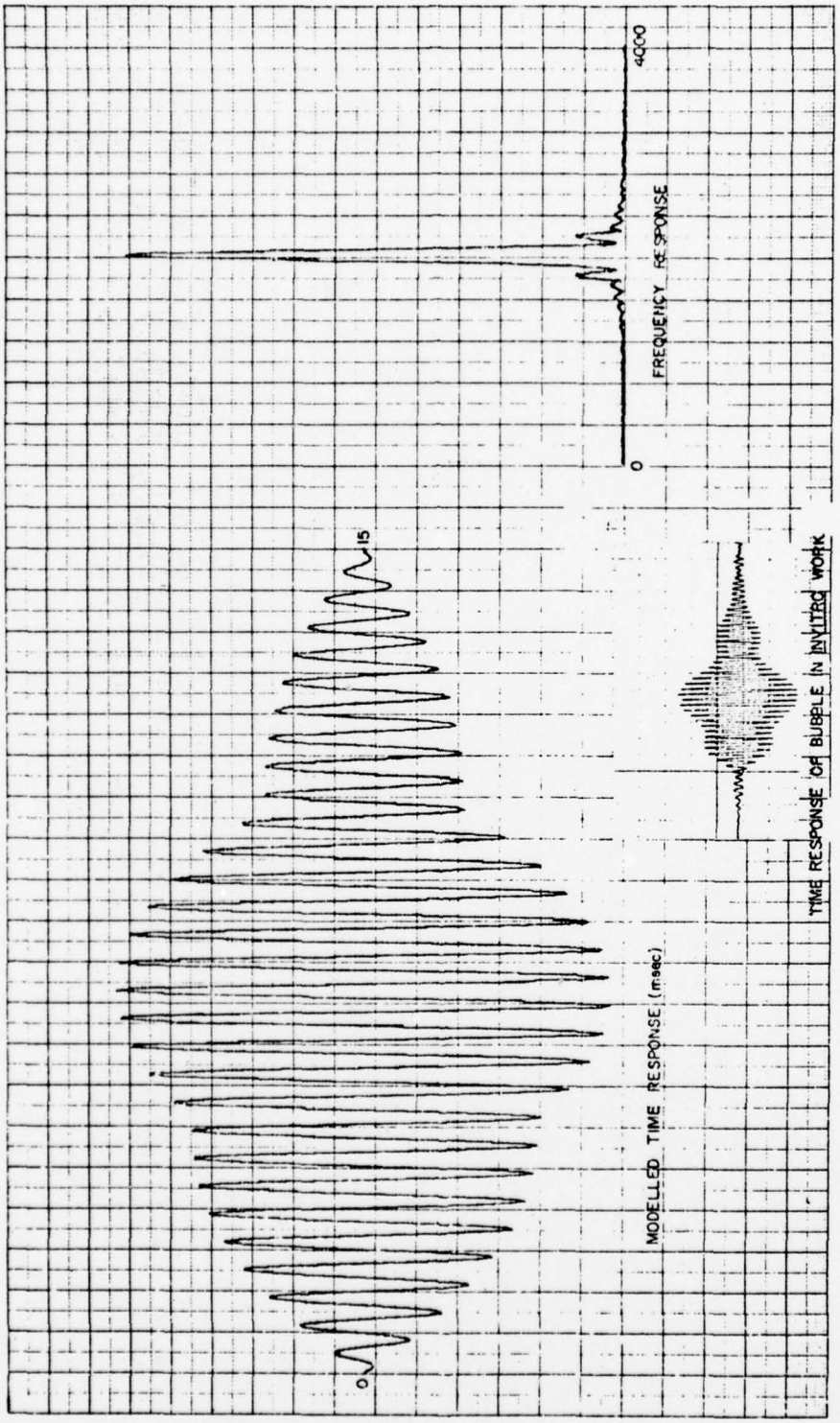

Figure 12. Time and frequency response of bubbles in the near field.

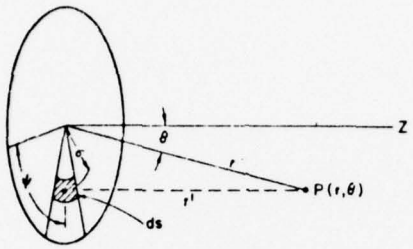

Figure 13. Circular transducer coordinate system.

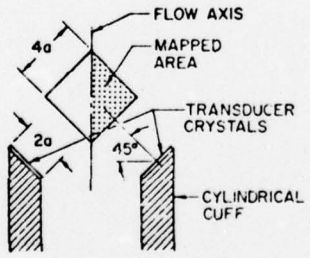

Figure 14. Cross-sectional view of cuff and mapped area.

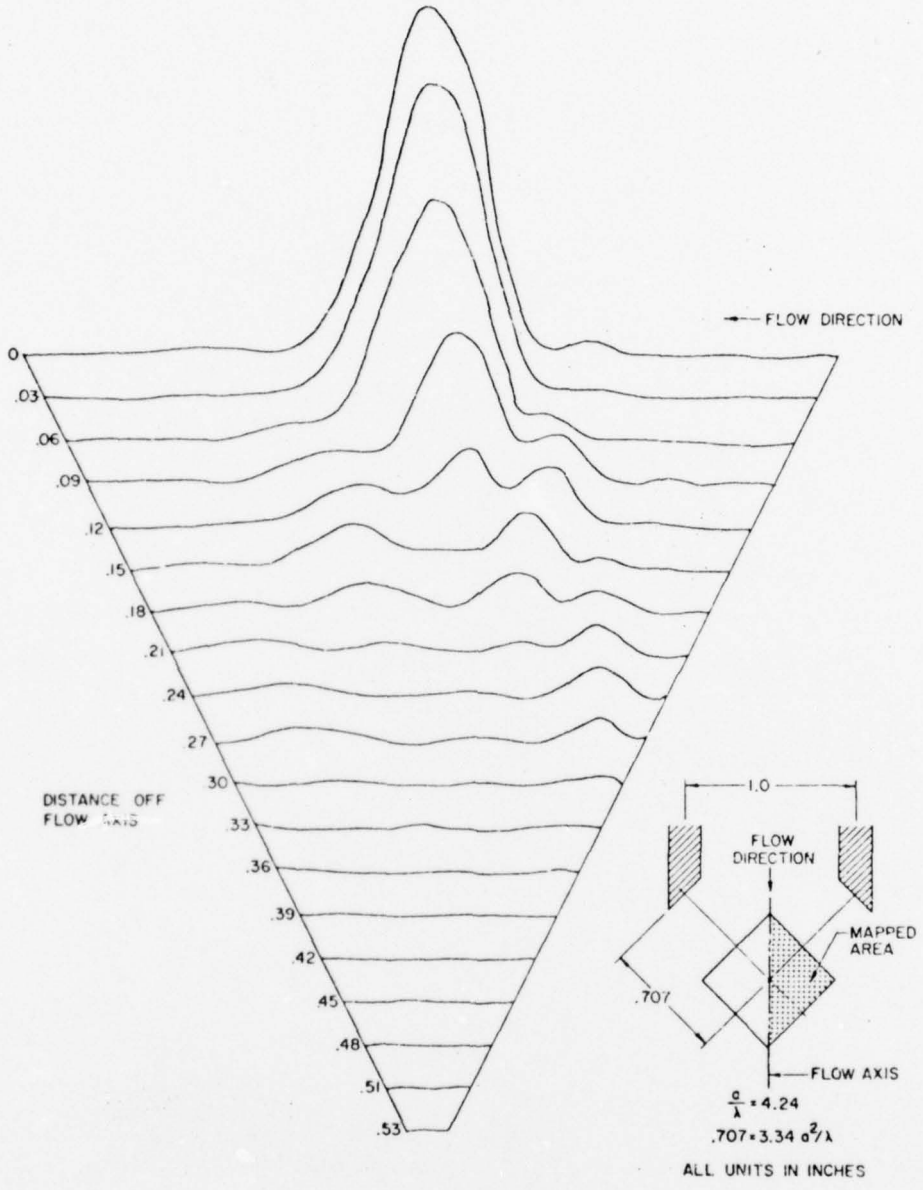

Figure 15. Relative pressure magnitude for large diameter cuff.

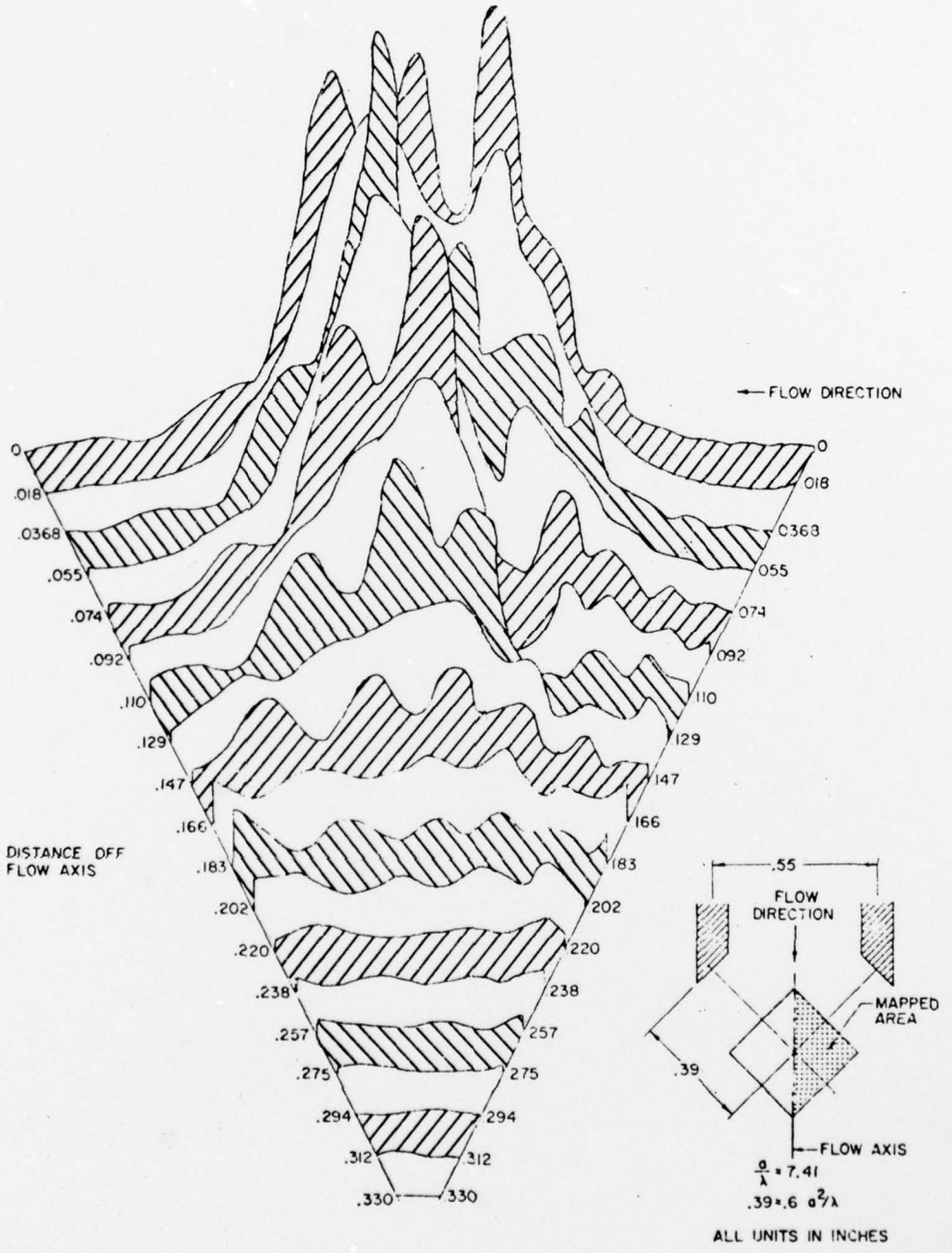

Figure 16. Relative pressure magnitude for small diameter cuff.

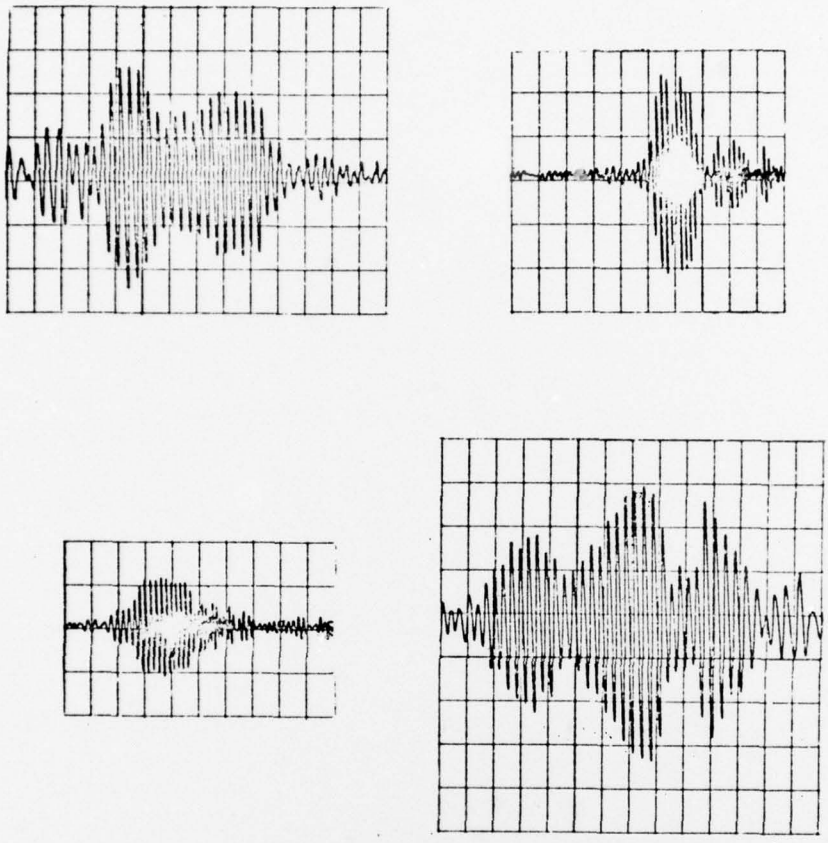

Figure 17. Examples of bubble signal envelopes detected in vitro using a small diameter cuff.

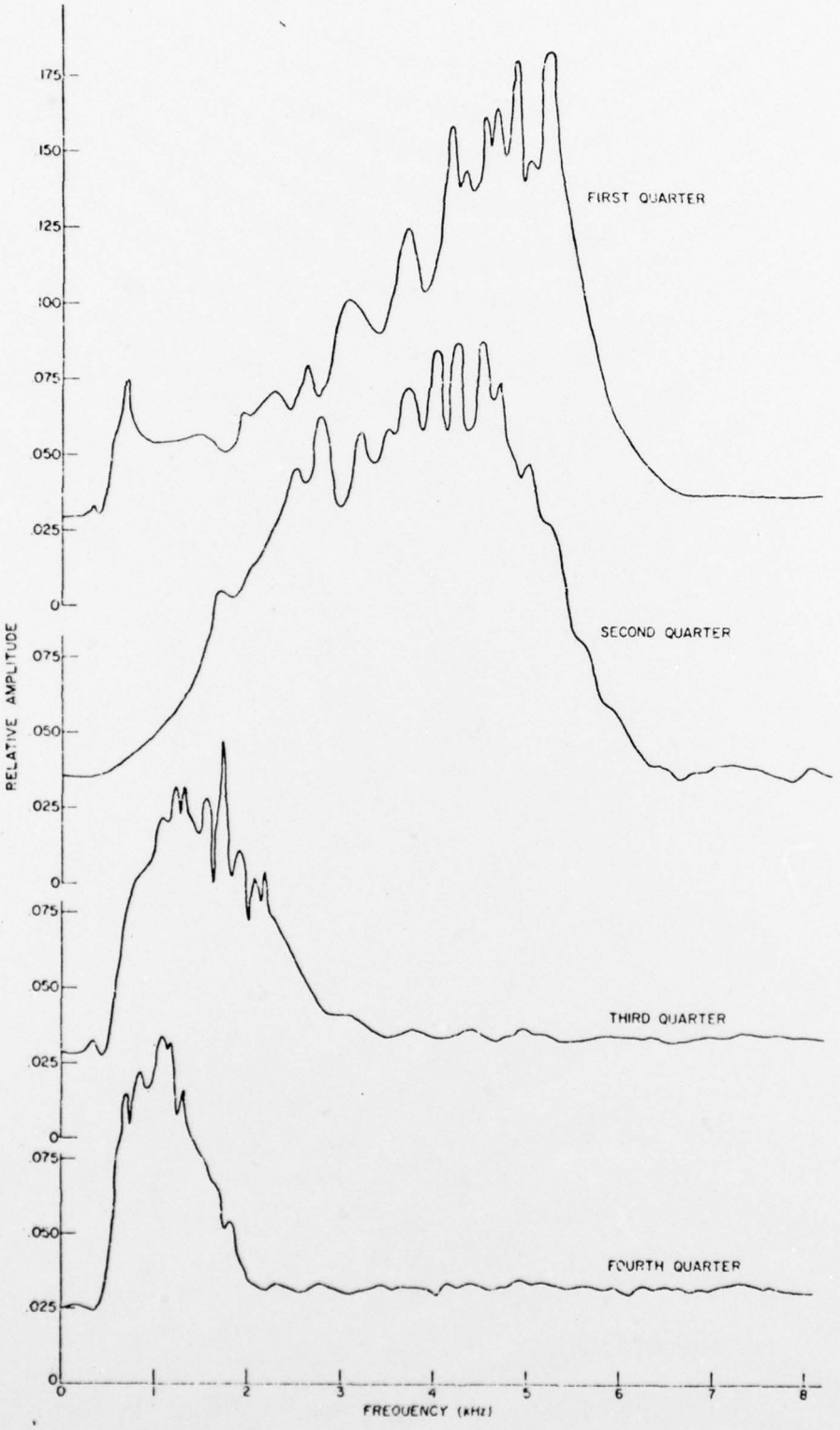

Figure 18. Normal pulmonary artery bloodflow spectra--goat data.

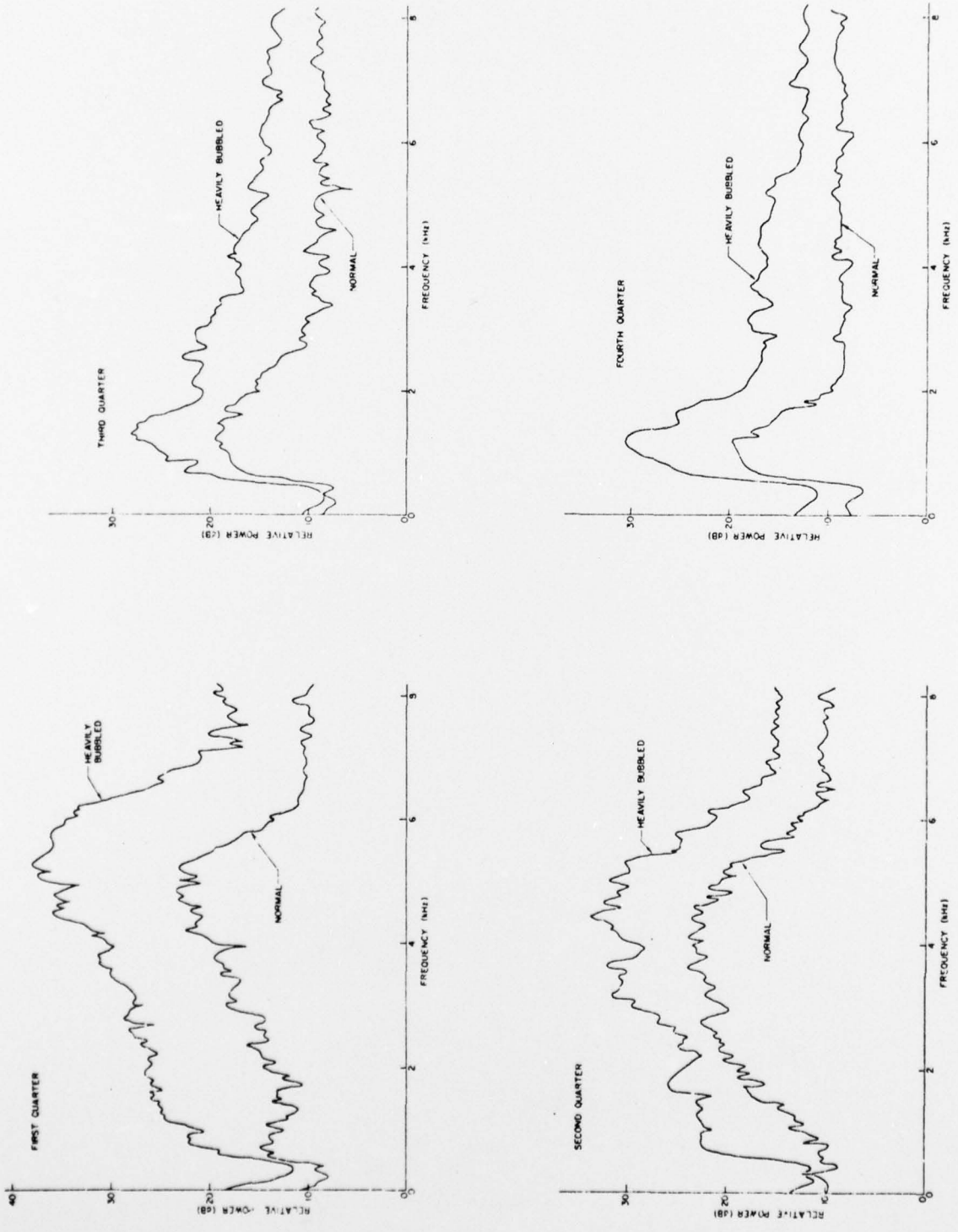

Figure 19. Bloodflow spectra for heart cycle quarters--goat data.

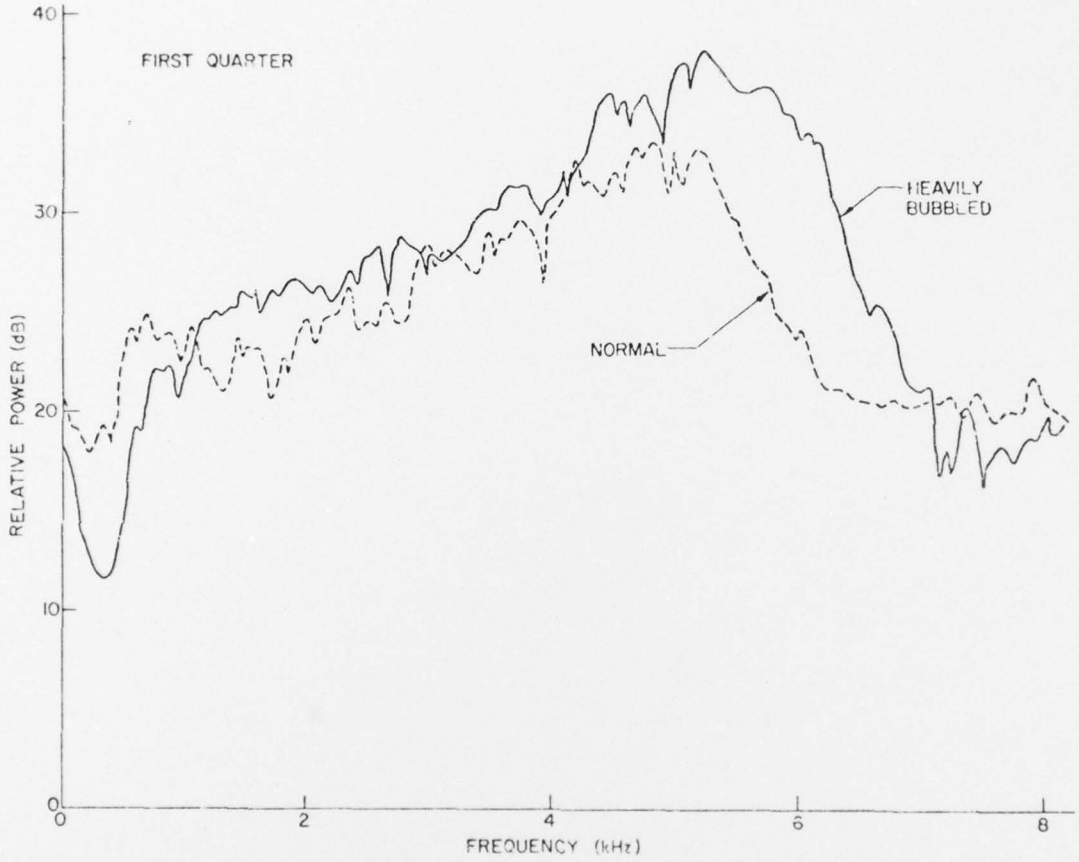

Figure 20. Comparison of normal and heavily bubbled bloodflow spectra--goat data.

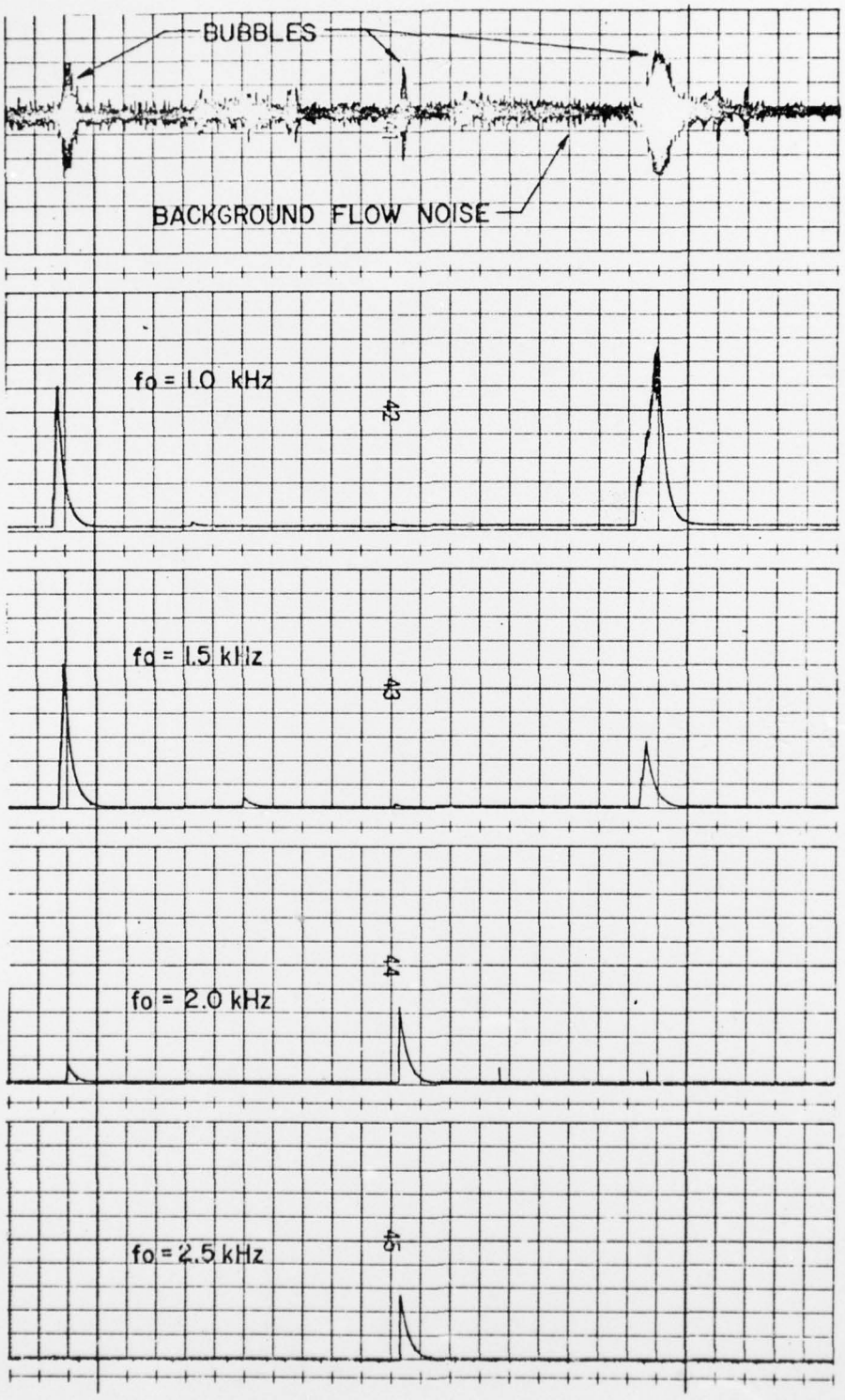

Figure 21. Embolus detection in four frequency bands centered as shown.

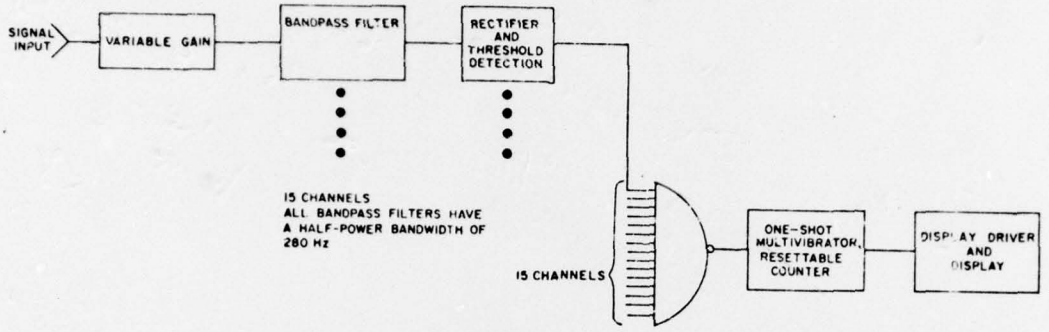

Figure 22. Block diagram of 15-channel emboli detector/counter system built for laboratory use early in the program.

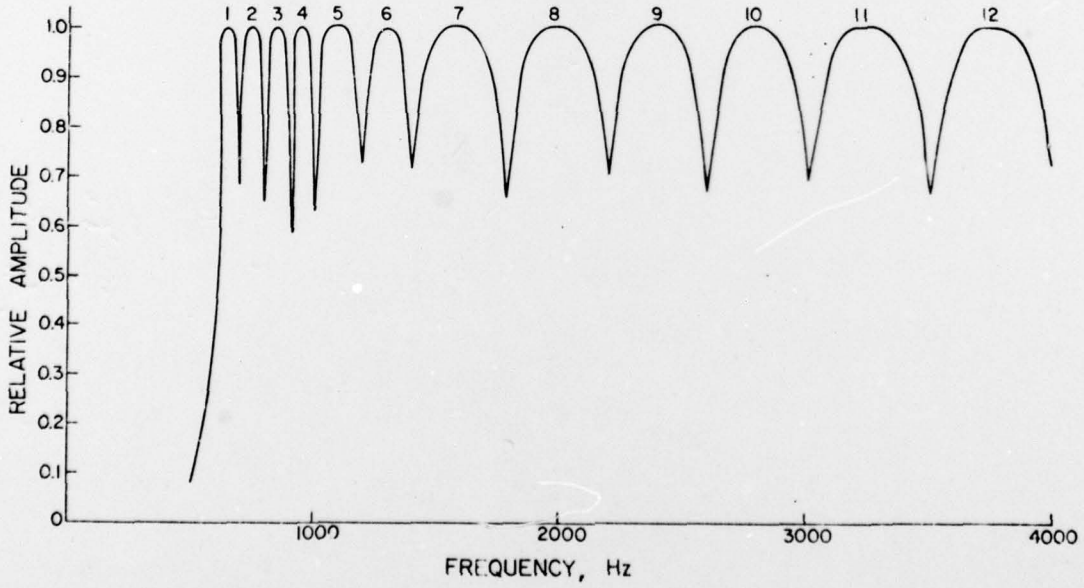

Figure 23. Frequency response of 12-channel counter.

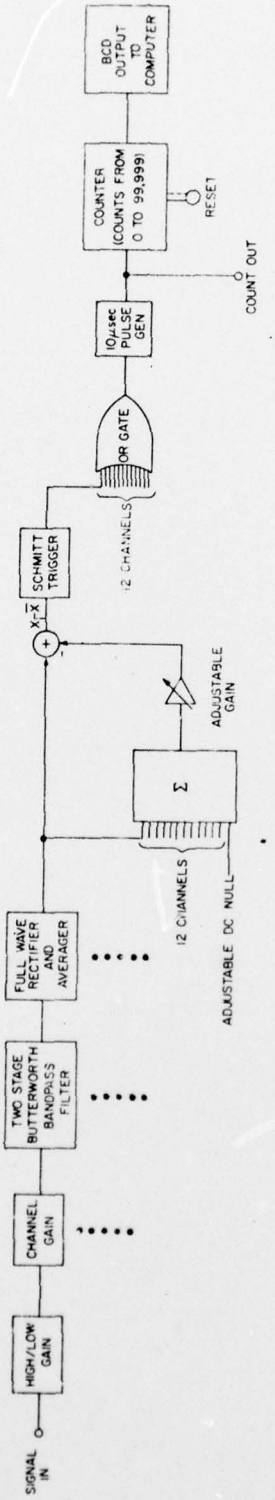

Figure 24. Block diagram of improved emboli detector/counter.

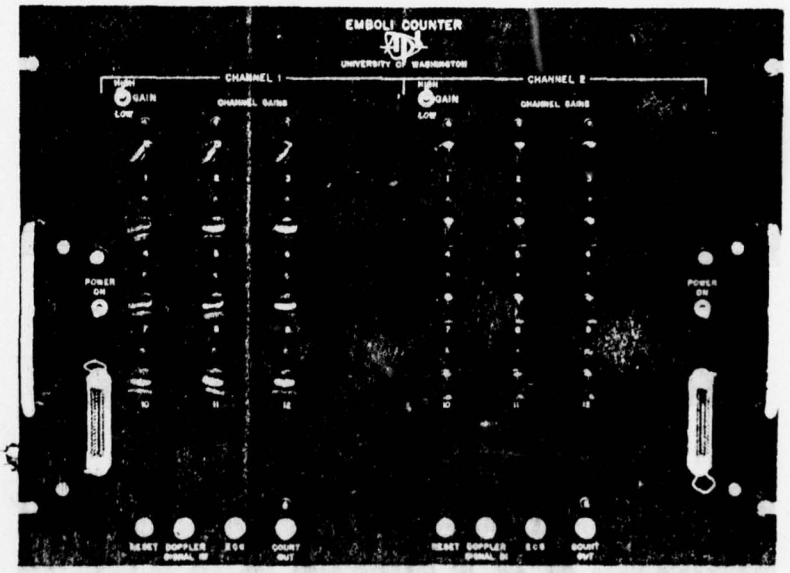

Figure 25a. Two-counter system. Front panel measures 19" x 13.97".

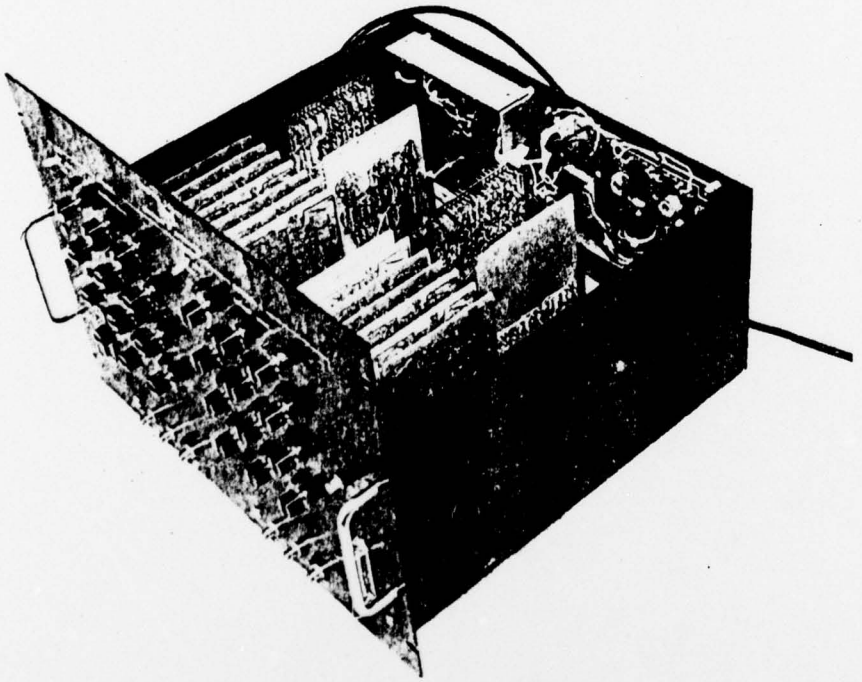

Figure 25b. Two-counter system, top view. Electronics box is 16" deep, 17.25" wide, and 8" high.

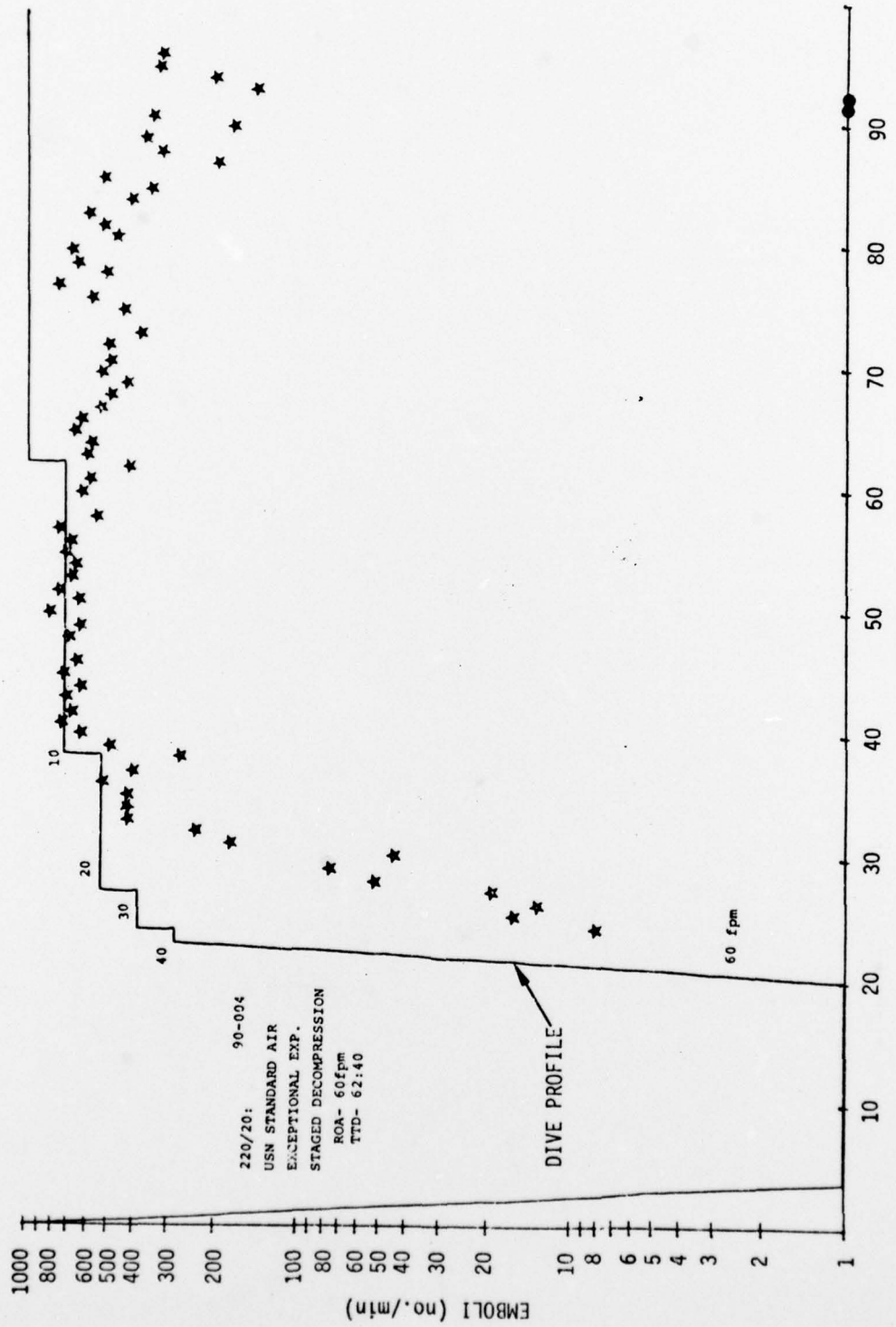

Figure 26. Emboli counts and dive profile without recompression.

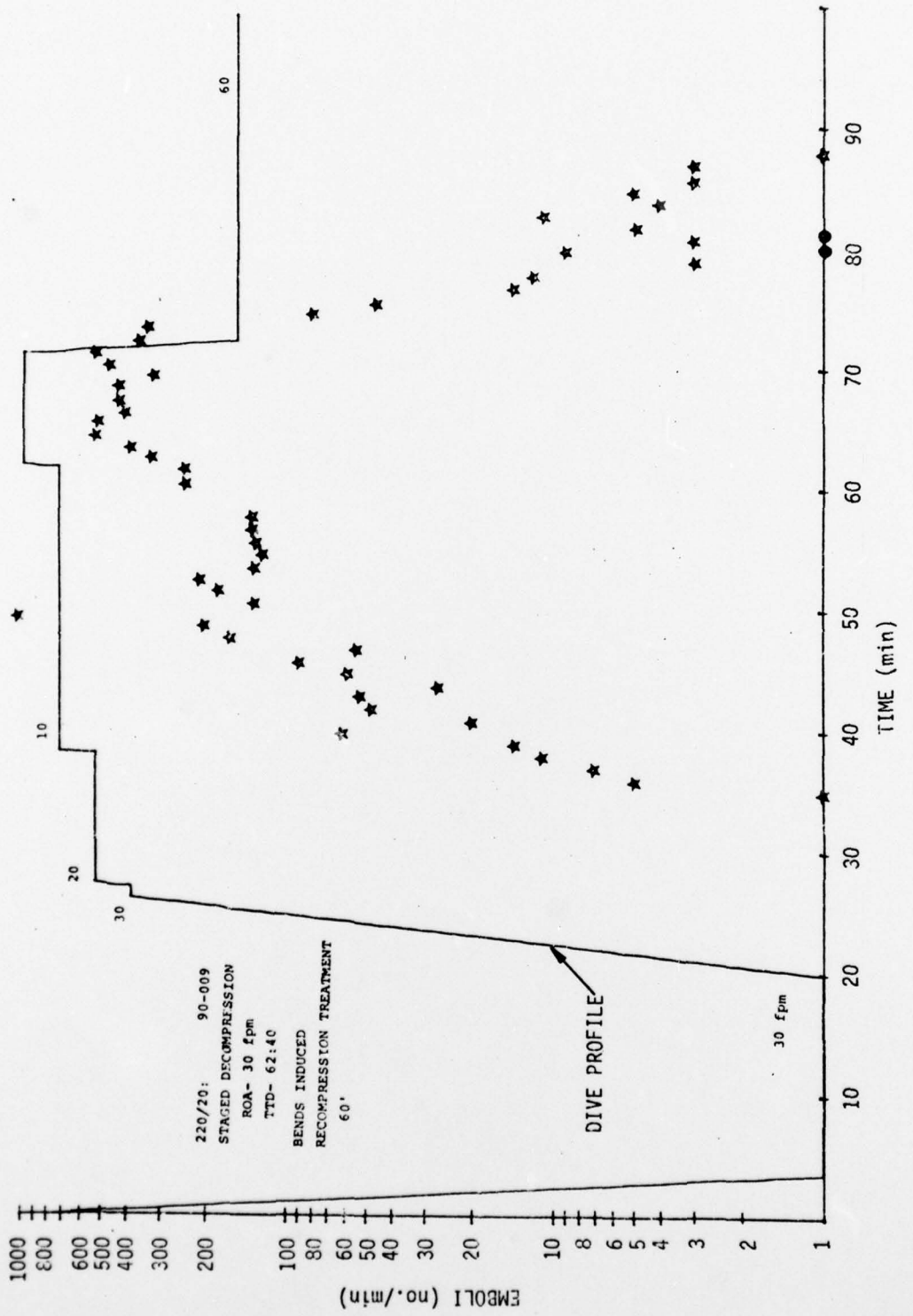

Figure 27. Emboli counts and dive profile with recompression.

PUBLICATIONS

Kent H. Smith, D.V.M., Ph.D.

Contract No. N00014-69-C-0402

1. Smith, K.H. The Relativity of Theoretical Tissue Gas Tensions and Doppler Detected Bubbles in the Vascular System. (Presented at First Annual Western Conference on Hyperbaric Medicine, Good Samaritan Hospital, Los Angeles, 1970).

2. Smith, K.H., and Spencer, M.P. Doppler Indices of Decompression Sickness; Their Evaluation and Use. Aerospace Med. 41:1396-1400, 1970.

3. Smith, K.H., and Johanson, D.C. Technical Report. ONR Contract N00014-C-0402, Project NR 101-750. 1970.

4. Smith, K.H. Application of Doppler Ultrasound to the Objective Detection of Decompression Sickness, and Etiology and Pathogenesis of Aseptic Bone Necrosis. (Abstract presented at BUMED-ONR Navywide Workshop in High Pressure Biomedical Research, U.S. Naval Submarine Medical Center, Groton, Conn., May, 1971).

5. Smith, K.H. and Stayton, R.L. Safe Decompression Procedures--Must They be Bubble Free? Sixth Symposium on Underwater Physiology, San Diego, July 6-10, 1975.

6. Smith, K.H.; Stegall, P.H.; and D'Aoust, B.G. Pathophysiology of Decompression Sickness, International Symposium on Man-in-the-Sea, Honolulu, Hawaii, July 13-15, 1975.

SECURITY CLASSIFICATION OF THIS PAGE (When Data Entered)

REPORT DOCUMENTATION PAGE

READ INSTRUCTIONS BEFORE COMPLETING FORM

1. REPORT NUMBER: N00014-69-C-0402	2. GOVT ACCESSION NO.
3. RECIPIENT'S CATALOG NUMBER	
4. TITLE (and Subtitle): Hyperbaric Decompression by Means of Bubble Detection	5. TYPE OF REPORT & PERIOD COVERED: Final Report
	6. PERFORMING ORG. REPORT NUMBER
7. AUTHOR(s): Kent H. Smith and Lee Stayton	8. CONTRACT OR GRANT NUMBER(s)
9. PERFORMING ORGANIZATION NAME AND ADDRESS: Virginia Mason Research Center, 1000 Seneca Street, Seattle, Washington 98101	10. PROGRAM ELEMENT, PROJECT, TASK AREA & WORK UNIT NUMBERS
11. CONTROLLING OFFICE NAME AND ADDRESS	12. REPORT DATE: April 20, 1978
	13. NUMBER OF PAGES: 135
14. MONITORING AGENCY NAME & ADDRESS (if different from Controlling Office): As above	15. SECURITY CLASS. (of this report)
	15a. DECLASSIFICATION/DOWNGRADING SCHEDULE

16. DISTRIBUTION STATEMENT (of this Report)

DISTRIBUTION STATEMENT A
Approved for public release;
Distribution Unlimited

17. DISTRIBUTION STATEMENT (of the abstract entered in Block 20, if different from Report)

18. SUPPLEMENTARY NOTES

Prepared as final report of contract #N00014-69-C-0402.

19. KEY WORDS (Continue on reverse side if necessary and identify by block number)

Doppler Bubble Detection. Decompression Sickness. Diving Decompression Table. Ultrasonic Devices. Hyperbaric.

20. ABSTRACT (Continue on reverse side if necessary and identify by block number)

Present decompression procedures, based on the Haldane concept, allow the maximum possible degree of supersaturation without producing decompression sickness in an attempt to provide the greatest rate of gas elimination and the shortest possible safe decompression. The initially large supersaturation values experienced in a Haldane type decompression were shown to predispose bubble formation. Using the Doppler detector implanted on the pulmonary artery or posterior vena cava in sheep and goats, we have demonstrated the presence of gaseous emboli in all Haldane model decompressions.

DD FORM 1 JAN 73 1473 EDITION OF 1 NOV 65 IS OBSOLETE
S/N 0102-LF-014-6601

over

SECURITY CLASSIFICATION OF THIS PAGE (When Data Entered)

(cont)

Emboli signals from implanted cuffs were clear with a high signal to noise ratio and were therefore adaptable for signal analysis and absolute quantitation with a gas emboli counter. Gas emboli-free ascent procedures were developed using the ultrasonic detector and the emboli counter.

These gaseous emboli when detected in large numbers heralded the onset of decompression sickness. Even in small numbers these emboli caused changes in platelet and fibrinogen survival times. We conclude that the most probable cause of bubble formation in a Haldane type decompression is the initial ascent rate and that gas emboli are pathogenic and should be eliminated to provide a truly safe decompression.